論文 / 著書情報
Article / Book Information

題目(和文)	不連続動特性をもつシステムに対する推定法とその応用
Title(English)	Estimation for Discontinuous Dynamical Systems and its Applications
著者(和文)	SrangSarot
Author(English)	Sarot Srang
出典(和文)	学位:博士（学術）, 学位授与機関:東京工業大学, 報告番号:甲第9668号, 授与年月日:2014年9月25日, 学位の種別:課程博士, 審査員:山北　昌毅,三平　満司,倉林　大輔,大山　真司,早川　朋久
Citation(English)	Degree:, Conferring organization: Tokyo Institute of Technology, Report number:甲第9668号, Conferred date:2014/9/25, Degree Type:Course doctor, Examiner:,,,,
学位種別(和文)	博士論文
Type(English)	Doctoral Thesis

Estimation for Discontinuous Dynamical Systems and its Applications

A dissertation presented

by

Sarot Srang

in Partial Fulfillment of the Requirements
for the Degree of Doctor of Philosophy

Supervisor

Associate Professor Masaki Yamakita

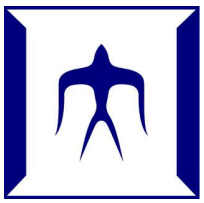

Department of Mechanical and Control Systems Engineering
Graduate School of Science and Technology
Tokyo Institute of Technology

August 20, 2014

Acknowledgments

I would like to express my deepest gratitude to my supervisor Associate Professor Masaki Yamakita for his invaluable advices and supports for many things related to my studies and social life. I would also like to thank to the committees, Professor Mitsuji Sampei, Professor Daisuke Kurabayashi, Associate Professor Shinji Ohyama and Associate Professor Tomohisa Hayakawa, who kindly spent time checking and approving this dissertation.

I would like to express my special gratitude to Dr. Keo Lychek, an instructor in my former class in Institute of Technology of Cambodia and also a former student in Yamakita laboratory, for introducing me to my supervisor before I came to Japan. Without his introduction, I might never have chance to study what I really like the most under the supervision of a very helpful and kind supervisor who always spends a lot of time instructing students.

I would like to thank to JICA that has set up a program called AUN/SEED.Net (Asian University Network for Southeast Asia Engineering Education Development) that awarded me a scholarship to study a Doctor degree for three years in Japan. I would like to especially thank to JICA staffs working at Tokyo International Center (TIC) for their very careful supports for my living environment.

I also have many special thanks to Mr. Masahiro Kawaguchi for being my helpful and friendly tutor in Yamakita laboratory for one year; I would like to thank my former seniors, Assistant Prof. Yuta Hanazawa, Dr. Sirichai Pornsarayouth and Dr. Yasuaki Kaneda for their guidance and discussions; I would also like to thank to former and current Yamakita laboratory members, such as Ms. Suthira Limkul, Mr. Kazuhiro Tanaka, Mr. Tadashi Sumioka, Mr. Yasuke Yashiro, Mr. Hiroyuki Suda, Mr. Kazuyoshi Odachi, Mr. Hiroaki Ishiyama, Mr. Terumitsu Hayashi, Mr. Hiroyuki Ohyama, Mr. Mikiya Hara, Mr. Yuto Noda, Mr. Yu Iemura, Mr. Umihiko Amanuma, Mr. Yongjae Kim, Mr. Hiroki Fujii, Mr. Yusuke Yaginuma, Mr. Mamoru Watanabe, Mr. Kwangwoo Seo, Mr. Ryo Yanase, Mr. Takayuki Morito and Mr. Doan Nhat Thanh for sometimes teaching Japanese to me and making enjoyable events; and I would like to thank Ms. Mari Kobayasi, secretary of Yamakita laboratory, for her kind support in terms of academic affair.

Last but not least, I am very grateful to my family including my parents, my wife, my brother and sister for their strong encouragement and cares of me.

Sarot Srang

Ookayama, Tokyo
June, 2014

Abstract

Discontinuous dynamical systems have been increasingly paid attention since they arise a large number of applications ranging from various physical to biological systems such as systems with friction, impact, bang-bang controllers, on-off controllers, sliding mode control and actuator nonlinearity like dead-zone, a group of robots which obey the law of "move away from the nearest other robot or environmental boundary," systems requiring discontinuous stabilization, nonsmooth harmonic oscillator, dynamical network with switching topology, and biological neural networks. There are riches of analysis on semistability, multistability and bifurcation in the form of differential inclusion using Filippov's convex method. However, *estimation techniques* of the prescribed systems have not been widely investigated. In this research, we account for stochastic model for such systems and estimation problems are explored.

Algorithms for estimation being considered consists of initialization, prediction (also called time update) and correction (also called measurement update), which is a Kalman-type estimation. Since the accuracy of prediction relies on the computation method itself which must deals with dynamical systems involving discontinuous vector field, this research is directed into three main scopes, investigation of computation accuracy at discontinuities, advantages of Filippov's convex method for both improvement on numerical accuracy and stability analysis of estimation in terms of observability, and realization of an appropriate filtering techniques for our proposed simplified model. However, these distinguished contributions are not written separately by chapter.

The common problem of computation accuracy of state around a discontinuity surface (called sliding surface if state is sliding) is chattering. It is largely incurred if Euler approximation is used as a numerical integration method. In this work, chattering of a particular one-dimensional system is explicitly detailed. Then extension of analysis on chattering to higher dimensional systems is made. A term, *trajectory error* is defined to characterize numerical accuracy on a sliding surface, and it plays an important role together with the improved computation approach and the proposed filtering technique, which is described below.

Filippov's convex method is extended to the use for improving computational accuracy of state near one or more sliding surfaces, i.e. it is used to avoid chattering and obtain attraction of state to the sliding surfaces if the state satisfies threshold conditions. The maximum trajectory errors corresponding to the surfaces are termed as the thresholds. A brief description of this method for n-dimensional systems with single and multiple sliding surfaces is given. This method is, moreover, a systematic fashion which grants stability analysis based on observability. It is shown that for a class of discontinuous dynamical systems the average vector field obtained from Filippov's convex method yields unobservability in estimation point of view. For instant, joint state and parameter model of a system with discontinuous

asymmetric friction model, where the coefficients of friction are to be estimated, is shown to result zero average vector field at zero velocity, so that the system is obviously unobservable. An other generic example for higher dimensional discontinuity surface is also given.

Suitable filtering techniques for discontinuous dynamical systems is mainly focused in this research. For Kalman-type filtering, unscented transformation, a nonlinear filtering framework, is superior to extended Kalman filter, which applies linearization technique, since it does not require partial derivatives as does the linearization technique that may incur severeness at discontinuity. To cover broad range systems, we propose that the discontinuous vector field is simplified as multiplication of known discontinuous basis function and parameter that evolves in time. The basis function is selected in such a way that stability of estimation is guaranteed. We use continuous-discrete unscented Kalman filter (CDUKF) to estimate the proposed model because it has been proved better than discrete time UKF. A particular feature is included to the algorithm, i.e. when system state lies on sliding surface, estimation is switched to computation of deterministic model as it is shown unobservable. Friction estimation for adaptive compensation in position control system is the main application example, which is used several times, meanwhile another generic example is also given. Simulation results of the two application examples show the robust performance of the method to clarify the potential use of simplification manner.

Furthermore, we consider the use of classical Kalman filter (KF) for a simplified linear time varying model, and CDUKF to estimate state and all unknown parameters of its original model. An example of tracking control of a stochastic system with actuator nonlinearity (dead-zone) is used to illustrate the performance of the both methods. For controller aspect, we also provide the elaboration of modification to an existing adaptive controller which can achieve exponential tracking of a class of nonlinear deterministic systems. The modification is made because the controller is not applicable for stochastic systems.

We also consider a new filtering approach which extends the existing receding-horizon nonlinear Kalman filter (RNKF) framework to incorporate with unscented transformation to yield a so-called receding-horizon unscented Kalman filter (RUKF). Again, it is applied to the friction estimation problem for adaptive compensation control of position. The simulation results of friction estimation and tracking performance obtained from using RUKF, classical UKF and CDUKF are compared and discussed.

Contents

List of Figures

List of Tables

Chapter 1

Introduction

Discontinuous dynamical systems which are modeled as a differential equations with discontinuous right-hand-side, have been increasingly paid attention since they arise a large number of applications ranging from various physical to biological systems such as systems with friction [1, 2, 3, 4], impact, bang-bang controllers, on-off controllers, sliding mode control and actuator nonlinearity like dead-zone; a group of robots which obey the law of "move away from the nearest other robot or environmental boundary;" systems requiring discontinuous stabilization; nonsmooth harmonic oscillator [4]; dynamical network with switching topology [5], genetic regulatory networks [6, 7] and biological neural networks with discontinuous activation function [8, 9].

In nonsmooth mechanics, the motion of rigid bodies is subject to velocity jumps and force discontinuities as a result of friction and impact [10]. Bang-bang controllers switch discontinuously between extreme values of the inputs to generate minimum-time trajectories from the initial to the final states [12]. Thermostats implement on-off controllers to regulate room temperature [13]. In the robotic manipulation of objects by means of mechanical contact [14], discontinuities occur naturally from interaction with the environment. Discontinuities are also intentionally designed to achieve regulation and stabilization. Sliding mode control [15, 16], for instant, uses discontinuous feedback controllers for stabilization. The resulting closed-loop system is discontinuous on a designed surface where the dynamics of the system is restricted to for stabilization. In robotics [17], it is of interest to induce emergent behavior in a swarm of robots by prescribing interaction rules among individual agents. Simple law such as "move away from the nearest other robot or environmental boundary" give rise to discontinuous dynamical systems. In adaptive control, [18] switching algorithms are employed to select the most appropriate controller from a given finite family to enhance robustness, ensure boundedness of the estimates, and prevent the system from stepping into undesired regions of the state space. An example of nonsmooth harmonic oscillator is a discontinuous spring force [4]. The spring does not exert any force when the mass is at the reference position. When the mass is displaced to the positive direction, the spring exerts a constant negative force, and vice versa. Many control systems cannot be stabilized by continuous state-dependent feedback. As a consequence, it is necessary to consider either time-dependent or discontinuous feedback [4]. In cooperative control, agents communicate via network. Since communication links among them are often unreliable due to multi-path effects and exogenous disturbances, the information exchange topologies in network systems are often dynamic. In particular, link failures or creations in network multi-agent systems result in switchings of the communication topology. Variation in network topology introduces

control input discontinuities, which in turn give rise to discontinuous dynamical systems [5]. In biological neural networks, the fundamental building block of the central nervous system is neuron (nerve cell). It behavior is best described in terms of the electrochemical potential gradient across the cell membrane. If the voltage gradient across the membrane increases to a critical threshold value then there is a subsequent abrupt step-like increase in the potential gradient, the action potential. This action potential is transmitted to other neurones. The dynamical model of biological neural network involves vector field in function of this action potential which can be modeled as discontinuous function which, then, yields discontinuous dynamical model of the system. The following is an example of second-order neural network with discontinuous neuron activations [8].

$$\begin{cases} \dot{x}_1 = -x_1 - \text{sign}(x_2) - \text{sign}(x_2), \\ \dot{x}_1 = -x_2 - \text{sign}(x_1) - \text{sign}(x_2), \end{cases}$$

where $\text{sign}(x_i) = 1$ for $x_i > 0$, $\text{sign}(x_i) = -1$ for $x_i < 0$, and $\text{sign}(0)$ is undefined.

Due to highly nonlinear property on discontinuity surface, there are difficulties in terms of engineering point of view. One of the common known problems is the present of chattering which ruins the accuracy of computation due to discretization method, e.g. Euler approximation. Various type of trajectory behaviors cannot be handled by using classical analysis like Lipschitz function. There are riches of analysis on stability by [4], semistability and finite-time semistability by [5], and multistability and bifurcations by [9]. These analyses are based on differential inclusion using Filippov's convex method. Although numerous interesting systems are described by discontinuous dynamical model with well analysis as described above, estimation for such systems has not been widely investigated. In this research, we account for stochastic model for such systems, and estimation problems are mainly considered. Applications of joint state and parameter estimation of certain systems for control purpose are well elaborated.

The celebrated Kalman filter (KF) and extended Kalman filter (EKF) are very powerful approaches for filtering and estimation problems, and they have been applied to various advanced engineering problems for more than four decades. Because EKF is applied to nonlinear systems, it has been widely used for prediction [19], estimation [20, 21], adaptive filtering [22], system identification [23, 24], state observation [25], training of neural networks [26], and many other areas, and its stability analysis was investigated by [27]. Despite its usefulness, many researchers had tried to find other nonlinear filtering approach. The classical (or discrete) unscented Kalman filter (UKF) was proposed by [28, 29]. It was, later, proved more robust than EKF in several cases [30]. In addition it can incorporated highly nonliner system including discontinuous dynamical systems since the propagation of prediction can be done via unscented transformation which does not require partial derivative as does linearization technique which must be used in the EKF algorithm. Based on continuous-time limit with respect to time step, [31] derived continuous-time unscented Kalman filter (CUKF), also called unscented Kalman-Bucy filter (UKBF), and analyzed by [32], and derived continuous-discrete unscented Kalman filter (CDUKF) by extending the fact that during the integration (propagation) interval of time update, the measurement covariance matrix is infinity which reflects the unavailability of measurement update during this interval. In addition, the latter one was proved to outperform the discrete UKF by showing simulation results of reentry vehicle tracking problem. Cubature Kalman filter (CKF) and continuous-discrete cubature Kalman filter, which are the special case of UKF and CDUKF respectively, were derived by the same authors [33, 34], and CDCKF were proved to outperform the CDUKF. However,

it is not suitable for estimation of discontinuous dynamical systems since its algorithm uses Itô-Taylor expansion of order 1.5 which requires first and second partial derivatives. Joint state and parameter estimation was considered [35, 36]. In [36], reduced-order unscented Kalman filter was proposed. For simplex sigma points, a general tractable algorithm is derived for large dimensional systems but with smaller and fixed rank (or rank approximation) of covariance matrix performed in Frobenius norm projection. Also, a fine algorithm of augmented state and parameter is systematically derived for both discrete and continuous time model. However, for the algorithms in [36], uncertainty term of process equation is not taken into account. In this research, in order to cover a broad rang of systems, we consider significant internal uncertainty of state model. We make simplification on the state equation as a multiplication of basis function, which is in terms of state variable, and parameter that evolves in time. As we mainly focus on discontinuous dynamical systems, the basis functions selected must involve discontinuities. If the model of a system is unknown or difficult to obtain, the basis function is arbitrarily selected, but must be within a limitation that stability of estimation is guaranteed. Estimation of this simplified systems is the core of our research. By intuition, simplification too far from the actual model may yield worse estimation performance although stability can be upheld. Hence, we also consider limitation of simplification that achieve superior performance.

Recently, receding-horizon nonlinear Kalman filter (RNKF) was proposed to handle estimation problems with state constraints [37]. This algorithm combines the receding-horizon framework with the EKF. It was proved that for unconstrained linear systems the RNKF results in a KF estimate for the current instant and smoothed estimates for the other instants of the receding horizon. This implies its robustness over the one-step-prediction framework of the classical EKF and possible UKF. As mentioned that EKF is not well-used with discontinuous dynamical systems, we propose the incorporation between the receding horizon framework and the unscented transformation, which is named receding-horizon unscented Kalman filter. This algorithm is applied to the proposed simplified model mentioned earlier.

1.1 Outline

This dissertation consists of sevens chapters, and its next contents are organized the follows.

Chapter 2: Kalman Filter for Linear and Nonlinear Systems
This chapter reviews the general stochastic models for discrete, continuous and continuous-discrete. We give a brief background and algorithms of some standard Kalman-type filtering algorithms including the celebrated Kalman filter, the extended Kalman filter, the unscented Kalman filter, and the continuous-discrete unscented Kalman filter.

Chapter 3: Friction Estimation using CDUKF for Adaptive Control
We introduce a joint state and parameter model of the velocity model of a DC motor in both deterministic and stochastic forms in this chapter. The parameters are the coefficients of Stribeck curve which are estimated online using CDUKF. Then friction can be estimated, and is used for adaptive compensation for a position control. We also present the stability analysis for a one-dimensional systems with continuum equilibria at discontinuity and show how to determine an appropriate sampling time to compute the system equations with a desired accuracy, then apply to the DC motor model. Observability of the estimation prob-

lem is also investigated in the Stribeck zone. Discussions and simulation results are given to illustrate the performance of the control method.

Chapter 4: Filippov's Convex Method for the Improvement of the Adaptive Control
We consider the same control scheme as in the previous chapter. But, we also include the coefficient of viscous friction in the parameter estimation. Fillippov approach for both single and multiple sliding surfaces is given. In order to obtain accurate computation when state orbits along sliding surface, we use the Filippov approach to avoid chattering and have the state attracted to the surface. Furthermore, by using the method observability on the sliding surface is discussed. Simulation and discussion on parameter estimation and control performance are described.

Chapter 5: Estimation of Discontinuous Dynamical Systems using CDUKF
In this chapter, we consider an effective estimation algorithm for system with multiple discontinuities. We propose that a discontinuous vector field of state equation is approximated as multiplication of known discontinuous basis function and parameter that evolves in time. The problem set up, i.e. estimation of joint state and parameter of our proposed model and limitation of bias basis function are presented. We investigate behavior or chattering around sliding surface for n_x-dimensional systems, and we also bring up the Filippov approach for accurate computation. Motivating example on estimation problem of a system with higher dimensional manifold of discontinuity surface is discussed. We, moreover, provide a particular algorithm for estimation of the joint state and parameter model using CDUKF in the form of less computational complexity. To show the robustness of the algorithm, two numerical examples are given.

Furthermore, we give a comparison of effectiveness between the ultimate simplification model that becomes linear time-varying model and a minor-simplification model. Then KF and CDUKF can be applied accordingly. A case study of tracking control of a class of dynamical system with actuator nonlinearity (specifically dead-zone) is explored. The existing controller which achieves exponential tracking is modified to fit with stochastic systems for implementation. Finally, Discussion and simulation results are reported.

Chapter 6: Receding-horizon UKF
In this chapter we introduce RUKF which incorporates the receding-horizon scheme and the unscented transformation. We give the formulation of the algorithm based on the framework of the RNKF. The problem of friction estimation for adaptive control is considered. Simulation results of using the classical UKF, CDUKF, and RUKF are compared and discussed.

Chapter 7: Conclusion
This chapter summaries all of our work, and points out the effectiveness as well as the limitation of our proposed methods. Moreover, we also provide some comments for extending this research.

Chapter 2

Kalman-Type Filtering for Linear and Nonlinear Systems

Kalman-type filtering algorithms are very powerful for application in many areas such as signal processing, control, optimization, etc... It is because the algorithms can be used for variety of online implementation. For a brief review, only some estimation algorithms for linear and nonlinear systems are described in this chapter. The contents in this chapter mainly refer to [31, 33, 34].

2.1 Kalman Filter

Consider a linear discrete-time system as following,

$$\begin{aligned} x_{k+1} &= Ax_k + Bu_k + v_k \\ z_{k+1} &= Cx_{k+1} + Du_{k+1} + w_{k+1}, \end{aligned} \tag{2.1.1}$$

where $x_k \in \mathbb{R}^{n_x}$, $u_k \in \mathbb{R}^{n_u}$ and $z_k \in \mathbb{R}^{n_z}$ are state, input and measurement of the dynamical system respectively; $A \in \mathbb{R}^{n_x \times n_x}$ is the system matrix and $C \in \mathbb{R}^{n_z \times n_x}$ is an observation matrix, both of which are assumed constants; $B \in \mathbb{R}^{n_x \times n_u}$ and $D \in \mathbb{R}^{n_z \times n_u}$ are some matrices; $v_k \in \mathbb{R}^{n_x}$ and $w_k \in \mathbb{R}^{n_z}$ are independent process and measurement noises at time k. They are assumed to be Gaussian with covariance matrix $Q \in \mathbb{R}^{n_x \times n_x}$ and $R \in \mathbb{R}^{n_z \times n_z}$ respectively, and independent of x_k and z_k.

The well-known Kalman filter algorithm for (2.1.1) is given by the follows.

- *Initialization*

  Select any initial state estimate and its positive definite error covariance matrix which are denoted as $\hat{x}_{0|0}$ and $P_{0|0}$ respectively.

- *Time Update*

$$\begin{aligned} \hat{x}_{k+1|k} &= A\hat{x}_{k|k} + Bu_k \\ P_{k+1|k} &= AP_{k|k}A^T + Q. \end{aligned} \tag{2.1.2}$$

- *Measurement Update*

$$\begin{aligned}
\hat{z}_{k+1|k} &= C\hat{x}_{k+1|k} + Du_{k+1} \\
P_{xz,k+1|k} &= P_{k+1|k}C^T \\
P_{zz,k+1|k} &= CP_{k+1|k}C^T + R \\
\hat{x}_{k+1|k+1} &= \hat{x}_{k+1|k} + P_{xz,k+1|k}P^{-1}_{zz,k+1|k}(z_k - \hat{z}_{k+1|k}) \\
P_{k+1|k+1} &= P_{k+1|k} - P_{xz,k+1|k}P^{-1}_{zz,k|k+1}P^T_{xz,k+1|k}.
\end{aligned} \tag{2.1.3}$$

In terms of the Kalman gain,

$$K_{k+1} = P_{xz,k+1|k}P^{-1}_{zz,k+1|k}, \tag{2.1.4}$$

the measurement update can be rewritten as

$$\begin{aligned}
\hat{x}_{k+1|k+1} &= \hat{x}_{k+1|k} + K_{k+1}(z_{k+1} - C\hat{x}_{k+1|k} - Du_{k+1}) \\
P_{k+1|k+1} &= P_{k+1|k} - K_{k+1}P_{zz,k+1|k}K^T_{k+1}.
\end{aligned} \tag{2.1.5}$$

2.2 Generalization of Kalman Filter for Nonlinear Systems

The general model of a nonlinear discrete-time system is given by

$$\begin{aligned}
x_{k+1} &= f_d(x_k, u_k) + v_k \\
z_{k+1} &= h_d(x_{k+1}, u_{k+1}) + w_{k+1},
\end{aligned} \tag{2.2.1}$$

where $x_k \in \mathbb{R}^{n_x}$ is the state of the dynamic system at discrete-time k; $u_k \in \mathbb{R}^{n_u}$ is input of the system; f_d and h_d are some known functions; $z_k \in \mathbb{R}^{n_z}$ is the measurement; v_k and w_k have the same definition and assumption as in the previous section. For ease of writing we denote the joint of the sets, $z_{1:j}$ and $u_{1:k}$, as

$$G_k = (z_{1:k}, u_{1:k}). \tag{2.2.2}$$

For Bayesian filter theory under the Gaussian domain, the key approximation taken to develop is that the predictive density $p(x_{k+1}|G_k)$ and the filter likelihood density $p(z_{k+1}|G_k)$ are both Gaussian, which eventually leads to a Gaussian posterior density $p(x_{k+1}|(G_{k+1})$. Under the Gaussian approximation, the functional recursion of the Bayesian filter reduces to an algebraic recursion operating only on means and covariances of various conditional densities encountered in the time and the measurement updates.

2.2.1 Time Update

In the time update, the Bayesian filter computes the mean $\hat{x}_{k+1|k}$ and the associated covariance $P_{k+1|k}$ of the Gaussian predictive density as

$$\hat{x}_{k+1|k} = \mathsf{E}[x_{k+1}|G_k] \tag{2.2.3}$$

where $\mathsf{E}[\cdot]$ is the statistical expectation operator. By substituting the first equation of (2.2.1) into (2.2.3), we obtain

$$\hat{x}_{k+1|k} = \mathsf{E}[f_d(x_k, u_k) + v_k|G_k]. \tag{2.2.4}$$

Since v_k is assumed to be independent zero-mean, we get

$$\begin{aligned}\hat{x}_{k+1|k} &= \mathsf{E}[f_d(x_k, u_k)|G_k] \\ &= \int_{\mathbb{R}^{n_x}} f_d(x_k, u_k) p(x_k|G_k) dx_k \\ &= \int_{\mathbb{R}^{n_x}} f_d(x_k, u_k) \mathcal{N}(x_k; \hat{x}_{k|k}, P_{k|k}) dx_k,\end{aligned} \tag{2.2.5}$$

where $\mathcal{N}(.,.)$ is the conventional symbol for a Gaussian density. Similarly for error covariance matrix, we obtain

$$\begin{aligned}P_{k+1|k} &= \mathsf{E}[(x_{k+1} - \hat{x}_{k+1|k})(x_{k+1} - \hat{x}_{k+1|k})^T|z_{1:k}] \\ &= \int_{\mathbb{R}^n} (x_{k+1} - \hat{x}_{k+1|k})(x_{k+1} - \hat{x}_{k+1|k})^T p(x_k|G_k) dx_k \\ &= \int_{\mathbb{R}^n} f_d(x_k, u_k) f_d^T(x_k, u_k) \mathcal{N}(x_k; \hat{x}_{k|k}, P_{k|k}) dx_k - \hat{x}_{k+1|k}\hat{x}_{k+1|k}^T + Q.\end{aligned} \tag{2.2.6}$$

2.2.2 Measurement Update

It is well known that the errors in the predicted measurements are zero-mean white sequences ([33] and the references therein). Under the assumption that these errors can be well approximated by the Gaussian, the filter likelihood density is written as

$$p(z_{k+1}|G_k) = \mathcal{N}(z_{k+1}; \hat{z}_{k+1|k}, P_{zz,k+1|k}) \tag{2.2.7}$$

where the predicted measurement is given by

$$\begin{aligned}\hat{z}_{k+1|k} &= \int_{\mathbb{R}^n} z_{k+1} p(x_{k+1}|G_k) dx_{k+1} \\ &= \int_{\mathbb{R}^n} h_d(x_{k+1}, u_{k+1}) \mathcal{N}(x_{k+1}; \hat{x}_{k+1|k}, P_{k+1|k}) dx_{k+1},\end{aligned} \tag{2.2.8}$$

and the associated covariance is defined by

$$\begin{aligned}P_{zz,k+1|k} &= \int_{\mathbb{R}^n} (z_{k+1} - \hat{z}_{k+1|k})(z_{k+1} - \hat{z}_{k+1|k})^T p(x_{k+1}|G_k) dx_{k+1} \\ &= \int_{\mathbb{R}^n} h_d(x_{k+1}, u_{k+1}) h_d^T(x_{k+1}, u_{k+1}) \mathcal{N}(x_{k+1}; \hat{x}_{k+1|k}, P_{k+1|k}) dx_{k+1} - \hat{z}_{k+1|k}\hat{z}_{k+1|k}^T + R.\end{aligned} \tag{2.2.9}$$

Therefore, the conditional Gaussian density of the joint state and measurement can be written as

$$p\left([x_{k+1}^T \quad z_{k+1}^T]^T|G_k\right) = \mathcal{N}\left(\begin{pmatrix} \hat{x}_{k+1|k} \\ \hat{z}_{k+1|k} \end{pmatrix}, \begin{pmatrix} P_{k+1|k} & P_{xz,k+1|k} \\ P_{xz,k+1|k}^T & P_{zz,k+1|k} \end{pmatrix}\right) \tag{2.2.10}$$

where the cross-covariance is

$$\begin{aligned}P_{xz,k+1|k} &= \int_{\mathbb{R}^n} (x_{k+1} - \hat{x}_{k+1|k})(z_{k+1} - \hat{z}_{k+1|k})^T p(x_{k+1}|G_k) dx_{k+1} \\ &= \int_{\mathbb{R}^n} x_{k+1} h_d^T(x_{k+1}, u_{k+1}) \mathcal{N}(x_{k+1}; \hat{x}_{k+1|k}, P_{k+1|k}) dx_{k+1} - \hat{x}_{k+1|k}\hat{z}_{k+1|k}^T.\end{aligned} \tag{2.2.11}$$

On the receipt of a new measurement z_{k+1}, the Bayesian filter computes the posterior density $p(x_{k+1}|G_{k+1})$ from (2.2.10) yielding

$$p(x_{k+1}|G_{k+1}) = \mathcal{N}(x_{k+1}; \hat{x}_{k+1|k}, P_{k+1|k+1}), \tag{2.2.12}$$

where

$$\begin{aligned} K_{k+1} &= P_{xz,k+1|k} P^{-1}_{zz,k+1|k} \\ \hat{x}_{k+1|k+1} &= \hat{x}_{k+1|k} + K_{k+1}(z_{k+1} - \hat{z}_{k+1|k}) \\ P_{k+1|k+1} &= P_{k+1|k} - K_{k+1} P_{zz,k+1|k} K^T_{k+1}. \end{aligned} \tag{2.2.13}$$

2.3 Extended Kalman Filter

Consider a nonlinear dynamical discrete-time system given by (2.2.1). The algorithm of the extended Kalman filter is based on linearization technique of nonlinear functions at the latest known estimate. By using Taylor series expansion, the propagation and measurement functions, f_d and h_d can be rewritten as the follows,

$$\begin{aligned} f_d(x_k, u_k) = f_d(\hat{x}_{k|k}, u_k) &+ \frac{1}{1!}\frac{\partial f_d}{\partial x}\bigg|_{x=\hat{x}_{k|k}} (x_k - \hat{x}_{k|k}) \\ &+ \underbrace{\frac{1}{2!}\frac{\partial^2 f_d}{\partial x^2}\bigg|_{x=\hat{x}_{k|k}} (x_k - \hat{x}_{k|k})^2 + \cdots}_{HOT} \end{aligned} \tag{2.3.1}$$

$$\begin{aligned} h_d(x_{k+1}, u_{k+1}) = h_d(\hat{x}_{k+1|k}, u_{k+1}) &+ \frac{1}{1!}\frac{\partial h_d}{\partial x}\bigg|_{x=\hat{x}_{k+1|k}} (x_{k+1} - \hat{x}_{k+1|k}) \\ &+ \underbrace{\frac{1}{2!}\frac{\partial^2 h_d}{\partial x^2}\bigg|_{x=\hat{x}_{k+1|k}} (x_{k+1} - \hat{x}_{k+1|k})^2 + \cdots}_{HOT}. \end{aligned} \tag{2.3.2}$$

By truncating the higher order terms (HOT) of (2.3.1) and (2.3.2) and denoting

$$\begin{aligned} A_k &= \frac{\partial f_d}{\partial x}\bigg|_{x=\hat{x}_{k|k}} \\ C_{k+1} &= \frac{\partial h_d}{\partial x}\bigg|_{x=\hat{x}_{k+1|k}}, \end{aligned} \tag{2.3.3}$$

then the linear approximations of f_d and h_d can be written as

$$\begin{aligned} f_d(x_k, u_k) &\approx f_d(\hat{x}_{k|k}, u_k) + A_k(x_k - \hat{x}_{k|k}) \\ h_d(x_{k+1}, u_{k+1}) &\approx h_d(\hat{x}_{k+1|k}, u_{k+1}) + C_{k+1}(x_{k+1} - \hat{x}_{k+1|k}). \end{aligned} \tag{2.3.4}$$

Hence, the extended Kalman filter of (2.2.1) with the linearization (2.3.4) is given by the follows.

- *Initialization*

  Select any initial state estimate and its positive definite error covariance matrix $\hat{x}_{0|0}$ and $P_{0|0}$ respectively.

- *Time Update*

$$\begin{aligned} \hat{x}_{k+1|k} &= f_d(\hat{x}_{k|k}, u_k) \\ P_{k+1|k} &= A_k P_{k|k} A_k^T + Q. \end{aligned} \tag{2.3.5}$$

- *Measurement Update*

$$\begin{aligned} \hat{z}_{k+1|k} &= h_d(\hat{x}_{k+1|k}, u_{k+1}) \\ P_{xz,k+1|k} &= P_{k+1|k} C_{k+1}^T \\ P_{zz,k+1|k} &= C_{k+1} P_{k+1|k} C_{k+1}^T + R \\ \hat{x}_{k+1|k+1} &= \hat{x}_{k+1|k} + P_{xz,k+1|k} P_{zz,k+1|k}^{-1} (z_{k+1} - \hat{z}_{k+1|k}) \\ P_{k+1|k+1} &= P_{k+1|k} - P_{xz,k+1|k} P_{zz,k|k+1}^{-1} P_{xz,k+1|k}^T. \end{aligned} \tag{2.3.6}$$

Similar to (2.1.5), the measurement update can be defined in terms of the Kalman gain, defined in (2.1.4), as followings,

$$\begin{aligned} \hat{x}_{k+1|k+1} &= \hat{x}_{k+1|k} + K_{k+1}[z_{k+1} - h_d(\hat{x}_{k+1|k}, u_{k+1})] \\ P_{k+1|k+1} &= P_{k+1|k} - K_{k+1} P_{zz,k+1|k} K_{k+1}^T. \end{aligned} \tag{2.3.7}$$

2.4 Unscented Kalman Filter

Consider a dynamical system (2.2.1). The heart of the UKF is the *unscented transformation*, which uses a set of $(2n_x + 1)$ sigma points to approximate the Gaussian posterior density $p(x_k|G_k)$ and the Gaussian predictive density $p(x_{k+1}|G_k)$ which are used in (2.2.5), (2.2.6), (2.2.8), (2.2.9) and (2.2.11) accordingly. The approximate probability density, denoted as $\Pi(x)$ of an n_x-dimensional random variable x with mean $\hat{x}$ and covariance P is given by

$$\Pi(x) = \sum_{i=0}^{2n_x} W_i \boldsymbol{\delta}(x - X_i), \tag{2.4.1}$$

where $\boldsymbol{\delta}(\cdot)$ is the Dirac delta function and the sigma points $\{X_i\}$ are selected to preserve the first and second moments, such that

$$\begin{aligned} X_0 &= \hat{x} \\ X_i &= \hat{x} + (\sqrt{(n_x + \lambda)P})_i \\ X_i &= \hat{x} - (\sqrt{(n_x + \lambda)P})_i \end{aligned} \tag{2.4.2}$$

with associated weights as the follows [31, 38],

- mean contraction weights

$$\begin{aligned} W_0^{(m)} &= \frac{\lambda}{n_x + \lambda} \\ W_i^{(m)} &= \frac{1}{2(n_x + \lambda)}, \quad i = 1, \ldots, 2n_x \end{aligned} \tag{2.4.3}$$

- covariance contraction weights:

$$\begin{aligned} W_0^{(c)} &= \frac{\lambda}{n_x + \lambda_n} + (1 - \alpha^2 + \beta) \\ W_i^{(c)} &= \frac{1}{2(n_x + \lambda)}, \quad i = 1, \ldots, 2n_x \end{aligned} \tag{2.4.4}$$

where the common intermediate value is

$$\lambda = \alpha^2(n_x + \kappa) - n_x. \tag{2.4.5}$$

The three controlling parameters have the following properties [38],

- Spreading factor α, limited to $0 < \alpha < 1$, which controls how the sigma points are selected from the sizes of the major axes of the uncertainty ellipsoid of the distribution ($\alpha \to 0$ concentrates sigma points while $\alpha \to 1$ applies no scaling)
- Contraction term β, limited to $\beta > 0$, which controls how higher-order moments of the transform are included in the contracted covariance ($\beta = 2$ for pure Gaussian distribution)
- Offset term κ, limited to $\kappa \geq 0$, which is used to guarantee positive-semidefiniteness of the contracted covariance ($\kappa = 0$ applies no offset)

Hence, a nonlinear expectation is approximately computed using the sigma-point set as

$$\begin{aligned} \mathsf{E}[f(x)] &\approx \int_{\mathbb{R}^{n_x}} f(x)\Pi(x)dx \\ &\approx \sum_{i=0}^{2n_x} W_i^{(m)} f(X_i) \\ \mathsf{var}[f(x)] &\approx \int_{\mathbb{R}^{n_x}} \left(f(x) - \mathsf{E}[f(x)]\right)\left(f(x) - \mathsf{E}[f(x)]\right)^T \Pi(x)dx \\ &\approx \sum_{i=0}^{2n_x} W_i^{(c)} \left(f(X_i) - \mathsf{E}[f(x)]\right)\left(f(X_i) - \mathsf{E}[f(x)]\right)^T. \end{aligned} \tag{2.4.6}$$

In matrix form the above equations can be rewritten as

$$\begin{aligned} \mathsf{E}[f(x)] &= f(X)w_m \\ \mathsf{var}[f(x)] &= f(X)Wf^T(X), \end{aligned} \tag{2.4.7}$$

where the set of sigma points X is

$$\begin{aligned} X &= [X_i] \\ &= [\hat{x} \quad \cdots \quad \hat{x}] + \sqrt{(n_x + \lambda)} \begin{bmatrix} 0 & \sqrt{P} & -\sqrt{P} \end{bmatrix}, \end{aligned} \tag{2.4.8}$$

and vector w_m and matrix W are defined as the follows [31],

$$\begin{aligned} w_m &= \begin{bmatrix} {W_0}^{(m)} \cdots {W_{2n_x}}^{(m)} \end{bmatrix}^T \\ W &= (I - [w_m \cdots w_m]) \\ &\quad \times \operatorname{diag}\left(\begin{bmatrix} {W_0}^{(c)} \cdots {W_{2n_x}}^{(c)} \end{bmatrix}\right) \\ &\quad \times (I - [w_m \cdots w_m])^T. \end{aligned} \tag{2.4.9}$$

Therefore, we can assemble the complet UKF as the followings:

- *Initialization*

  Select any initial mean and its positive definite error covariance matrix $\hat{x}_{0|0}$ and $P_{0|0}$ respectively.

- *Time Update*

$$\begin{aligned} X_{k|k} &= [\hat{x}_{k|k} \quad \cdots \quad \hat{x}_{k|k}] \\ &\quad + \sqrt{n_x + \lambda}\,[0 \quad \sqrt{P_{k|k}} \quad -\sqrt{P_{k|k}}] \\ X_{k+1|k} &= f_d(X_{k|k}, u_k) \\ \hat{x}_{k+1|k} &= X_{k+1|k} w_m \\ P_{k+1|k} &= X_{k+1|k} W X_{k+1|k}^T + Q. \end{aligned} \tag{2.4.10}$$

- *Measurement Update*

$$\begin{aligned} X_{k+1|k}^{(r)} &= [\hat{x}_{k+1|k} \quad \cdots \quad \hat{x}_{k+1|k}] \\ &\quad + \sqrt{n_x + \lambda}\,[0 \quad \sqrt{P_{k+1|k}} \quad -\sqrt{P_{k+1|k}}] \\ Z_{k+1|k} &= h_d(X_{k+1|k}^{(r)}, u_{k+1}) \\ \hat{z}_{k+1|k} &= Z_{k+1|k} w_m \\ P_{xz,k+1|k} &= X_{k+1|k}^{(r)} W Z_{k+1|k}^T \\ P_{zz,k+1|k} &= Z_{k+1|k} W Z_{k+1|k}^T + R \\ K_{k+1} &= P_{xz,k+1|k} P_{zz,k+1|k}^{-1} \\ \hat{x}_{k+1|k+1} &= \hat{x}_{k+1|k} + K_{k+1}(z_{k+1} - \hat{z}_{k+1|k}) \\ P_{k+1|k+1} &= P_{k+1|k} - K_{k+1} P_{zz,k+1|k} K_{k+1}^T. \end{aligned} \tag{2.4.11}$$

  where $X_{k+1|k}^{(r)}$ is called the set of resampled sigma points. Note that the computation of square root of a matrix, $\sqrt{P}$, can be done using Cholesky factorization"chol(P)".

2.5 Continuous-Discrete Unscented Kalman Filter

According to [31] and the reference therein, in many signal processing systems the sensor measurements are obtained at discrete instances of time either due to sampling, due to processing delays in the device or because the sensor operates in scans. Still in the Nature time is continuous, not discrete, and for this reason often a physically more realistic approach than discrete-time filtering or continuous-time filtering is *continuous-discrete filtering*. In continuous-discrete filtering the state dynamics are modeled as continuous-time stochastic processes, and the measurements are obtained at discrete instances of time. This differs from discrete-time filtering because in that approach both dynamics and measurements are modeled as discrete-time processes.

The continuous-discrete filtering models described here have the general form as (see [34] and the reference therein)

$$\begin{aligned} dx(t) &= f(x(t), t)dt + \sqrt{Q_c}\, d\boldsymbol{\beta}(t), \\ z_k &= h_d(x(t_k), t_k) + w_k, \end{aligned} \tag{2.5.1}$$

where $x(t) \in \mathbb{R}^{n_x}$ and $z_k \in \mathbb{R}^{n_z}$ are state and measurement respectively; the function f is called the drift function; $\boldsymbol{\beta}(t) \in \mathbb{R}^{n_x}$ is standard Brownian motion with increment $d\boldsymbol{\beta}(t)$ that is independent of $x(t)$; $Q_c \in \mathbb{R}^{n_x \times n_x}$ is called the diffusion matrix, also known as the spectral density matrix or gain matrix of the process noise; the function h_d is the measurement model function; and w_k is a zero-mean Gaussian measurement noise with covariance matrix $R \in \mathbb{R}^{n_z \times n_z}$. The optimal solution of (Bayesian) continuous-discrete filtering is to recursively compute the posterior distribution,

$$p(x(t_k)|z_1, \ldots, z_k), \tag{2.5.2}$$

where t_k is the time of measurement z_k. By using optimal prediction the corresponding distribution can also be computed for all time instances before the next measurement $t \in [t_k, t_{k+1})$. There are several kinds of approximation on how to compute the posterior distribution in that CDUKF derived by [31] is one of the powerful methods. Before the algorithm is describe, we give a brief of continuous-discrete EKF (CDEKF).

Applying Euler approximation to the stochastic differential of (2.5.1) over the time interval $(t, t+\delta)$ yields

$$x(t+\delta) = x(t) + \delta f(x(t), t) + \sqrt{Q_c}e, \tag{2.5.3}$$

where the n_x-dimensional Gaussian random variable e is related to the standard Gaussian random variable $u = \frac{d\beta}{dt}$ via $e = \sqrt{\delta}u \sim \mathcal{N}(0, \delta I_{n_x})$ with I_{n_x} being used to denote the n_x-dimensional identity matrix. Taking the expectation yields

$$\mathsf{E}[x(t+\delta)] = \mathsf{E}[x(t)] + \delta \mathsf{E}[f(x(t), t)]. \tag{2.5.4}$$

Since $x(t)$ is independent of v, the associated error covariance matrix satisfies

$$\mathsf{var}[x(t+\delta)] = \mathsf{var}[x(t) + \delta f(x(t), t)] + \delta Q_c. \tag{2.5.5}$$

Historically, CDEKF is the first applicable continuous-discrete nonlinear filter which was derived in [39] as generalization of the classical EKF. To approximately solve the moment equations given by (2.5.4) and (2.5.5) over the time interval (t_k, t_{k+1}), the CDEKF uses the first-order Taylor series, which expands $f(x(t), t)$ around the latest known estimate $\hat{x}_{k|k} = \mathsf{E}[x_k|z_{1:k}]$, i.e.

$$\begin{aligned} f(x(t), t) = f(\hat{x}_{k|k}, k) + \frac{1}{1!}\frac{\partial f}{\partial x}\bigg|_{x=\hat{x}_{k|k}} (x(t) - \hat{x}_{k|k}) \\ \underbrace{+ \frac{1}{2!}\frac{\partial^2 f}{\partial x^2}\bigg|_{x=\hat{x}_{k|k}} (x(t) - \hat{x}_{k|k})^2 + \cdots}_{HOT} \end{aligned} \tag{2.5.6}$$

Consider the case where $t = t_k$ and $(t+\delta) = t_{k+1}$, which also implies that $\delta = T$, the relative time interval of measurement. If the HOT is truncated, substituting (2.5.6) into (2.5.4) yields the predicted estimate

$$\begin{aligned} \hat{x}_{k+1|k} &= \mathsf{E}[x_{k+1}|z_{1:k}] \\ &\approx \hat{x}_{k|k} + T f(\hat{x}_{k|k}, k). \end{aligned} \tag{2.5.7}$$

Similarly, substituting the truncated (2.5.6) into (2.5.5) yields the predicted state error covariance matrix following,

$$\begin{aligned} P_{k+1|k} &= \mathsf{var}[x_{k+1}|z_{1:k}] \\ &\approx (I_{n_x} + Tf_x(k))P_{k|k}(I_n + Tf_x(k))^T + TQ_c. \end{aligned} \tag{2.5.8}$$

where

$$f_x(k) = \left.\frac{\partial f}{\partial x}\right|_{x=\hat{x}_{k|k}}.$$

The predicted state estimate (2.5.7) and its error covariance (2.5.8) collectively form the time-update of the CDEKF.

CDUKF, similar to UKF, uses unscented transformation which was described in the previous section. (2.5.5) can be elaborated as

$$\begin{aligned} \mathsf{var}[x(t+\delta)] &= \mathsf{E}[(x(t) + \delta f(x(t),t) - \mathsf{E}[x(t) + \delta f(x(t),t)]) \\ &\quad \times (x(t) + \delta f(x(t),t) - \mathsf{E}[x(t) + \delta f(x(t),t)])^T] + \delta Q_c \\ &= \mathsf{E}[((x(t) - \mathsf{E}[x(t)]) + \delta(f(x(t),t) - \mathsf{E}[f(x(t),t)])) \\ &\quad \times ((x(t) - \mathsf{E}[x(t)]) + \delta(f(x(t),t) - \mathsf{E}[f(x(t),t)]))^T] + \delta Q_c \\ &= \mathsf{E}[(x(t) - \mathsf{E}[x(t)])(x(t) - \mathsf{E}[x(t)])^T] \\ &\quad + \delta\mathsf{E}[(x(t) - \mathsf{E}[x(t)])(f(x(t),t) - \mathsf{E}[f(x(t),t)])^T] \\ &\quad + \delta\mathsf{E}[(f(x(t),t) - \mathsf{E}[f(x(t),t)])(x(t) - \mathsf{E}[x(t)])^T] \\ &\quad + \delta^2\mathsf{E}[(f(x(t),t) - \mathsf{E}[f(x(t),t)])(f(x(t),t) - \mathsf{E}[f(x(t),t)])^T] + \delta Q_c \\ &= \mathsf{var}[x(t)] + \delta\mathsf{cov}[x(t), f(x(t),t)] + \delta\mathsf{cov}[f(x(t),t), x(t)] \\ &\quad + \delta^2\mathsf{var}[f(x(t),t), f(x(t),t)] + \delta Q_c. \end{aligned} \tag{2.5.9}$$

By neglecting terms of the order δ^2, the predicted state-error covariance matrix (2.5.5) is simplified to the following approximate result,

$$\mathsf{var}[x(t+\delta)] \approx \mathsf{var}[x(t)] + \delta\left(\mathrm{cov}[x(t), f(x(t),t)] + \mathrm{cov}[f(x(t),t), x(t)] + Q_c\right). \tag{2.5.10}$$

As δ tends to zero, the moments equations in (2.5.4) and (2.5.10) can be expressed in vector and matrix differential equations, respectively, as followings:

$$\frac{d}{dt}\mathsf{E}[x(t)] = \mathsf{E}[f(x,t),t] \tag{2.5.11}$$

$$\frac{d}{dt}\mathsf{var}[x(t)] = \mathrm{cov}[x(t), f(x(t),t)] + \mathrm{cov}[f(x(t),t), x(t)] + Q_c. \tag{2.5.12}$$

Given that x_k at time t_k is Gaussian distributed with the mean $\mathsf{E}[x(t_k)|z_{1:k}] = \hat{x}_{k|k}$ and covariance $\mathsf{var}[x(t_k)|z_{1:k}] = P_{k|k}$, then $\hat{x}_{k+1|k}$ and $P_{k+1|k}$ are obtained as follows: First, the operations $\mathsf{E}[\cdot]$ and $\mathrm{cov}[\cdot]$ that present on the right-hand side of (2.5.11) and (2.5.12) are approximated by the unscented transformation as discussed above. Then the results are numerically integrated up to time t_{k+1}; the Runge-Kutta method is used as a numerical integration tool in [31]. To compute the predicted state and its error covariance more accurately at time t_{k+1}, an m-step prediction over the "small" time intervals of length δ, where $\delta = (t_{k+1} - t_k)/m = T/m$ and the integer $m > 1$, is usually performed in a recursive manner.

On the receipt of a new measurement z_{k+1}, the posterior density is obtained by fusing z_{k+1} with the predictive density using Bayes' rule. Because the measurement-update relies only on the measurement equation, which is modeled in discrete time for a continuous-discrete state-space model case, the measurement-updates of the CDEKF and CDUKF reduce to that of the EKF and UKF, respectively.

Applying the unscented transformation (2.4.7) to (2.5.11) yields the time update of CDUKF. The complete algorithm of CDUKF is given by the follows:

- *Initialization*

  Select any initial mean and its positive definite error covariance matrix $\hat{x}_{0|0}$ and $P_{0|0}$ respectively.

- *Time Update*

  During the measurement interval $[kT \quad (k+1)T]$, integrate the differential equations of mean and its error covariance (2.5.13) and (2.5.14) starting with the initial condition $\hat{x}_{k|k}$ and $P_{k|k}$:

$$\begin{aligned} X(t) &= [\hat{x}(t) \quad \cdots \quad \hat{x}(t)] \\ &\quad + \sqrt{n_x + \lambda} \begin{bmatrix} 0 & \sqrt{P(t)} & -\sqrt{P(t)} \end{bmatrix} \\ \dot{\hat{x}}(t) &= f\left(X(t), t\right) w_m \qquad (2.5.13) \\ \dot{P}(t) &= X(t) W f^T\left(X(t), t\right) + f\left(X(t), t\right) W X^T(t) + Q_c \qquad (2.5.14) \end{aligned}$$

  At the end of time update the latest mean and its error covariance matrix are assigned to be $\hat{x}_{k+1|k}$ and $P_{k+1|k}$.

- *Measurement Update*

  The measurement update of CDUKF is identical to that of the UKF defined by (2.4.11).

Chapter 3

Friction Estimation using CDUKF for Adaptive Control

In this Chapter, we consider an application of continuous-discrete Unscented Kalman Filter to estimate state and friction for a position control system with Stribeck + viscous friction. Adaptive compensation of friction is integrated to the system. The coefficients of Stribeck curve are estimated on-line from joint state and parameter model by using CDUKF algorithm. To select sampling time appropriately for estimator, the stability and accuracy at low velocity of deterministic system are analysed. We finally presents the simulation results of a torque-controlled DC motor model to illustrate the performance of the position control system with PID controller using friction compensation since conventional PID controller are easily modified.

3.1 Introduction

In mechanical control system, regulation and trajectory tracking are very important for machine tools and robotic systems in regards to precision. One of the most challenging issue is friction which always exists between two relatively movable contacted surfaces of mechanical joints. Many researchers studied its model over decades, [1, 2, 3, 40, 41]. Its highly nonlinear properties around zero such as Stribeck effect and switching-like behavior cause some significant problems such as imprecise position regulation, large tracking lag and undesired limit cycles. A control technique to overcome the problems is compensation which can be found in [3, 42, 43, 44, 45, 46, 47, 48, 49, 50, 51]. There were two types of compensation, fixed and adaptive, which were used in those literatures. [47] studied a fixed friction compensation for which the parameters of friction model are estimated off-line for an observer-based compensations. It is shown that a good performance of the system can be obtained if the controller and the observer gains are properly tuned. However, this control strategy cannot deal with the variation of friction parameters in time.

Some literatures such as [42, 44, 45] and [50] studied adaptive compensation for static model of friction whereas [43] and [49] considered dynamic model, LuGre model, where partial parameters of friction are estimated on-line. In those papers, except [42], the convergence of model-based control system was proved by using Lyapunov method. Only [43] considered the changes of friction parameters in two different cases, the changes due to normal load and variation of temperature for a model of torque-controlled DC motor. In that work, experi-

ments for regulation and tracking on adaptive systems with PID controller were performed. The results show good performance since the impulse-like tracking errors disappear. However, the adaptation technique requires known nominal values of several parameters, which must be identified from individual experiments, and trial and error method. In [51], an extended Kalman-Bucy filter (EKBF) was used to estimate friction which was modeled as second-order random walk. Intuitively, the gap of uncertainty for friction model is large. It is known that stability of estimation can be guaranteed if large diffusion matrix of process noise is used for estimation algorithm. However, the estimation exhibits oscillation of estimate friction as seen in [51]. Only position tracking is considered in that paper, and experimental results show that even though the contributions of estimate friction from different compensation methods have remarkably different wave form, it results almost the same magnitude of tracking error. In our research we use an other method which can estimate friction more accurately, can cope with sudden change of friction and can deal with both regulation and tracking.

We consider unscented Kalman filter which is originally proposed by [28] to estimate joint state and parameter model of a torque-controlled DC motor with Stribeck + viscouse friction where the coefficients of Stribeck curve and viscous coefficient are assumed to vary in time. This algorithm is appropriate for estimation of highly nonlinear dynamical system and the system with discontinuous-right-hand-side since the propagation of prediction and correction can be done via unscented transform whereas extended Kalman filter requires partial derivatives for linearization which is not defined at discontinuity. In addition, it has been applied successfully in many cases, and it has been shown to have better performance than the extended Kalman filter [30]. The continuous-discrete version of unscented Kalman filter is derived by [31] and proved to outperform its discrete version by showing simulation result of reentry vehicle tracking problem. Recently, joint state and parameter estimation has been considered by [35, 36]. In [36] reduced-order unscented Kalman filter is proposed. For any number of sigma points (but not smaller than number of simplex sigma points), the authors derived a general tractable algorithm for a large dimensional system but with smaller and fixed rank (or rank approximation) of covariance matrix performed in Frobenius norm projection. Accurate parameter estimation is validated by simulation results. Since the dimension of our system is small, we consider a full rank of covariance matrix, and hence we adopt continuous-discrete unscented Kalman filter (CDUKF) algorithm from [31] to estimate our model. This algorithm estimates friction on-line, and then it is used for compensation in position controls. Using the proposed method, we can avoid time-consuming for identification of normal value of several friction parameters used in [43] through individual experiments.

3.1.1 Optimal Solution for a Stochastic Model

Recall the general form of continuous-discrete filtering model discussed in the previous chapter:

$$\begin{aligned} dx(t) &= f(x(t), t)dt + \sqrt{Q_c}d\boldsymbol{\beta}(t), \\ z_k &= h_d(x(t_k), t_k) + w_k, \end{aligned} \tag{3.1.1}$$

where $x(t) \in \mathbb{R}^{n_x}$ and $z_k \in \mathbb{R}^{n_z}$ are state and measurement respectively; the function f is called the drift function, and it is discontinuous or piecewise function for this research; $\boldsymbol{\beta}(t) \in \mathbb{R}^{n_x}$ is standard Brownian motion with increment $d\boldsymbol{\beta}(t)$ that is independent of $x(t)$; $Q_c \in \mathbb{R}^{n_x \times n_x}$ is called the diffusion matrix, also known as the spectral density matrix or gain

matrix of the process noise; the function h_d is the measurement model function; and w_k is a zero-mean Gaussian measurement noise with covariance matrix $R \in \mathbb{R}^{n_z \times n_z}$. The dynamic model (3.1.1) can be also written in terms of white noise $v_c(t) = \sqrt{Q_c}\frac{d\beta(t)}{dt}$ as

$$\dot{x}(t) = f(x(t), t) + v_c(t). \tag{3.1.2}$$

The algorithm that will be used for estimation of such system is the CDUKF which was given in the previous chapter.

3.1.2 Stochastic Model of a Torque-Controlled DC Motor

For ease of writing and reading from this section on, velocity and angular velocity terms are equivalently used. Before introducing the stochastic model of a torque-controlled DC motor, we give its deterministic dynamical model as following,

$$\dot{\omega}(t) = \frac{1}{J}\Big(u(t) - (\alpha_0 + \alpha_1 e^{-(\omega/\omega_s)^2} + \alpha_2|\omega|)\text{sign}(\omega)\Big) \tag{3.1.3}$$

where ω is angular velocity; J is the total moment of inertia of the motor; $u(t)$ is control torque; ω_s is called Stribeck velocity and assumed to be known, and its value used in this work is the same as that used in [43]; $\alpha_0 + \alpha_1$ is static friction; α_0 is Coulomb friction; and α_2 is viscous friction coefficient. The stochastic differential equations where velocity and coefficients Stribeck curve, α_0, α_1, are considered as state variables, $x = [x_1, x_2, x_3]^T = [\omega, \alpha_0, \alpha_1,]^T$ can be written as follows,

$$\begin{aligned} \dot{x}_1(t) &= \frac{1}{J}(u(t) - F_f) + v_{c1}(t) \\ \dot{x}_2(t) &= v_{c2}(t) \\ \dot{x}_3(t) &= v_{c3}(t) \end{aligned} \tag{3.1.4}$$

where $v_{c1}(t)$, $v_{c2}(t)$ and $v_{c3}(t)$ are white Gaussian process noises with diffusion matrix Q_c; and F_f is friction torque which is defined as following,

$$\begin{aligned} g_v &= x_2 + x_3 e^{-(x_1/\omega_s)^2}, \\ F_f &= (g_v + x_4|x_1|)\text{sign}(x_1). \end{aligned} \tag{3.1.5}$$

The graphical model of friction in (3.1.5) is shown in Fig. 3.1. Seen in the figure, the zones with negative slop are due to Stribeck effect.

We assume that we can measure velocity, and then the measurement model is as follow,

$$z_k = Hx_k + w_k, \tag{3.1.6}$$

where w_k is zero-mean Gaussian measurement noise with known variance, and $H = [1, 0, 0]$. All the parameters used for computing the actual plant (3.1.4), (3.1.5) and (3.1.6) are selected from [43].

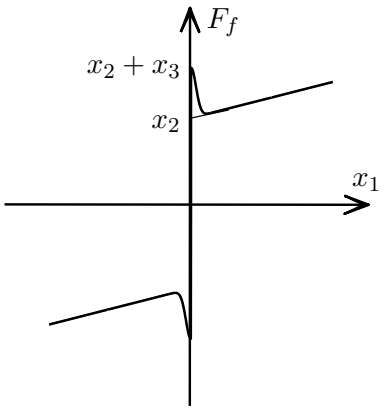

Figure 3.1: Friction model with known viscous coefficient

3.2 Analysis of a System with an Equilibrium at Discontinuity

3.2.1 Numerical Accuracy

Consider a one-dimensional deterministic system following,

$$\dot{x} = f(u) - g(x)\text{sign}(x). \tag{3.2.1}$$

Assumption 3.1

1. A continuous function $f : \mathbb{R} \longmapsto \mathbb{R}$ and $f(0) = 0$
2. $g(x) \geq 0 \ \forall x \in \mathbb{R}$ and $0 \leq \underline{\gamma} \leq g(x) \leq \overline{\gamma}$ for $|x| < \varepsilon$
3. $x(0) = x_0 > 0$

From this assumption, $x(t) = 0$ is an equilibrium of (3.2.1) if input u approaches to zero, and then this equation becomes

$$\dot{x} = -g(x)\text{sign}(x). \tag{3.2.2}$$

Taking a Lyapunov function as following,

$$V(x) = \frac{1}{2}x^2, \tag{3.2.3}$$

and then taking its first derivative with respect to time, we obtain

$$\dot{V} = x\dot{x} = -xg(x)\text{sign}(x) = -g(x)|x| < 0 \tag{3.2.4}$$

$\forall x \in \mathbb{R}$, which yields

$$V(x(t)) \leq V(x(0)) \Leftrightarrow (x(t))^2 \leq (x_0)^2, \text{ or } |x(t)| \leq x_0. \tag{3.2.5}$$

Inequality (3.2.5) implies that the system (3.2.2) is stable, i.e. $x(t)$ converges to zero. Since $0 \leq \underline{\gamma} \leq g(x) \leq \overline{\gamma}$, we can have $W = \sqrt{2V} = |x|$ satisfying the differential inequality following,

$$\frac{\partial^+ W}{\partial t} = \frac{\sqrt{2}\dot{V}}{2\sqrt{V}} = -\frac{\sqrt{2}g(x)}{2} \leq -\frac{\sqrt{2}\underline{\gamma}}{2}. \tag{3.2.6}$$

By integrating both side of this inequality, we obtain

$$W(x(t)) \leq W(x(0)) - \gamma t, \text{ or } |x(t)| \leq x_0 - \gamma t \tag{3.2.7}$$

where γ is equal to $\sqrt{2}\underline{\gamma}/2$ which is non-negative. Inequality (3.2.7) indicates that $x(t)$ reaches zero at a finite time, which cannot be realized with numerical simulation using discrete time computation that is to say chattering occurs around zero. For a certain function $f(x)$, the amplitude of chattering depends on sampling time and the type of numerical integration methods, for example, Euler method, Rung-Kutta method etc... In most cases, Euler method seems to exhibit chattering with largest amplitude for the same sampling time. Thus, we try to show how to define the amplitude of chattering for Euler method. Equation (3.2.1) can be approximated as

$$x_{k+1} = x_k - f(x_k)\text{sign}(x_k)\delta, \tag{3.2.8}$$

where δ is sampling time. In some cases, for example control system with symmetric model using integrator action, the behavior of chattering at steady-state can be defined by

$$x_{k+1} \approx -x_k. \tag{3.2.9}$$

Substituting (3.2.8) into (3.2.9) yields

$$x_k \approx \frac{1}{2} f(x_k)\text{sign}(x_k)\delta, \text{ or} \tag{3.2.10}$$

$$A_m = |x_k| \approx \frac{1}{2} f(x_k)\delta, \tag{3.2.11}$$

where A_m is called the amplitude of chattering. The equation (3.2.11) can be solved analytically or numerically if the sampling time δ is selected, or instead of solving this equation, we can select the amplitude of the chattering upon a desired accuracy of the system (3.2.1). The sampling time δ can be, thus, determined afterward. For example, if the condition following,

$$A_m = |x(t)| < \epsilon, \tag{3.2.12}$$

is necessary, then by substituting the equation (3.2.11) into the inequality (3.2.12), we obtain

$$\frac{1}{2} f(x)\delta \leq \epsilon. \tag{3.2.13}$$

This inequality is satisfied if any value of δ satisfies the inequality following

$$\frac{1}{2}\overline{\gamma}\delta \leq \epsilon \tag{3.2.14}$$

since $\underline{\gamma} \leq f(x) \leq \overline{\gamma}$. Hence,

$$\delta \leq \frac{2\epsilon}{\overline{\gamma}}. \tag{3.2.15}$$

This inequality is crucially used to determine the value of sampling time to simulate the system (3.2.1) with accuracy, ϵ, around its switching-like equilibrium if the upper-bound value $\overline{\gamma}$ of the function $f(x)$ is known.

3.2.2 Application to a torque-controlled DC motor model

At steady state if we assume that the input torque, u, of the system (3.1.3) is zero, then the system becomes

$$\dot{\omega} = -\frac{1}{J}(\alpha_0 + \alpha_1 e^{-(\omega/\omega_s)^2} + \alpha_2|\omega|)\text{sign}(\omega) \tag{3.2.16}$$

which is stable at the equilibrium $\omega_e = 0$. Thus the system (3.2.16) is identical to (3.2.1), where

$$f(\omega) = \frac{1}{J}(\alpha_0 + \alpha_1 e^{-(\omega/\omega_s)^2} + \alpha_2|\omega|) > 0 \tag{3.2.17}$$

$\forall\omega \in \mathbb{R}$ since α_0, α_1 and α_2 are positive coefficients, and it satisfies the condition, $\underline{\gamma} \leq f(\omega) \leq \overline{\gamma}$ for $|\omega| < \epsilon$. Since the behaviour of Stribeck effect represented by $e^{-(\omega/\omega_s)^2}$ shown in Fig. 3.2 is highly nonlinear around equilibrium, the simulation accuracy ϵ should be in the interval of this effect. If it is too large, a simulation as well as estimation cannot capture this effect. One particular value of ϵ is the abscise of the inflection point of the function, i.e. $\epsilon = \frac{\omega_s}{\sqrt{2}}$. From the figure, the function $f(\omega)$ defined in (3.2.17) is bounded as shown below

$$f(\omega) \leq \frac{1}{J}(\alpha_0 + \alpha_1) = \overline{\gamma} \tag{3.2.18}$$

for $|\omega| \leq \epsilon$. By substituting the value of $\epsilon = \frac{\omega_s}{\sqrt{2}}$ and $\overline{\gamma}$ defined in (3.2.18), we obtain

$$\delta \leq \frac{\sqrt{2}\omega_s J}{\alpha_0 + \alpha_1}. \tag{3.2.19}$$

This inequality implies that a larger of sampling time can be selected if moment of inertia is larger.

3.2.3 Observability

To check the observability of the system (3.1.4) and (3.1.6), we consider its general discrete time model (e.g. using Euler-Maruyama method) of the joint state and parameter as following,

$$\begin{aligned} x_{k+1} &= f_d(x_k, u_k) + v_k \\ y_k &= h_d(x_k) + w_k. \end{aligned} \tag{3.2.20}$$

The nonlinear observability matrix is defined as

$$U(x_k) = \begin{bmatrix} \frac{\partial h_d}{\partial x}(x_k) \\ \frac{\partial h_d}{\partial x}(x_{k+1})\frac{\partial f_d}{\partial x}(x_k) \\ \vdots \\ \frac{\partial h_d}{\partial x}(x_{k+n_x-1})\frac{\partial f_d}{\partial x}(x_{k+n_x-2})\cdots\frac{\partial f_d}{\partial x}(x_k) \end{bmatrix} \tag{3.2.21}$$

where n_x is the number of process equations. The most significant behavior of the system occurs when the Stribeck zones influence the system. Thus, we consider the observability of the dynamical systems (3.1.4), (3.1.5) and (3.1.6) at an x_k where the angular velocity is equal to ϵ. By numerically computing the system (3.2.20), we find that the observability matrix (3.2.21) has full rank.

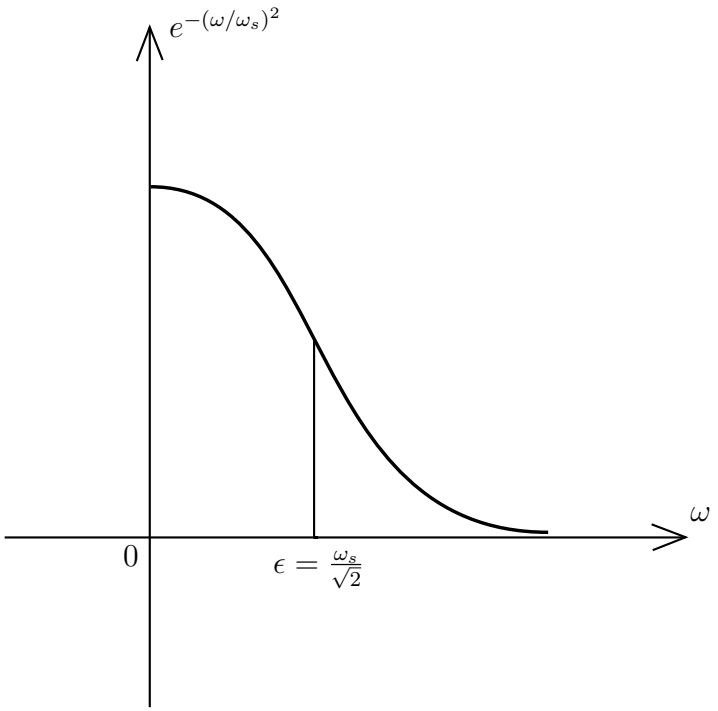

Figure 3.2: Exponential term of Stribeck curve

3.3 Simulation and discussions

Adaptive friction compensation + load compensation with PID controller is considered. Thus, the feedback control input is defined by

$$u = J\ddot{\theta}_r + e(K_p + \frac{K_i}{s} + K_d s) + \hat{F}_f, \tag{3.3.1}$$

where $e = \theta_r - \theta$ is the position error; θ_r is the desired position, which is assumed to be twice differentiable; $\hat{F}_f$ is friction estimated from the system (3.1.4); and K_p, K_i and K_d are PID parameters. The block diagram of the control system is shown in Fig. 3.3. For regulation control, failure of compensation at velocity around zeros occurs when the sign of the estimate velocity is opposite to that of the true one. This causes limit cycle to exist. In our control technique we use the desired angular velocity to switch off the compensation when its absolute value is less than a threshold ϵ, which is defined as the amplitude of the chattering expected to be exhibited by the estimator. Also in this zone, we temporarily stop the estimator to avoid the divergent of the estimation. In addition, because the estimate velocity is memorized during this zone, we calculate the estimate friction using the measured velocity whose sign may change, and, hence, make proper compensation in some instants. In practice, if velocity is measured by an encoder, its sign may not change, so we can use the dither-like technique for the compensation of friction in function of the modified velocity following,

$$\hat{\omega}_m(t) = \hat{\omega}(t) + \epsilon \ \text{sign}(r(t)) \tag{3.3.2}$$

where $\hat{\omega}(t)$ is estimate velocity, and $r(t)$ is a random signal which may change its sign, for example a white noise.

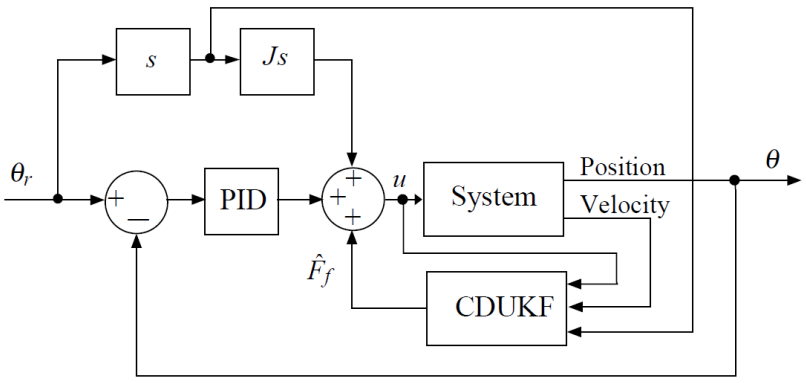

Figure 3.3: Block diagram of adaptive control

Some initial parameters are selected as follows: the spectral density of process noise, $Q_c = 10^{-7} \times \text{diag}([1\ 0\ 0])$, the variance of measurement noise, $R = 10^{-7}$, the initial covariance, $P_0 = 10^{-9} \times \text{diag}([1\ 1\ 1])$. The initial estimation of states is set to be a zero vector. It has been known that the numerical calculation of integration method at velocity around zero of system with friction induces large error of velocity, [1]. The error depends on the solver used. For example, ode1 (Euler), which is adopted to simulate our true system produces large error in comparison with other solvers. The error of this method is the chattering which was described in Section 3.2.1. For the estimation algorithm, ode4 (Runge-Kutta) is used to compute the differential equations of mean and covariance. This solver also produces some error at velocity around zero. Thus, the sampling time for the simulation of both the true plant and the estimator should be small enough. The sampling time for estimator is defined by inequality (3.2.19), i.e. $\delta \leq \frac{\sqrt{2}\omega_s J}{\alpha_0 + \alpha_1}$, where $\alpha_0 + \alpha_1$ is unknown stiction friction. However, it is not difficult to identify this parameter experimentally at zero velocity. In our simulation we also consider a sudden change of α_0 and α_1 by 2 times. We thus select the value of stiction friction twice as large as that used in [43]. We finally obtain the value of sampling time, $\delta \leq 4.6 \times 10^{-5}$. Then we use 4×10^{-5} seconds for sampling time of estimator, 2×10^{-5} seconds for sampling time of simulated plant, and 8×10^{-5} seconds for time interval of measurement update. To ensure numerical stability and have fast convergent of estimation, an extra additive matrix ΔQ_c, which is discussed in [32], is needed, and its value used for our simulation is, $\Delta Q_c = 10^{-6} \times \text{diag}([10\ 1\ 0.7])$. For system without friction compensation, good performance of position control can be obtained if high gain and derivative action of the controller are assigned. However, the drawback of high gain controller is that in practice, the system with compliant drive train may be lead to instability, and the actuator may reach the saturated point. In our simulation, the parameters of PID controller are the same as those used in [43]. For position regulation, the performances of systems with and without friction compensation are almost the same (Fig. 3.4 and Fig. 3.5). It is similar to the experimental result in [43]. Fig. 3.6 is the desired signal of tracking. Fig. 3.7 indicates the computational behavior of velocity around zero. It does not look like a symmetric chattering because we include noise in the simulation, and the control input $u(t)$ is not exactly zero. The simulated true system itself shows non-physical behavior, and so does the estimation. So, of course, estimation is not accurate. However, for the velocity far from zero the estimation is very accurate, as clearly seen at the both end of the graphs in the figure. Estimation of the

parameter α_0 is relatively accurate, which is shown in Fig. 3.8. Whereas, the estimation of the parameter α_1 is not accurate after 50 seconds. It is because friction around zero velocity (regardless the viscous term) increases twice. Then the expected velocity chattering interval of the computation for estimation covers the Stribeck zone almost entirely, whereby the parameter can only be detected. One important notice is that although the estimation of α_1 is not accurate, the both estimate parameters compensate each other to yield a relatively accurate friction estimation as shown in Fig. 3.10. Therefore, the performance of system with friction compensation is much improved, which is illustrated by Fig. 3.11. This result is comparable to that done by [43].

3.4 Summery

In adaptive friction compensation for a position-controlled system, we presents a new adaptive technique using CDUKF to estimate Stribeck + viscous friction. A model of a DC motor is considered. Its dynamic equations are modeled as stochastic differential equations in that the coefficients of Stribeck curve are considered as state variables as they are assumed to be varied in time due to the changes of normal load and/or temperature. The performance of the control system with PID controller is investigated. The simulation shows that the control system with friction compensation outperforms the system without friction compensation. For real-time application, an experiment is necessary. From the expression, $\delta \leq \sqrt{2}\omega_s J/(\alpha_0+\alpha_1)$, it is recommended that a larger moment of inertia be attached to motor in order to select a larger sampling time for estimation algorithm, and accurate estimation still can be expected.

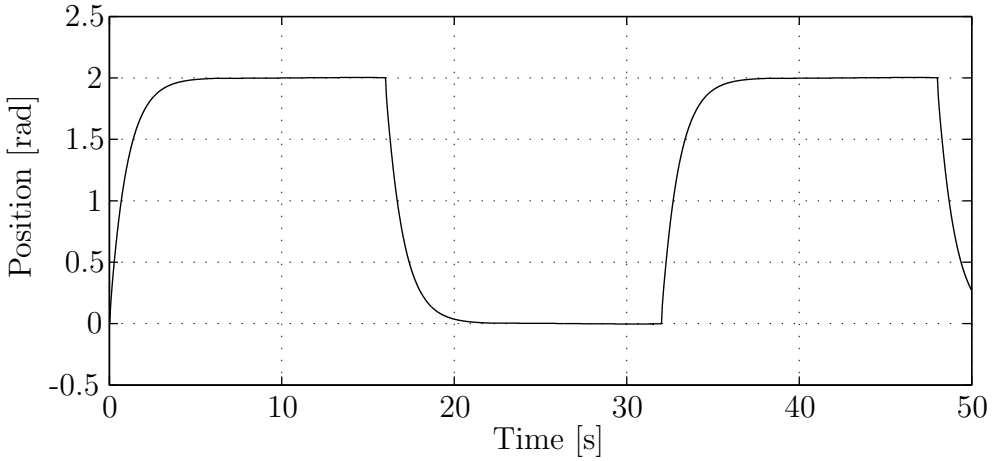

Figure 3.4: Regulation reference

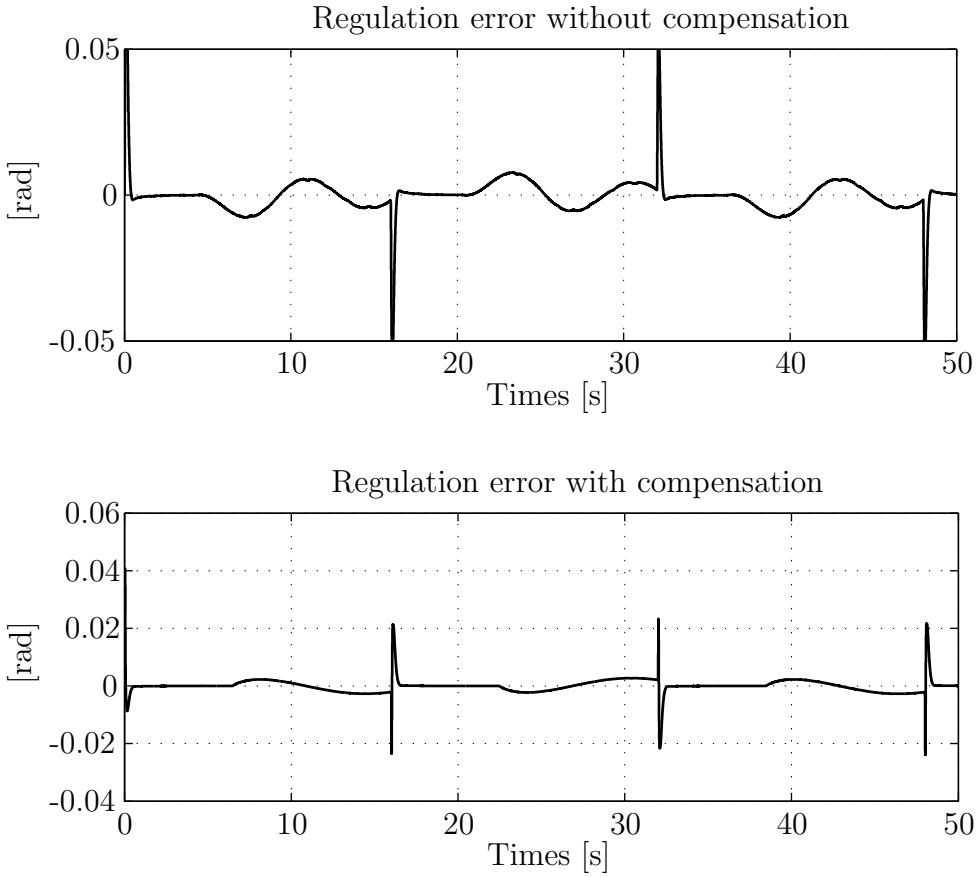

Figure 3.5: Regulation performance

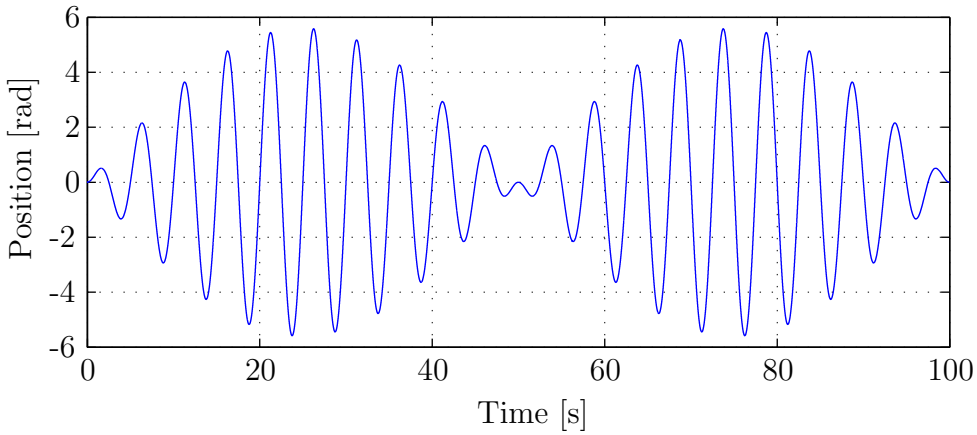

Figure 3.6: Tracking reference

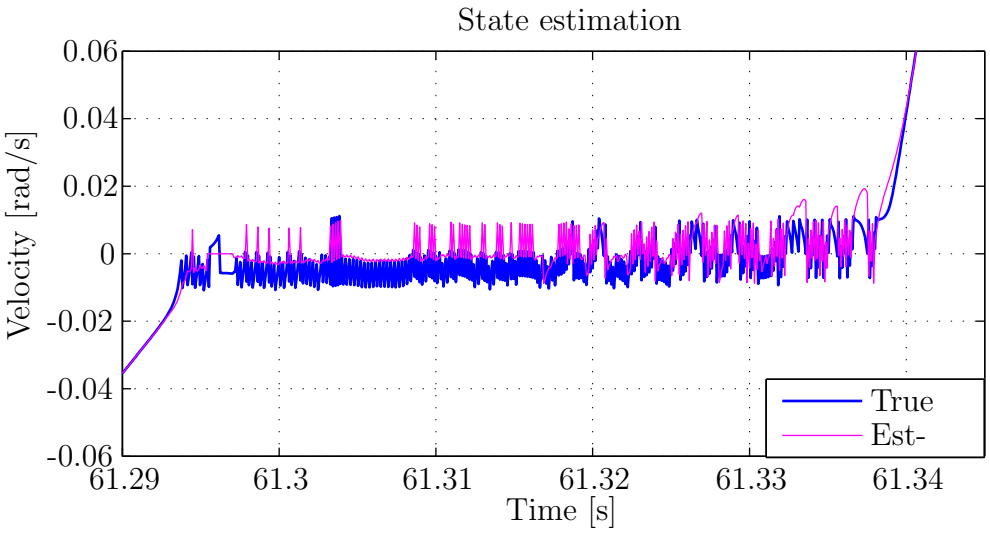

Figure 3.7: State estimation at zero velocity

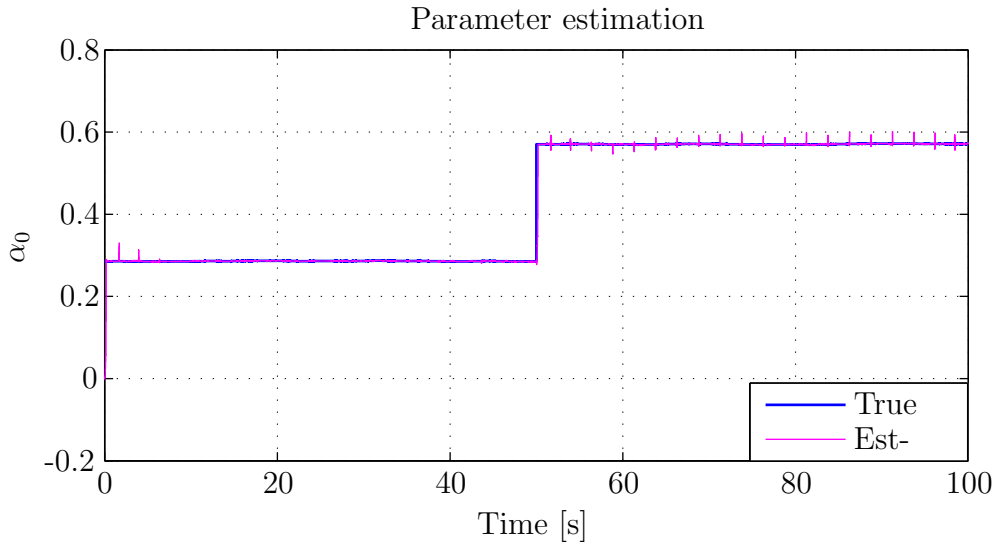

Figure 3.8: Parameter estimation, α_1

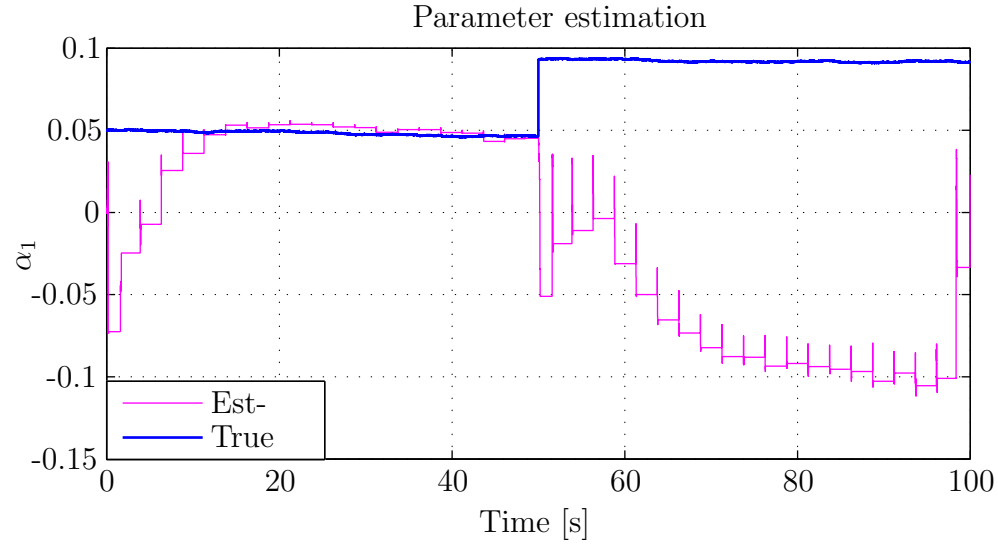

Figure 3.9: Parameter estimation, α_2

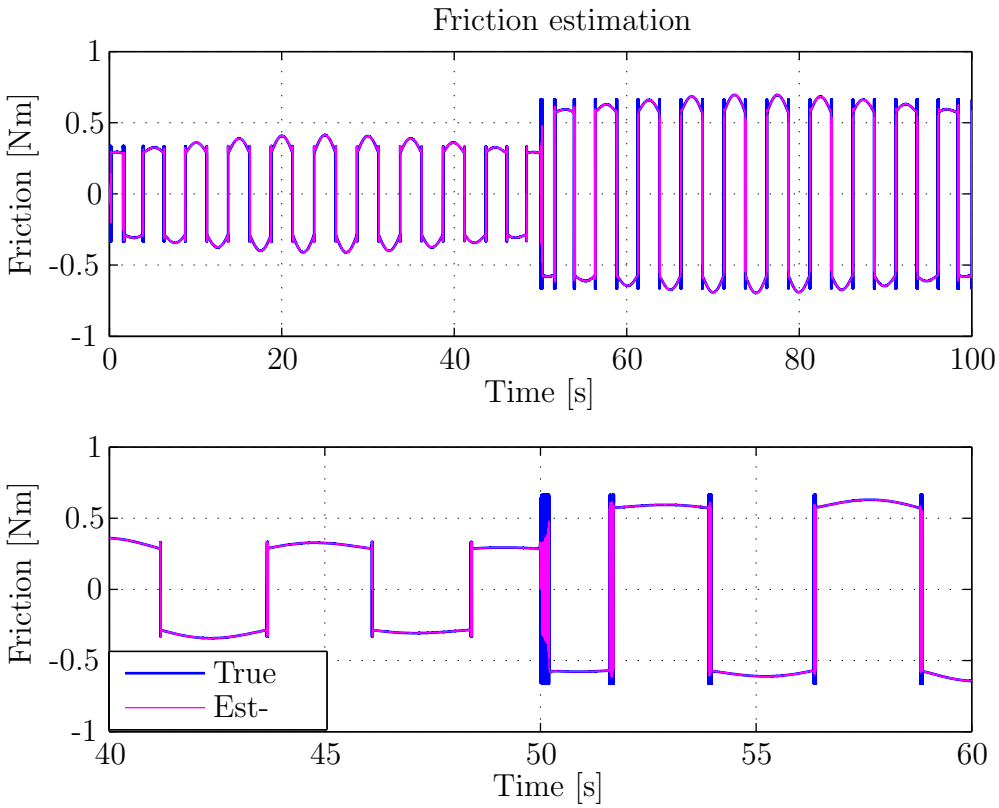

Figure 3.10: Friction estimation

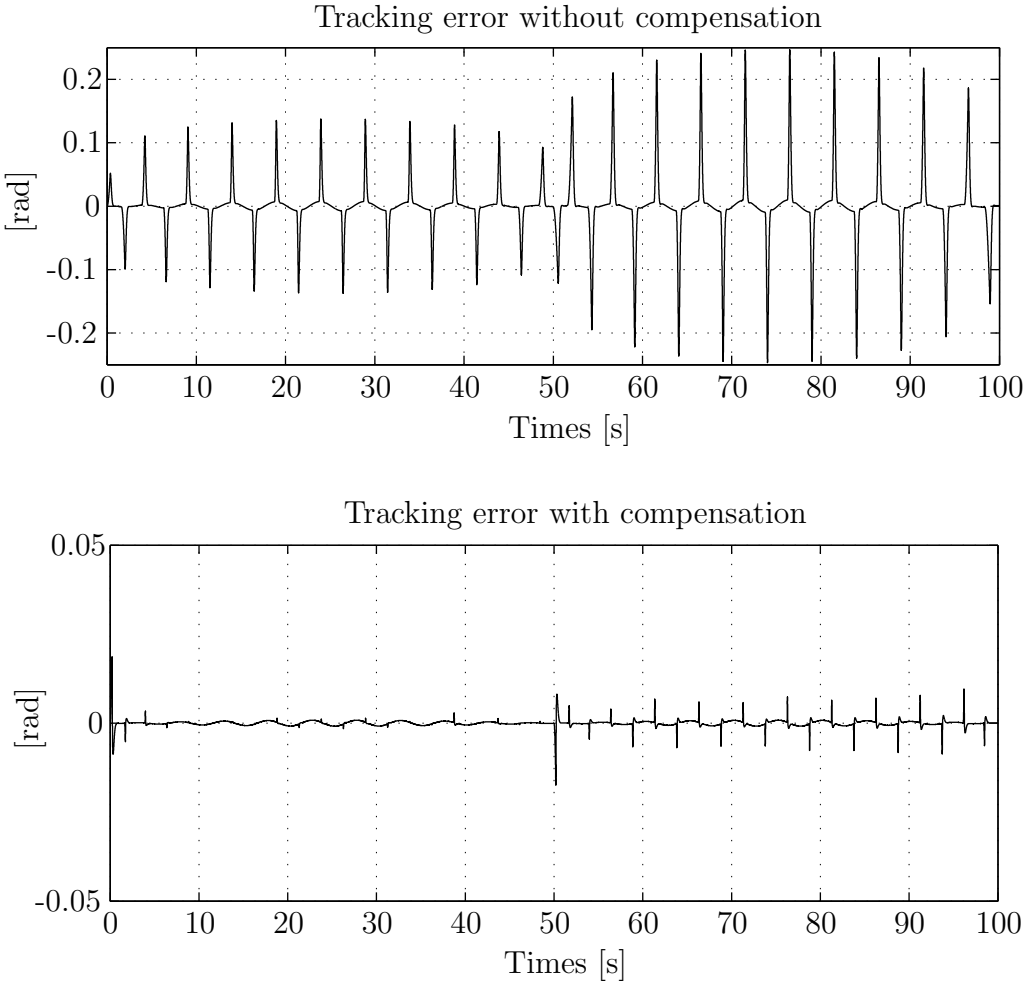

Figure 3.11: Tracking performance

Chapter 4

Filippov's Convex Method for the Improvement of the Adaptive Control

In this Chapter, we consider joint state and parameter estimation for a system with Stribeck friction, where coefficients of Stribeck curve and viscous coefficient are considered as state variables together with velocity. As friction model is discontinuous, for its estimation we use continuous-discrete unscented Kalman filter for which the propagation of prediction and correction can be done via unscented transform. The estimate friction is then used for compensation in position control system with PID controller and load compensation. On the estimation we discuss the observability of the joint state and parameter model. We find that the model is unobservable at zero velocity by using Filippov's convex method. To avoid divergence of parameter estimation we propose temporary stop of parameter update at velocity around zero, which is defined by a threshold. At the same time, we use Filippov approach joined with attraction to manifold to avoid chattering and have velocity approach to zero. The judgement of performance for our proposed method is made from simulation results.

4.1 Introduction

In the previous Chapter, we only estimated two parameters of the friction model, α_1 and α_2, while the coefficient of viscous friction is assumed constant and identified independently in advance. We will extend the scope by taking the variation of viscous coefficient into account. This is because in reality, viscous coefficient may change due to variation of temperature which is the main factor changing the viscosity of lubricant. Again we use continuous-discrete unscented Kalman filter to estimate stat and friction parameters.

Since accurate estimation must rely on computation itself during time update, we consider a reliable numerical tool to accurately compute the differential equations for time update of the CDUKF algorithm. There is a wide variety of numerical methods for solving ordinary differential equations (ODEs) and many of them are routinely used in established software, e.g. MATLAB ([52] and reference therein). However, most of these algorithms require that the ODEs are sufficiently smooth, while the system being considered includes discontinuity. Such system requires special numerical treatment for computation which will be described in the coming sections.

4.2 Computation of Filippov Systems

A class of systems with discontinuous vector fields are called Filippov systems. What characterizes such a system is the division of the state space into disjoint subregions, such that in each such region the defining vector field is smooth. The boundaries between the different regions will be referred to as discontinuity surfaces. This section covers a brief theoretical background of Filippov's convex method and is mostly referred to [52].

4.2.1 Systems with Single Discontinuity Surface

A general dynamical system is written by

$$\dot{x} = f(x,t) \tag{4.2.1}$$

where $x \in \mathbb{R}^{n_x}$. To begin with discontinuity, let us assume that the state space consists of only two regions, S_i and S_j, separated by a discontinuity surface Σ_{ij}, which is defined by a smooth scalar function $\sigma_{ij}(x)$ such that

$$\Sigma_{ij} = \{x \in \mathbb{R}^{n_x} \mid \sigma_{ij}(x) = 0\}, \tag{4.2.2}$$

and where

$$\begin{aligned} S_i &= \{x \in \mathbb{R}^{n_x} \mid \sigma_{ij}(x) > 0\} \\ S_j &= \{x \in \mathbb{R}^{n_x} \mid \sigma_{ij}(x) < 0\}. \end{aligned} \tag{4.2.3}$$

Therefore, the dynamical equation (4.2.1) can be rewritten as

$$\dot{x} = \begin{cases} F_i(x,t), & x \in S_i \\ F_j(x,t), & x \in S_j \end{cases} \tag{4.2.4}$$

where $F_i(x,t)$ and $F_j(x,t)$ are sufficiently smooth. Then, applying the Filippov's convex method to the equation (4.2.4) yields a differential inclusion as following [53],

$$\dot{x}(t) \in \begin{cases} \{F_i(x,t)\}, & x \in S_i \\ \overline{co}(F_i, F_j), & x \in \Sigma_{ij} \\ \{F_j(x,t)\}, & x \in S_j, \end{cases} \tag{4.2.5}$$

where $\overline{co}(F_i, F_j)$ is the minimal closed convex set containing F_i and F_j, i.e. $\overline{co}(F_i, F_j) = \{f \in \mathbb{R}^{n_x} : f = \lambda(x)F_i + (1-\lambda(x))F_j, \lambda(x) \in [0,1]\}$.

A sliding surface refers to a discontinuity surface on which the state is theoretically sliding. Numerically, the state orbit, however, incurs chattering which bounces around the surface. For computation approach to avoid chattering, (4.2.5) is written as follow [52],

$$\dot{x}(t) = \begin{cases} F_i(x,t), & x \in \hat{S}_i, \\ \hat{F}_{ij}(x,t), & x \in \hat{\Sigma}_{ij}, \\ F_j(x,t), & x \in \hat{S}_j, \end{cases} \tag{4.2.6}$$

where the sliding surface, $\hat{\Sigma}_{ij}$ is a set including Σ_{ij} and its neighborhood, i.e. $\hat{\Sigma}_{ij} = \{x \in \mathbb{R}^{n_x} \mid |\sigma_{ij}(x)| < \epsilon\}$, $\hat{S}_i = \{x \in \mathbb{R}^{n_x} \mid \sigma_{ij}(x) > \epsilon\}$, $\hat{S}_j = \{x \in \mathbb{R}^{n_x} \mid \sigma_{ij}(x) < -\epsilon\}$, where ϵ is a threshold for interval of a discontinuity surface. Then, the sliding vector field is given by

$$\hat{F}_{ij}(x,t) = \frac{F_i(x,t) + F_j(x,t)}{2} + \frac{F_j(x,t) - F_i(x,t)}{2}\mu_{ij}(x) - C\sigma_{ij}(x)\left(\partial\sigma_{ij}/\partial x\right)^T \tag{4.2.7}$$

where

$$\mu_{ij}(x) = 1 - 2\lambda(x) = -\frac{(\partial\sigma_{ij}/\partial x)(F_i + F_j)}{(\partial\sigma_{ij}/\partial x)(F_j - F_i)}, \tag{4.2.8}$$

and C, constant of attraction, is positive. The last term of the right-hand-side of (4.2.7) is added in purpose of regional attraction [52], and the remaining term is called Utkin's equivalent control [15]. The solution of (4.2.6) is absolutely continuous.

4.2.2 Systems with a Number of Discontinuity Surfaces

In the previous section, we have only considered a single discontinuity surface. However, we can nevertheless extend the method to an arbitrary number of surfaces. The only thing one has to do is to assure uniqueness of orbits constrained to the discontinuity surfaces. This is done by only considering a special class of Filippov systems where the vector fields in the different regions of stat space are dependent. To compute orbits along the various discontinuity surfaces we will here use Filippov's convex method instead of Utkin's equivalence method to show how that approach can be implemented and is more straightforward.

Assume that in system (4.2.1), there are N discontinuity surfaces Σ_i described by N scalar smooth functions $\sigma_i(x)$. Then the vector field of (4.2.1) can be written as [52],

$$f(x,t) = f_{\text{orig}}(x,t) + \sum_{i=1}^{N} \Delta_i^f(x,t)\mu_i(x) \tag{4.2.9}$$

where

$$\mu_i(x) = \begin{cases} 1, & \sigma_i(x) > 0, \\ [0,1], & \sigma_i(x) = 0, \\ 0, & \sigma_i(x) < 0. \end{cases} \tag{4.2.10}$$

The introduced base vector field $f_{\text{orig}}(x,t)$ is defined from the vector field when $\sigma_i(x) < 0$ for all i, and the individually additional term $\Delta_i^f(x,t)$ can, then, be defined using the condition $\sigma_i(x) > 0$ in (4.2.10).

To define $\mu_i(x)$ when the system (4.2.1) is sliding, we must consider that the system state may orbit along two or more sliding surfaces simultaneously. Let S be a set of index of sliding surface along which the system state orbits and N_S be total element number of S. Then the condition $\frac{\partial\sigma_i(x)}{\partial x} f(x,t) = 0$ for $i \in S$ must hold. By using (4.2.9), this condition can be elaborated as

$$\frac{\partial\sigma_i(x)}{\partial x} f_{\text{orig}}(x,t) + \frac{\partial\sigma_i(x)}{\partial x} \sum_{k=1}^{N} \Delta_k^f(x,t)\mu_k(x) = 0. \tag{4.2.11}$$

Denote

$$\begin{aligned} \{\alpha_1, \ldots, \alpha_{N_S}\} &= \{\mu_i(x)\} \\ \{\beta_1, \ldots, \beta_{N_S}\} &= \{\sigma_i(x)\} \\ \{\gamma_1, \ldots, \gamma_{N_S}\} &= \{\Delta_i^f(x,t)\} \end{aligned} \tag{4.2.12}$$

for $i \in S$. From (4.2.11) and (4.2.12), we obtain

$$\begin{bmatrix} \alpha_1 \\ \vdots \\ \alpha_{N_S} \end{bmatrix} = \begin{bmatrix} \frac{\partial\beta_1}{\partial x}\gamma_1 & \cdots & \frac{\partial\beta_1}{\partial x}\gamma_{N_S} \\ \vdots & \cdots & \vdots \\ \frac{\partial\beta_{N_S}}{\partial x}\gamma_1 & \cdots & \frac{\partial\beta_{N_S}}{\partial x}\gamma_{N_S} \end{bmatrix}^{-1} \begin{bmatrix} \frac{\partial\beta_1}{\partial x}\widetilde{f}(x,t) \\ \vdots \\ \frac{\partial\beta_{N_S}}{\partial x}\widetilde{f}(x,t) \end{bmatrix}, \tag{4.2.13}$$

where

$$\widetilde{f}(x,t) = f_{\text{orig}}(x,t) + \sum_{k\in\{\{1,\ldots,N\}\setminus S\}} \Delta_k^f(x,t)\frac{\text{sign}(\sigma_k(x))+1}{2}.$$

It is considered that $\mu_i(x)$ defined by (4.2.12) and (4.2.13) may satisfy $\mu_i(x) \notin [0,1]$ which means that the system state is not constrained to the i^{th} discontinuity surface. Denote a set $S' = \{i \in S \mid \ \mu_i(x) \notin [0,1]\}$. Thus, (4.2.9) can be rewritten as

$$\begin{aligned} f(x,t) = f_{\text{orig}}(x,t) & \\ &+ \sum_{i\in\{\{1,\ldots,N\}\setminus S\}} \Delta_i^f(x,t)\frac{\text{sign}(\sigma_i(x))+1}{2} \\ &+ \sum_{i\in\{S\setminus S'\}} \Delta_i^f(x,t)\mu_i(x) \\ &+ \sum_{i\in S'} \Delta_i^f(x,t)\frac{\text{sign}(\mu_i(x))+1}{2}. \end{aligned} \tag{4.2.14}$$

We consider a class of discontinuous dynamical systems which have a property of semistability, or finite-time semistability [54]. For computation, chattering always occurs around sliding surface since the system state never reaches any sliding surface in finite time. In order to improve computational accuracy, we define an interval for sliding surface as $|\sigma_i(x)| < \epsilon_i$, where ϵ_i is a threshold which will be defined for n_x-dimensional systems in the next chapter; and term of attraction to the sliding surface is added to the average vector field defined in (4.2.14). Therefore, approximation of average vector field can be written as

$$\begin{aligned} f(x,t) = f_{\text{orig}}(x,t)\theta(t) & \\ &+ \sum_{i\in\{\{1,\ldots,N\}\setminus S\}} \Delta_i^f(x,t)\frac{\text{sign}(\sigma_i(x))+1}{2} \\ &+ \sum_{i\in\{S\setminus S'\}} \Delta_i^f(x,t)\mu_i(x) \\ &+ \sum_{i\in S'} \Delta_i^f(x,t)\frac{\text{sign}(\mu_i(x))+1}{2} \\ &- \sum_{i\in\{S\setminus S'\}} C_i\sigma_i(x)\left(\frac{\partial\sigma_i(x)}{\partial x}\right)^T, \end{aligned} \tag{4.2.15}$$

where C_i is positive if the condition $|\sigma_i(x)| < \epsilon_i$ is satisfied; and it is zero otherwise.

4.3 Joint State and Parameter model for a DC Motor

4.3.1 Model

The stochastic differential equations where velocity and friction coefficients, α_0, α_1 and α_2, are considered as state variables, $x = [x_1, x_2, x_3, x_4]^T = [\omega, \alpha_0, \alpha_1, \alpha_2]^T$ can be written as

follows,

$$\begin{aligned}\dot{x}_1(t) &= (u(t) - F_f)/J + v_{c1}(t)\\ \dot{x}_2(t) &= v_{c2}(t)\\ \dot{x}_3(t) &= v_{c3}(t)\\ \dot{x}_4(t) &= v_{c4}(t)\end{aligned} \tag{4.3.1}$$

where $v_{c1}(t)$, $v_{c2}(t)$,v_{c3} and $v_{c4}(t)$ are white Gaussian process noises with diffusion matrix Q_c; and F_f is friction torque which is defined as following,

$$\begin{aligned}g_v &= x_2 + x_3 e^{-(x_1/\omega_s)^2},\\ F_f &= (g_v + x_4|x_1|)\text{sign}(x_1)\end{aligned} \tag{4.3.2}$$

and illustrated by Fig. 4.1.

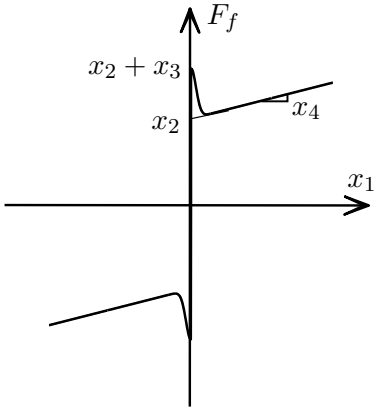

Figure 4.1: Unknown-parameter friction model

We assume that we can measure velocity, and then the measurement model is as follow,

$$z_k = Hx_k + w_k, \tag{4.3.3}$$

where w_k is zero-mean Gaussian measurement noise with known variance, and $H = [1, 0, 0, 0]$. All the parameters used for computing the actual plant (4.3.1), (4.3.2) and (4.3.3) are selected from [43].

4.3.2 Observability

The same as the observability analysis in the previous chapter, the observability matrix can be defined by the equation (3.2.21) for the general discrete time equation (3.2.20). It is found observable at non-zero velocity, but if we consider the observability of the system when it orbits along the sliding surface i.e. zero velocity, by using (4.2.7) and (4.2.10) for the system (4.3.1) and (4.3.2), then (4.3.1) becomes

$$\begin{bmatrix}\dot{x}_1\\ \dot{x}_2\\ \dot{x}_3\\ \dot{x}_4\end{bmatrix} = \begin{bmatrix}0\\ 0\\ 0\\ 0\end{bmatrix} - \begin{bmatrix}C_1 x_1\\ 0\\ 0\\ 0\end{bmatrix} \tag{4.3.4}$$

if

$$|u| \leq x_2 + x_3 = \alpha_0 + \alpha_1,$$

and the measurement model remains the same as (4.3.3). It can be clearly seen that the system of (4.3.4) and (4.3.3) is not observable, and, hence, its estimation diverges. One possible solution that we use to avoid divergence is to temporarily stop updating the three parameters, $x_2,\ x_3$, and x_4, while the state velocity, x_1, is still updated.

4.4 Adaptive Friction Compensation

Adaptive friction compensation + load compensation with PID controller is considered. The block diagram of the control system is shown in Fig. 4.2. The feedback control input is defined as

$$u = J\ddot{\theta}_r + e(K_p + \frac{K_i}{s} + K_d s) + \hat{F}_f, \tag{4.4.1}$$

where $e = \theta_r - \theta$ is position error; θ_r is position reference, which is assumed to be twice differentiable; $\hat{F}_f$ is estimated friction from the system (4.3.1) using continuous-discrete unscented Kalman filter; and K_p, K_i and K_d are PID parameters. Without compensation, we tune these parameters to get the best result for regulation and tracking differently, but with compensation, we use the same parameters for both. We select these parameters from [43], but only $0.05K_i$ is used for integrator coefficient.

We test a system that the three parameter are assumed to suddenly increase twice due to increasing normal load and variation of temperature after 50 seconds of running time until the final time, 100 seconds. In our simulation, Euler-Maruyama and Runge-Kutta method (ode4) are used for plant and the estimation algorithm respectively. Some constants used for plant and estimation algorithm are shown in Table 5.1. Since we can never have realistic simulation at velocity around zero, we intentionally create model uncertainty by selecting different threshold ϵ and constant of attraction C for actual plant and estimator. To cope with model uncertainty, and to guarantee stability of estimation, large diffusion matrix Q_c is required, [32].

Table 4.1: Simulation parameters

Constant	Plant	Estimator
Q_c	10^{-7}diag([1 100 10 1])	10^{-6}diag([800 10 10 1])
R	10^{-7}	1.5×10^{-7}
x_0	$[0\ \alpha_0\ \alpha_1\ \alpha_2]^T$	$[0\ 0\ 0\ 0]^T$
P_0	–	$10^{-8}I$
ϵ	0.001	0.005
C	100	50

Simulation results of regulation and tracking control are depicted from Fig. 4.3 to Fig. 4.12.

- *Regulation:* In Fig. 4.3, we show position reference and error in the case of no compensation. With compensation, the lower graph of Fig. 4.4 indicates that the error is reduced, which is comparable to the work of [43], and the control torque, the upper

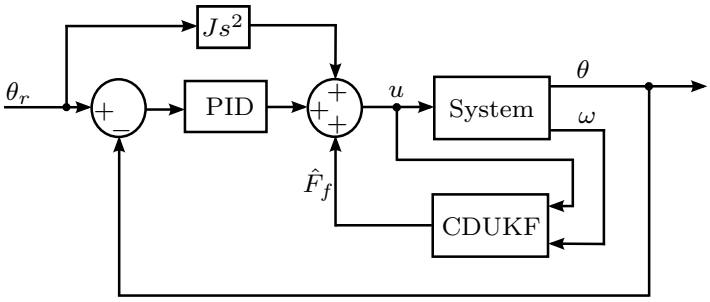

Figure 4.2: Block diagram of adaptive control without the use of desired velocity

graph, is actuated within suitable range. It is resulted from the robustness of velocity and parameter estimation as shown in Fig. 4.5, 4.6 and 4.7. α_0 and α_1 quickly converge to the actual value. Even though α_2, the upper graph of Fig. 4.7 seems to be sensitive at high velocity (during the change of desired value of regulation), it converges to its actual value when the system is regulating. Furthermore, viscous friction around zero velocity is small, so it does not significantly disturb the system performance.

As we select a very large element of Q_c corresponding to velocity, the estimate value oscillates about the actual one. At zero velocity of actual system, it results the estimate velocity in the Stribeck zone which yields estimate friction less than the actual one. Therefore, over compensation can be avoided.

- *Tracking:* Tracking reference is depicted in the upper graph of Fig. 4.8, and the lower graph is tracking error of system without compensation. It is clearly seen that velocity, all the parameters, and, thus, friction shown in Fig. 4.10, 4.11 and 4.12 can be estimated accurately. Hence, compensation method significantly reduces tracking error as seen in the lower graph of Fig. 4.9. In comparison with [51] (case: contact up), we use larger stiction friction ($\alpha_0 + \alpha_1$) and smaller moment of inertia, but our proposed method results smaller magnitude of tracking error regardless the error around the time of the abrupt change of friction parameters.

$Sampling\ time for\ true\ system$	5×10^{-5}
$Sampling\ time\ for\ estimation\ algorithm$	1×10^{-4}
$Sampling\ time\ for\ measurement$	2×10^{-4}
$Spectral\ density\ of\ process\ noise$	$10^{-7}I$
$Variance\ of\ measurement\ noise$	10^{-7}
$Initial\ covariance$	10^{-9}
$Initial\ estimation\ of\ states$	$[0, 0, 0]^T$

4.5 Summery

Estimation algorithm is very robust for various stochastic systems. However, its straightforward application for estimating friction of joint state and parameter model of a dynamical

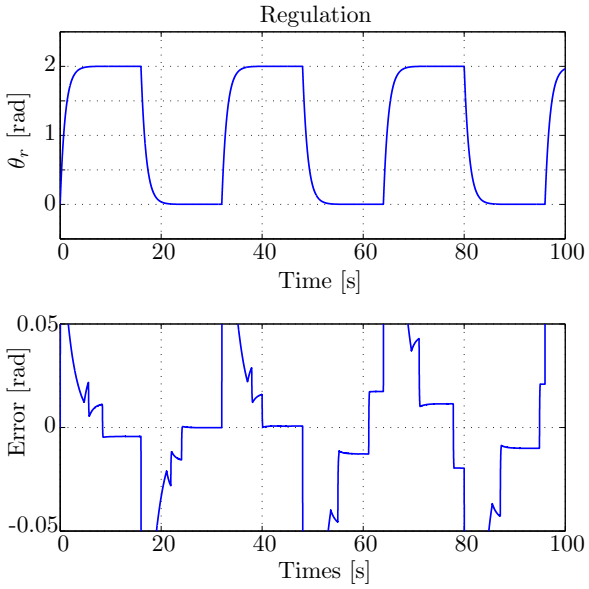

Figure 4.3: Regulation performance without friction compensation

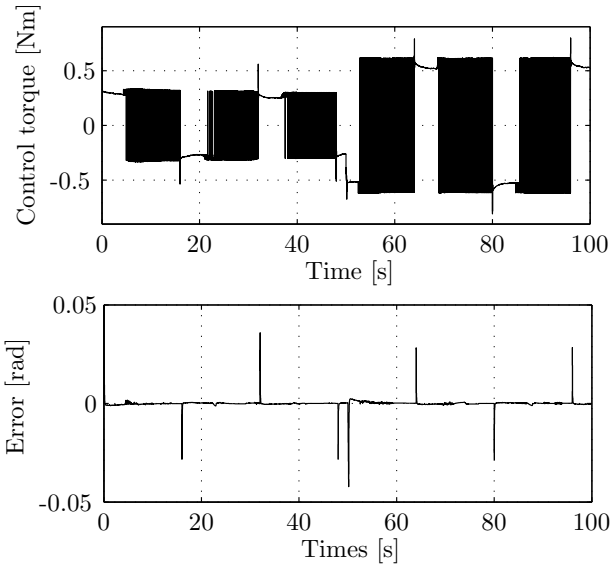

Figure 4.4: Regulation performance with friction compensation

system with Stribeck friction becomes unrealizable since the sliding vector field yields unobservable under the sense of Filippov method. Therefore estimation diverges. To avoid divergent of the estimation we temporary stop parameter update in both prediction and correction step. The simulation result shows good performance of both position regulation and tracking. Our proposed method can be also applied to estimate a model with multiple discontinuities. The extended works from ours is to estimate friction with hysteresis at Stribeck zones which is usually involved in hydraulic system and to implement to real-time system.

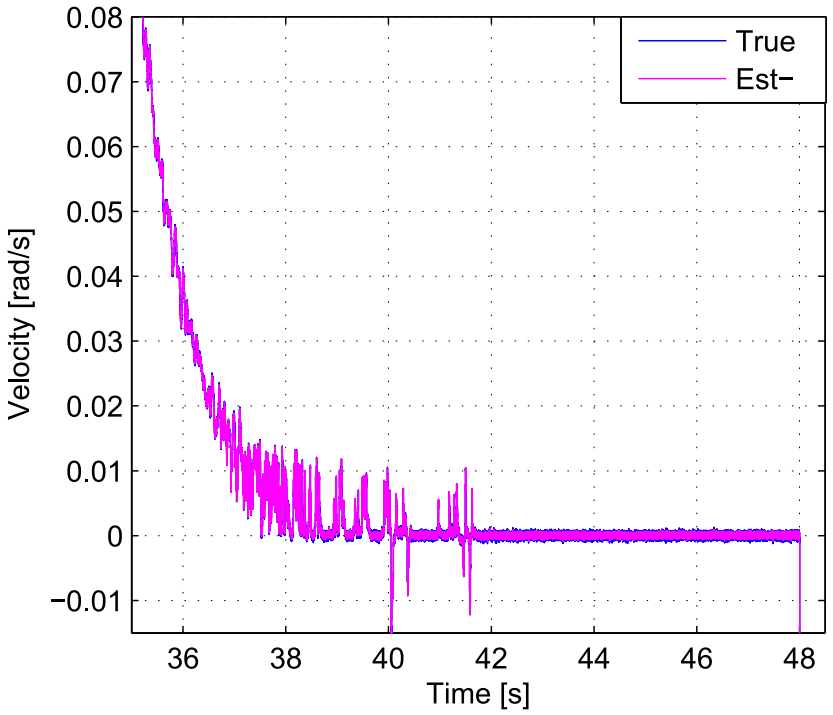

Figure 4.5: Velocity estimation around zero in regulation case

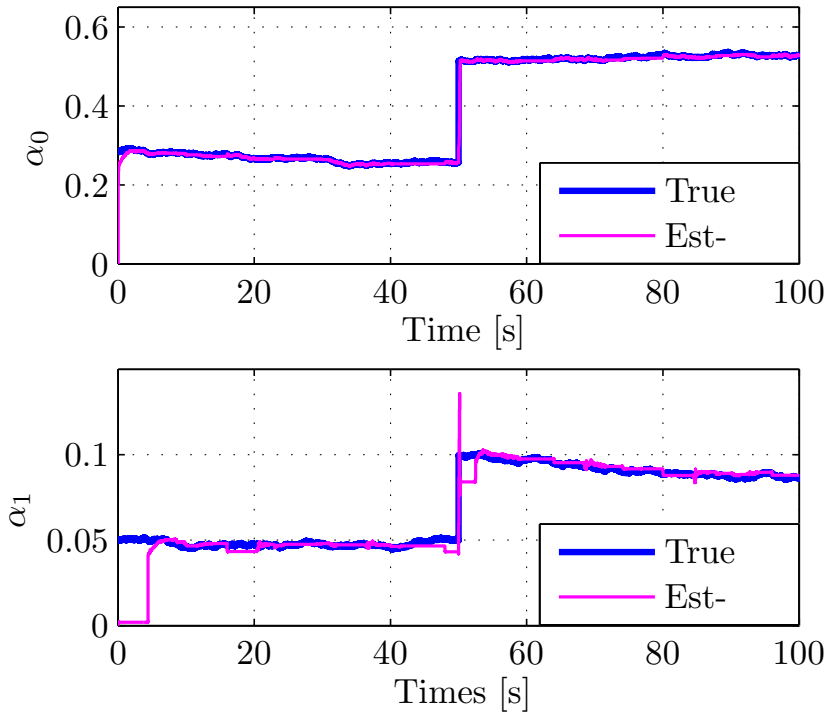

Figure 4.6: Parameter estimation, α_0 and α_1 in regulation case

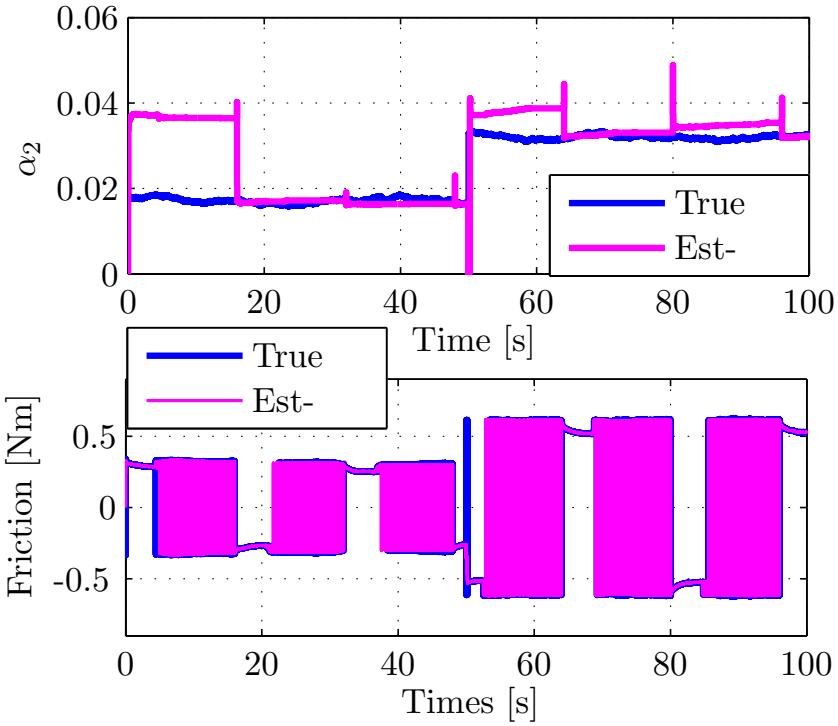

Figure 4.7: Parameter, α_2, and friction estimation in regulation case

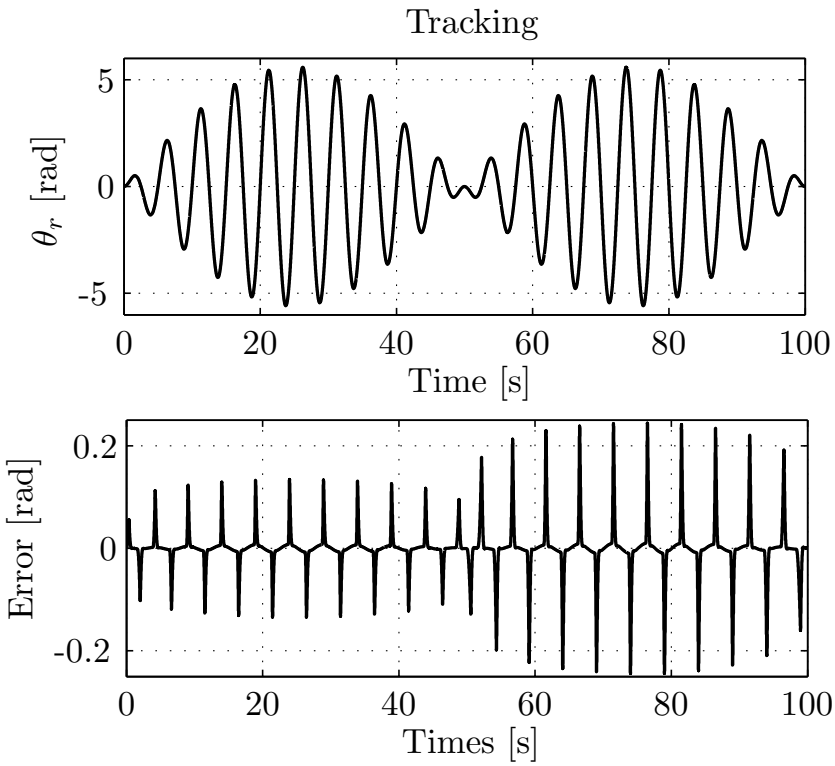

Figure 4.8: Tracking performance without friction compensation

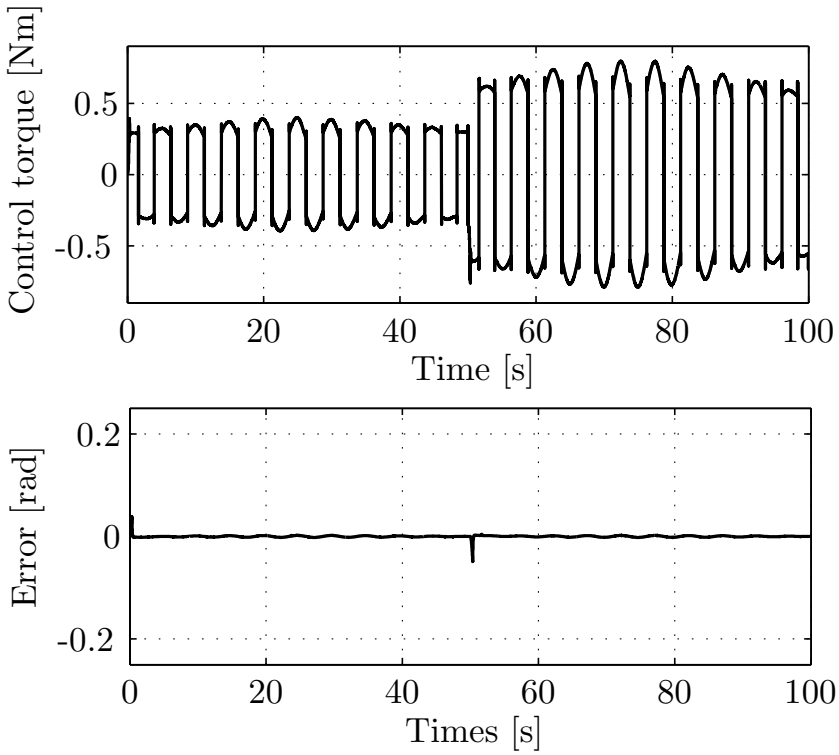

Figure 4.9: Tracking performance with friction compensation

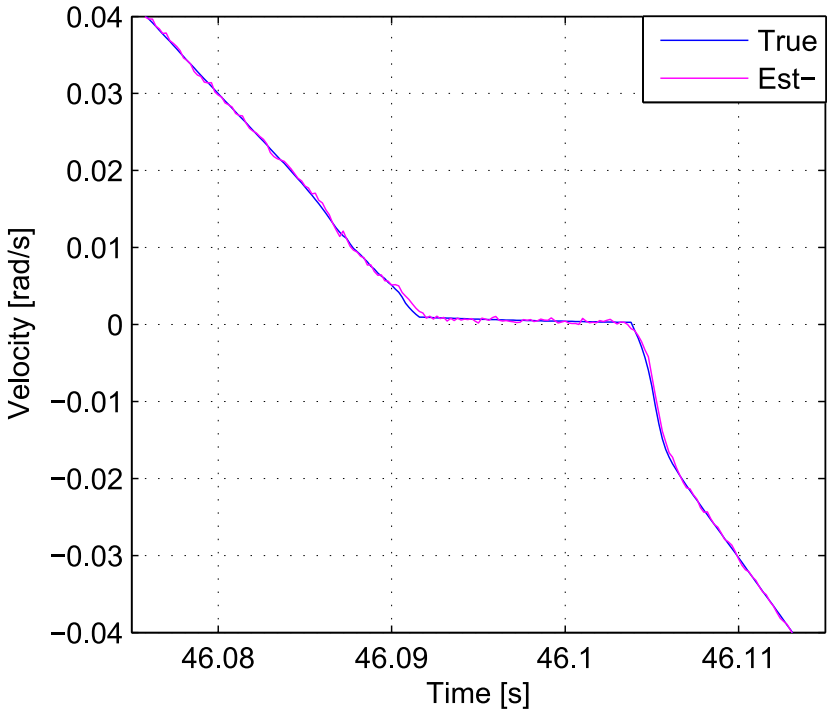

Figure 4.10: Velocity estimation around zero in tracking case

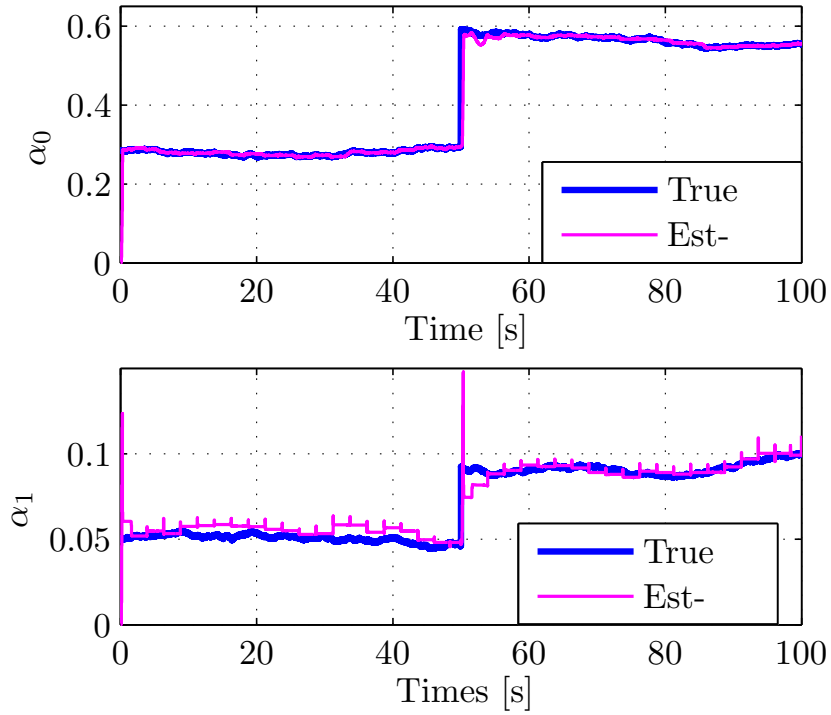

Figure 4.11: Parameter estimation, α_0 and α_1 in tracking case

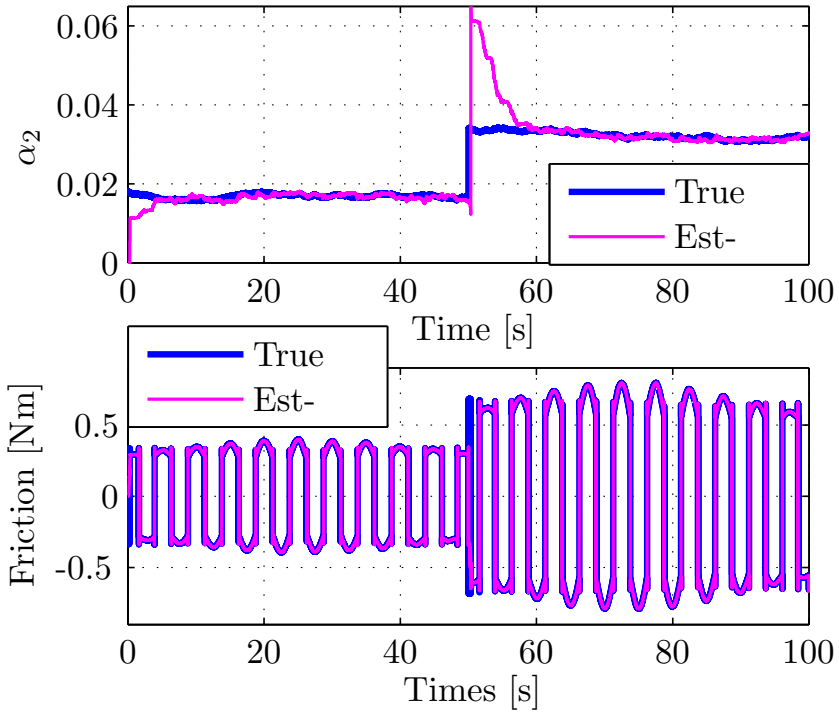

Figure 4.12: Parameter, α_2, and friction estimation in tracking case

Chapter 5

Estimation for n_x-Dimensional Systems with Multiple Discontinuities

5.1 Introduction

In this chapter, computational behavior on sliding surface(chattering for higher dimension) is investigated. In order to cover a broad range of systems, we propose to structure the model of state equation as multiplication of basis function, which is in term of state variable, and parameter that evolves in time. As we mainly focus on discontinuous systems, the basis functions considered must involve discontinuities. If the model of a system is unknown or difficult to obtain, the basis function is arbitrarily chosen, but must be within a limitation that stability of estimation is guaranteed. We still use continuous-discrete unscented Kalman filter to estimate the proposed model, but it is given in the form of less computational complexity. A particular feature is included to the algorithm i. e. when system state orbits along sliding surface, estimation is switched to computation of deterministic model as it is shown unobservable by using Filippov's convex method. Extension of the Filippov's convex method is also used in order to obtain accurate computation (avoiding chattering) along sliding surface. Simulation results of two numerical examples are provided to show the robustness of the algorithm.

5.2 Problem Set up

In most practical applications, stochastic systems are physically modeled in continuous-discrete form [34]

$$\begin{aligned} dx(t) &= f(x,t)dt + \sqrt{Q}_c d\beta(t) \\ z_k &= h_d(x_k, t_k) + w_k, \end{aligned} \tag{5.2.1}$$

where $x(t) \in \mathbb{R}^{n_x}$ and $z_k \in \mathbb{R}^{n_z}$ are state and measurement respectively; $f(x,t)$ is called drift function; $\beta(t)$ is standard Brownian motion; $Q_c \in \mathbb{R}^{n_x \times n_x}$ is called the diffusion matrix; h_d is measurement model function; w_k is zero-mean Gaussian measurement noise with covariance matrix R. In terms of white noise $v_c(t) = \sqrt{Q_c}\frac{d\beta(t)}{dt}$ with spectral density Q_c, the model (5.2.1) can be rewritten as

$$\begin{aligned} \dot{x}(t) &= f(x,t) + v_c(t) \\ z_k &= h_d(x_k, t_k) + w_k. \end{aligned} \tag{5.2.2}$$

The function $f(x,t)$ is assumed to be the optimal model for the system state, and the term $v_c(t)$ accounts for model uncertainty and process noise and is assumed to be bounded. The function $f(x,t)$ is restructured as

$$f(x,t) = \Phi^T_{\text{ideal}}(x,t)\theta_{\text{ideal}} \tag{5.2.3}$$

where $\Phi^T_{\text{ideal}}(x,t)$ is called basis function, and θ_{ideal} is constant parameter vector. Then, the filtering problem (5.2.2) can be equivalently written in the form of join state and parameter model

$$\begin{aligned} \begin{bmatrix} \dot{x}(t) \\ \dot{\theta}_{\text{ideal}}(t) \end{bmatrix} &= \begin{bmatrix} \Phi^T_{\text{ideal}}(x,t)\theta_{\text{ideal}} + v_c(t) \\ 0 \end{bmatrix} \\ z_k &= h_d(x_k, t_k) + w_k. \end{aligned} \tag{5.2.4}$$

In some practices, it is difficult to obtain accurate model of the drift function due to uncertainty of physical effect or/and empirical parameter (see the second application example in Section 5.5). In this work, we, therefore, investigate filtering problem where the drift function is reformulated as

$$\Phi^T_{\text{ideal}}(x,t)\theta_{\text{ideal}} = \Phi^T(x,t)\theta_{\text{ideal}} + \mathcal{E}(x,t,\theta_{\text{ideal}}), \tag{5.2.5}$$

where $\Phi(x,t)$ is approximate basis function, and $\mathcal{E}(x,t,\theta_{\text{ideal}})$ is model error which is latter considered as disturbance. To account for this disturbance, we consider a compensation by the following replacement,

$$\Phi^T(x,t)\theta_{\text{ideal}} \leftarrow \Phi^T(x,t)\theta(t), \tag{5.2.6}$$

where $\theta(t)$ evolves in time, which is governed by the following equation,

$$\dot{\theta}(t) = \nu(t), \tag{5.2.7}$$

where $\nu(t)$ is assumed to be white Gaussian noise. One may consider $\nu(t)$ a different type of noise and apply an appropriate estimation algorithm. In our work we specifically consider Kalman-type filtering.

From (5.2.4)-(5.2.7), we obtain

$$\begin{aligned} \begin{bmatrix} \dot{x}(t) \\ \dot{\theta}(t) \end{bmatrix} &= \begin{bmatrix} \Phi^T(x,t)\theta(t) \\ 0 \end{bmatrix} + \begin{bmatrix} \mathcal{E}(x,t,\theta_{\text{ideal}}) + v_c(t) \\ \nu(t) \end{bmatrix} \\ z_k &= h_d(x_k, t_k) + w_k, \end{aligned} \tag{5.2.8}$$

The filtering problem (5.2.2) becomes estimation problem of join state and parameter model (5.2.8). In the same manner, [55] considered spatial field estimation where the basis function is not in function of time. For autonomous system, the basis function in our problem formulation is similar to that in [55].

The filtering algorithm for continuous-discrete model derived by [31] is CDUKF. It is obtained from the combination of *time update* of UKBF with setting infinity spectral density matrix of measurement noise, and *measurement update* of discrete UKF. There are concrete evidences proving stability of UKF and UKBF [56, 32]. Under certain assumptions, estimation error of UKF and UKBF are bounded in mean square if the noise terms are bounded (*Theorem 1* of [56] and *Theorem 3.1* of [32]). We extend this fact for CDUKF since, in [31],

it is proved to outperform UKF by simulation result of reentry vehicle tracking problem. The boundedness of the noise term of (5.2.8) implies boundedness of $\mathcal{E}(x, t, \theta_{\text{ideal}})$, i.e.

$$\mathcal{E}(x, t, \theta_{\text{ideal}})\mathcal{E}^T(x, t, \theta_{\text{ideal}}) \leq \gamma I_{n_x} \tag{5.2.9}$$

for all $x \in \mathbb{R}^{n_x}$ and $t > 0$, where γ is positive. Therefore, (5.2.9) is necessary condition for limitation of the choice of bias basis function introduced in (5.2.5), which guarantees stability of estimation using CDUKF.

5.3 Computational accuracy improvement for Filippov Systems

In the previous section, we introduce the problem set up which is reformulated as joint state and parameter, where multiplication of a bias basis function and parameter is considered as simplification for state equation. In this section, we specifically investigate computational behavior of the system where the basis function involves discontinuities.

5.3.1 Chattering

Consider a state equation following,

$$\dot{x}(t) = f(x, t) \tag{5.3.1}$$

where $x \in \mathbb{R}^{n_x}$, and $f(x, t)$ is discontinuous vector field. Let Σ be a set of discontinuity surface described by a scalar smooth function $\sigma(x)$. Then the set is defined by $\Sigma = \{x \in \mathbb{R}^{n_x} \mid \sigma(x) = 0\}$.

In general, the sate orbit of (5.3.1) may crosses or theoretically lies on the surface after reaching in finite time. A discontinuity surface that the system state lies on is called sliding surface. We will investigate numerical accuracy in the worst case in which the system (5.3.1) has at least one sliding surface. Numerically, chattering around the surface is induced, which is illustrated in Fig. 5.1. In this work, we investigate namely trajectory error due to chattering for the n_x-dimensional system (5.3.1) using Euler method whose computation exhibits largest error in comparison with Rung-Kutta and other numerical integration methods. Euler approximation of (5.3.1) is written as

$$x_{k+1} = x_k + f(x_k, t_k)\Delta t \tag{5.3.2}$$

where Δt is sampling time.

Suppose that (5.3.1) has continuum equilibria along sliding surface, i. e. $f(x_s, t) = 0$ for $x_s \in \Sigma$. Then, the system state, theoretically, reaches the continuum equilibria in finite time for any $x_0 \in \mathbb{R}^{n_x}$ [54]. For (5.3.2), assume that an ideal sampling time $\Delta t'$ is selected in such way that at time $k^*\Delta t'$, the state x_{k^*} reaches the surface Σ. Then, we obtain $f(x_{k^*}, t_{k^*}) = 0$, and thus (5.3.2) becomes

$$x_{k^*+1} = x_{k^*}, \tag{5.3.3}$$

which means that the computational state never leaves the surface once it reaches, and, hence, it does not generate trajectory error. However, in practice, we never find any ideal

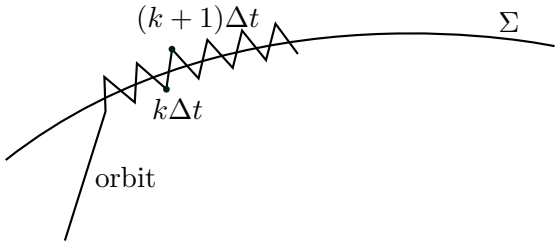

Figure 5.1: Chattering

sampling time, so the computational state does not reach the surface, but bounces around the surface.

Consider trajectory error $\epsilon(x_p)$ around sliding surface, which is generated by neighborhood $x_p \in \mathcal{B}_\delta(x_s)$, where $x_s \in \Sigma$ and δ is positive. We, thus, have $f(x_p, \tau) \neq 0$, where τ is corresponding time at which computational state of (5.3.2) becomes x_p. We define

$$\begin{aligned} \epsilon(x_p) &= \sigma(x_{p+1}) \\ &= \sigma(x_p + f(x_p, \tau)\Delta t). \end{aligned} \tag{5.3.4}$$

It is often the case to consider that maximum trajectory error can be defined by

$$\epsilon_{max} = \sup_{x_s \in \Sigma} \left(\sup_{\tau > 0} \sup_{x_i \to x_s} |\sigma(x_i + f(x_i, \tau)\Delta t)| \right) \tag{5.3.5}$$

if Δt is small enough, and $f(x, \tau)$ is smooth for $x \in \mathcal{B}_\delta(x_s)$ except its center. For autonomous system, $f(x, t) = f(x)$, then (5.3.5) becomes

$$\epsilon_{max} = \sup_{x_s \in \Sigma} \left(\sup_{x_i \to x_s} |\sigma(x_i + f(x_i)\Delta t)| \right). \tag{5.3.6}$$

An example of a 4-dimensional systems with discontinuous vector field is given as following,

$$\begin{aligned} \dot{x}_1(t) &= \text{sign}(x_3(t) - x_4(t)) \\ \dot{x}_2(t) &= 2\ \text{sign}(x_4(t) - x_3(t)) + 6\ \text{sign}(x_1(t) - x_2(t)) \\ \dot{x}_3(t) &= 5\ \text{sign}(x_4(t) - x_3(t)) + \text{sign}(x_2(t) - x_1(t)) \\ \dot{x}_4(t) &= 4\ \text{sign}(x_3(t) - x_4(t)) + 3\ \text{sign}(x_1(t) - x_2(t)) \end{aligned} \tag{5.3.7}$$

where its simulation result is shown in Fig. 5.2.

5.3.2 Filippov Approach

The deterministic state equation of (5.2.8) can be written as

$$\dot{x}(t) = f(x, t) = \Phi^T(x, t)\theta(t), \tag{5.3.8}$$

where $\Phi(x)$ is a discontinuous-function matrix and $\theta(t)$ is a parameter vector. In order to improve computational accuracy, we define an interval for sliding surface as $|\sigma_i(x)| < \frac{\epsilon_i}{2}$,

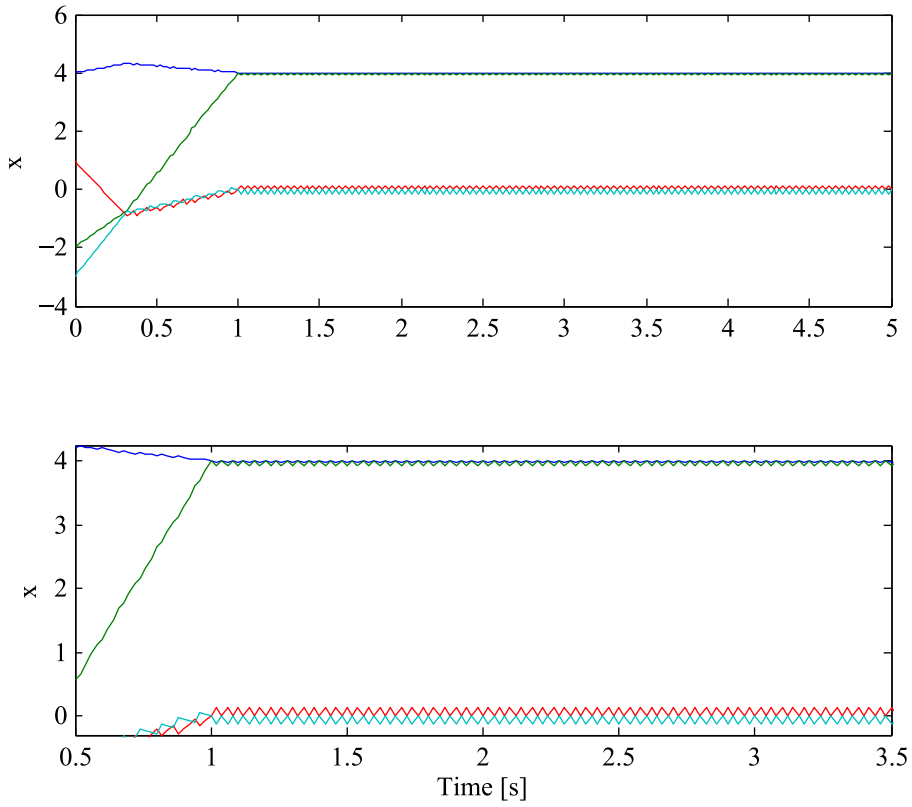

Figure 5.2: Simulation without Filippov approach: Existence of chattering in time frame

where ϵ_i is a threshold computed by (5.3.5) or (5.3.6).

$$\begin{aligned}\Phi^T(x,t)\theta(t) = \Phi^T_{\text{orig}}(x,t)\theta(t) \\ + \sum_{i\in\{\{1,\dots,N\}\setminus S\}} \Delta_i^T(x,t)\theta(t)\frac{\text{sign}(\sigma_i(x))+1}{2} \\ + \sum_{i\in\{S\setminus S'\}} \Delta_i^T(x,t)\theta(t)\mu_i(x) \\ + \sum_{i\in S'} \Delta_i^T(x,t)\theta(t)\frac{\text{sign}(\mu_i(x))+1}{2} \\ - \sum_{i\in\{S\setminus S'\}} C_i\sigma_i(x)\left(\frac{\partial\sigma_i(x)}{\partial x}\right)^T,\end{aligned} \tag{5.3.9}$$

where C_i is positive if the condition $|\sigma_i(x)| < \frac{\epsilon_i}{2}$ is satisfied; and it is zero otherwise. By applying the Filippov approach to the example (5.3.7), chattering is eliminated as illustrated in Fig. 5.3.

5.4 Estimation Algorithm

There are numerous robust estimation algorithms in literatures, but only CDUKF is a low-computational algorithm, which covers wide range of practical applications as it is formulated

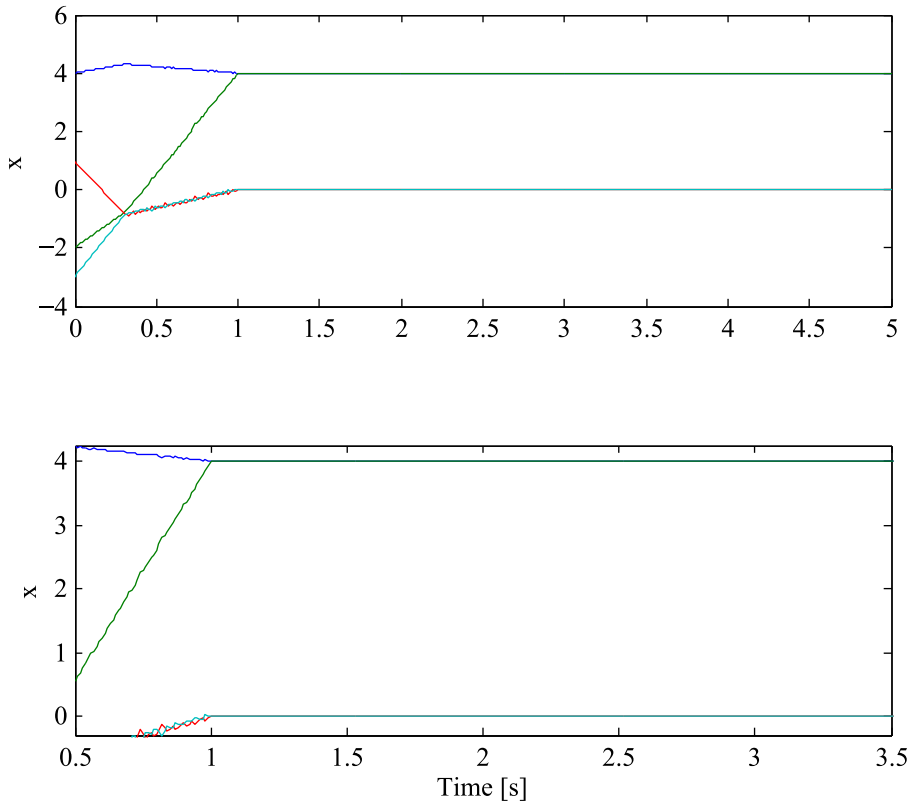

Figure 5.3: Simulation with Filippov approach: No existence of chattering in time frame

for hybrid filtering and it can cope with highly nonlinear systems, especially discontinuous systems, and models with consequential uncertainty.

To handle estimation of the join state and parameter model (5.2.8), it is crucial to investigate observability of the system. Since the deterministic model of (5.2.8) is discontinuous, Filippov's convex method is used for observability analysis on sliding surfaces.

5.4.1 Motivating Example

Consider an autonomous deterministic system with one sliding surface as following [5],

$$\begin{aligned}
\dot{x}_1(t) &= \theta_1 \text{sign}(x_2(t) - x_1(t)) \\
\dot{x}_2(t) &= \theta_2 \text{sign}(x_1(t) - x_2(t)) \\
\dot{\theta}_1(t) &= 0 \\
\dot{\theta}_2(t) &= 0 \\
z_k &= \begin{bmatrix} x_{1k} \\ x_{2k} \end{bmatrix} = \begin{bmatrix} 1 & 0 & 0 & 0 \\ 0 & 1 & 0 & 0 \end{bmatrix} \begin{bmatrix} x_{1k} \\ x_{2k} \\ \theta_{1k} \\ \theta_{2k} \end{bmatrix}.
\end{aligned} \tag{5.4.1}$$

If the state does not lies on sliding surface, which means that $x_1 \neq x_2$, the terms, $\text{sign}(x_2 - x_1)$ and $\text{sign}(x_1 - x_2)$, are denoted as ± 1 and ∓ 1 respectively, then the system (5.4.1) is in the

form of linear system. Therefore, observability matrix can be defined as

$$\begin{bmatrix} 1 & 0 & 0 & 0 \\ 0 & 1 & 0 & 0 \\ 0 & 0 & \pm 1 & 0 \\ 0 & 0 & 0 & \mp 1 \end{bmatrix}$$

which has full rank and implies that the system (5.4.1) is observable. However, if the system state of (5.4.1) lies on sliding surface, $\sigma(x) = x_2 - x_1 = 0$, the state equation can be written in the form following,

$$\begin{aligned} \dot{x}(t) &= \Phi_{\text{orig}}^T(x)\theta(t) + \Delta^T(x)\theta(t)\mu_(x), \\ \dot{\theta}(t) &= 0. \end{aligned} \tag{5.4.2}$$

where

$$\begin{aligned} x(t) = [x_1(t) \quad x_2(t)]^T,\ \theta(t) = [\theta_1(t) \quad \theta_2(t)]^T, \\ \Phi_{\text{orig}}(x) = \begin{bmatrix} -1 & 0 \\ 0 & 1 \end{bmatrix},\ \text{and}\ \Delta(x) = \begin{bmatrix} 2 & 0 \\ 0 & -2 \end{bmatrix} \end{aligned} \tag{5.4.3}$$

By using (4.2.13), $\mu(x) = \frac{1}{2}$ is attained. Substituting (5.4.3) and $\mu(x) = \frac{1}{2}$ into (5.4.2) coupled with measurement equation of (5.4.1), we obtain

$$\begin{aligned} \dot{x}(t) &= 0, \\ \dot{\theta}(t) &= 0, \\ z_k &= \begin{bmatrix} I & 0 \end{bmatrix} \begin{bmatrix} x_k \\ \theta_k \end{bmatrix} \end{aligned} \tag{5.4.4}$$

It is intuitively concluded that (5.4.4) is unobservable. Hence, estimation of system (5.4.1) or the proposed problem set up (5.2.8) in Section 5.2 may diverge when system state orbits along any sliding surface. In order to avoid divergence, we propose a switch from estimation problem to computation of deterministic system. It is remarkable that if the actual system state is constrained to a mathematically known discontinuity surface, the computation of deterministic system, then, results convergence to the surface by the attraction term, $-\sum_{i\in\{S\setminus S'\}} C_i\sigma_i(x)\left(\frac{\partial\sigma_i(x)}{\partial x}\right)^T$ in (5.3.9). This implies robustness of the proposed method.

5.4.2 Proposed Estimation Algorithm

CDUKF algorithm is implemented for our proposed problem formulation which is simply written as

$$\begin{aligned} \begin{bmatrix} \dot{x}(t) \\ \dot{\theta}(t) \end{bmatrix} &= \begin{bmatrix} \Phi^T(x,t)\theta(t) \\ 0 \end{bmatrix} + v_c'(t) \\ z_k &= h_d(x_k, t_k) + w_k, \end{aligned} \tag{5.4.5}$$

where $x(t)$ and $\theta(t)$ are n_x-dimensional state and n_θ-dimensional parameter respectively, and $v_c'(t)$ is white Gaussian noise with spectral density Q'. Denote $n = n_x + n_\theta$; $\hat{\Sigma}_i = \{x \in \mathbb{R}^{n_x} \mid\ |\sigma_i(x)| < \frac{1}{2}\epsilon_i\}$, a set of interval sliding surface, $S = \{i \in \{1, \ldots, N\} \mid\ |\sigma_i(x)| < \frac{1}{2}\epsilon_i\}$,

a set of index of interval sliding surface within which the system state orbits; and $S' = \{i \in S \mid \ \mu_i(x) \notin [0,1]\}$, a set of index of interval discontinuity surface to which the system state is not constrained. Our proposed algorithm is provided in a form of less computational complexity as follows.

Algorithm (Hybrid UKF)

1. UKF associated weights, $W_r^{(m)}$, and $W_r^{(c)}$, then w_m and W; $\quad r = 0, \ldots, 2n$

2. Initilization $\quad \hat{x}_{0|0}$, $\hat{\theta}_{0|0}$, $P_{0|0}$

3. Time update
   During $t \in [kT \quad (k+1)T]$, do the following tasks:
   • If
   $$\hat{x}(t) \in \bigcup_{i \in S} \hat{\Sigma}_i$$
   - Calculate $\{\mu_i(\hat{x})\}$ by the followings,
   $$\begin{aligned} \{\alpha_1, \ldots, \alpha_{N_S}\} &= \{\mu_i(\hat{x})\} \\ \{\beta_1, \ldots, \beta_{N_S}\} &= \{\sigma_i(\hat{x})\} \\ \{\gamma_1, \ldots, \gamma_{N_S}\} &= \{\Delta_i^T(\hat{x}, t)\hat{\theta}(t)\} \end{aligned}$$

$$\begin{bmatrix} \alpha_1 \\ \vdots \\ \alpha_{N_S} \end{bmatrix} = \begin{bmatrix} \frac{\partial \beta_1}{\partial x}\gamma_1 & \cdots & \frac{\partial \beta_1}{\partial x}\gamma_{N_S} \\ \vdots & \cdots & \vdots \\ \frac{\partial \beta_{N_S}}{\partial x}\gamma_1 & \cdots & \frac{\partial \beta_{N_S}}{\partial x}\gamma_{N_S} \end{bmatrix}^{-1} \begin{bmatrix} \frac{\partial \beta_1}{\partial x}\widetilde{f}(\hat{x}, t) \\ \vdots \\ \frac{\partial \beta_{N_S}}{\partial x}\widetilde{f}(\hat{x}, t) \end{bmatrix},$$

   where

$$\widetilde{f}(\hat{x}, t) = \Phi_{\text{orig}}^T(\hat{x}, t)\hat{\theta}(t) + \sum_{k \in \{\{1,\ldots,N\} \setminus S\}} \Delta_k^T(\hat{x}, t)\hat{\theta}(t)\frac{\text{sign}(\sigma_k(\hat{x})) + 1}{2}.$$

   - Integrate
   $$\begin{aligned} \dot{\hat{x}}(t) = {} & \Phi_{\text{orig}}^T(\hat{x}, t)\hat{\theta}(t) \\ & + \sum_{i \in \{\{1,\ldots,N\} \setminus S\}} \Delta_i^T(\hat{x}, t)\hat{\theta}(t)\frac{\text{sign}(\sigma_i(\hat{x})) + 1}{2} \\ & + \sum_{i \in \{S \setminus S'\}} \Delta_i^T(\hat{x}, t)\hat{\theta}(t)\mu_i(\hat{x}) \\ & + \sum_{i \in S'} \Delta_i^T(\hat{x}, t)\hat{\theta}(t)\frac{\text{sign}(\mu_i(\hat{x})) + 1}{2} \\ & - \sum_{i \in \{S \setminus S'\}} C_i\sigma_i(\hat{x})\left(\frac{\partial \sigma_i(\hat{x})}{\partial x}\right)^T \\ \dot{P}(t) = {} & 0 \qquad \text{(covariance matrix is memorized)} \end{aligned}$$

• else
- Sampling

$$\begin{aligned}\mathcal{X}(t) = &\left[\begin{bmatrix} \hat{x}(t) \\ \hat{\theta}(t) \end{bmatrix}, \quad \cdots \quad , \begin{bmatrix} \hat{x}(t) \\ \hat{\theta}(t) \end{bmatrix} \right] \\ &+ \sqrt{n+\lambda} \begin{bmatrix} 0 & \sqrt{P(t)} & -\sqrt{P(t)} \end{bmatrix} \\ X(t) = [I_{n_x} \mid 0]\mathcal{X}(t), &\quad \Theta(t) = [0 \mid I_{n_\theta}]\mathcal{X}(t)\end{aligned}$$

Denote that $[\cdot]_r$ is the $(r+1)^{\text{th}}$ column of $[\cdot]$.
- Compute

$$f_r(\mathcal{X}(t),t) = \Phi^T([X(t)]_r,t)[\Theta(t)]_r + \sum_{i=1}^{N} \Delta_i^T([X(t)]_r,t)[\Theta(t)]_r \frac{\text{sign}(\sigma_i([X(t)]_r)) + 1}{2}$$

$$(r = 0, \ldots, 2n)$$

$$\hat{f}(\mathcal{X}(t),t) = \sum_{r=0}^{2n} W_r^{(m)} f_r(\mathcal{X}(t),t)$$

- Starting with initial condition $\hat{x}_{k|k}$ and $P_{k|k}$, integrate

$$\begin{aligned}\dot{\hat{x}}(t) =& \hat{f}(\mathcal{X}(t),t) \\ \dot{P}(t) =& \sum_{r=0}^{2n} W_r^{(c)} \left(\begin{bmatrix} ([X(t)]_r - \hat{x}(t))(f_r(\mathcal{X}(t),t) - \hat{f}(\mathcal{X}(t),t))^T & 0 \\ ([\Theta(t)]_r - \hat{\theta}(t))(f_r(\mathcal{X}(t),t) - \hat{f}(\mathcal{X}(t),t))^T & 0 \end{bmatrix} \right. \\ &\left. + \begin{bmatrix} ([X(t)]_r - \hat{x}(t))(f_r(\mathcal{X}(t),t) - \hat{f}(\mathcal{X}(t),t))^T & 0 \\ ([\Theta(t)]_r - \hat{\theta}(t))(f_r(\mathcal{X}(t),t) - \hat{f}(\mathcal{X}(t),t))^T & 0 \end{bmatrix}^T \right) + Q',\end{aligned}$$

At the end of the time update, the latest mean and covariance are assigned as $\hat{x}_{k+1|k}$ and $P_{k+1|k}$. Since during the time update, the parameter vector is not updated, at the end of this interval the predicted parameter is assigned as $\hat{\theta}_{k+1|k} = \hat{\theta}_{k|k}$.

4. Measurement update
At time $(k+1)T$,
• if

$$\hat{x}_{k|k} \in \bigcup_{i \in S} \hat{\Sigma}_i, \quad k \leftarrow k+1, \text{ then go to step 3.}$$

• else
- Resampling

$$\begin{aligned}\mathcal{X}_{k+1|k}^{(r)} = &\left[\begin{bmatrix} \hat{x}_{k+1|k} \\ \hat{\theta}_{k+1|k} \end{bmatrix}, \quad \cdots \quad , \begin{bmatrix} \hat{x}_{k+1|k} \\ \hat{\theta}_{k+1|k} \end{bmatrix} \right] \\ &+ \sqrt{n+\lambda} \begin{bmatrix} 0 & \sqrt{P_{k+1|k}} & -\sqrt{P_{k+1|k}} \end{bmatrix} \\ X_{k+1|k}^{(r)} = &[I_{n_x} \mid 0]\mathcal{X}_{k+1|k}^{(r)}\end{aligned}$$

- Compute

$$
\begin{aligned}
[Z_{k+1|k}]_r &= h_d([X^{(r)}_{k+1|k}]_r, t_k) \\
\hat{z}_{k+1|k} &= \sum_{r=0}^{2n} W_r^{(m)} [Z_{k+1|k}]_r \\
P_{zz,k+1|k} &= \sum_{r=0}^{2n} W_r^{(c)} ([Z_{k+1|k}]_r - \hat{z}_{k+1|k})([Z_{k+1|k}]_r - \hat{z}_{k+1|k})^T + R \\
P_{xz,k+1|k} &= \sum_{r=0}^{2n} W_r^{(c)} \left([\mathcal{X}^{(r)}_{k+1|k}]_r - \begin{bmatrix} \hat{x}_{k+1|k} \\ \hat{\theta}_{k+1|k} \end{bmatrix} \right) ([Z_{k+1|k}]_r - \hat{z}_{k+1|k})^T \\
K_{k+1} &= P_{xz,k+1|k} P^{-1}_{zz,k+1|k} \\
\begin{bmatrix} \hat{x}_{k+1|k+1} \\ \hat{\theta}_{k+1|k+1} \end{bmatrix} &= \begin{bmatrix} \hat{x}_{k+1|k} \\ \hat{\theta}_{k+1|k} \end{bmatrix} + K_{k+1}(z_k - \hat{z}_{k+1|k}) \\
P_{k+1|k+1} &= P_{k+1|k} - K_{k+1} P_{zz,k+1|k} K_{k+1}^T \\
k &\leftarrow k+1, \text{ then go to step 3.}
\end{aligned}
$$

Remark 5.1: In order to avoid computational burden of calculating ϵ_i in the algorithm, ϵ_i should be pre-computed using (5.3.5) or (5.3.6). Its value depends on completely known model for estimation. Since our proposed problem formulation involves to-be-estimated parameter, it is considered to limit upper and lower bound of the parameter for pre-computation of ϵ_i. For some cases, e.g. control systems involving integrator action, one may select smaller ϵ_i since the controller action makes the systems converge to sliding surface almost exponentially before the orbit incurs chattering. Therefore, for simulation the value of ϵ_i is very useful for beginning.

5.5 Application Examples

To clarify the robustness of the algorithm, simulation results of two numerical examples are given. The first example has ideal formulation, i. e. exact basis function, and involves two sliding surfaces. For the second example, there is only one sliding surface, and we consider a different basis function from the actual one.

5.5.1 Generic Example

Consider a continuous-discrete filtering model following,

$$
\begin{aligned}
\dot{x}_1 &= p_1 \text{sign}(x_3 - x_4) + u_1(t) + v_{c1}(t) \\
\dot{x}_2 &= p_2 \text{sign}(x_4 - x_3) + p_3 \text{sign}(x_1 - x_2) + u_2(t) + v_{c2}(t) \\
\dot{x}_3 &= p_4 \text{sign}(x_4 - x_3) + p_5 \text{sign}(x_2 - x_1) + u_3(t) + v_{c3}(t) \\
\dot{x}_4 &= p_6 \text{sign}(x_3 - x_4) + p_7 \text{sign}(x_1 - x_2) + u_4(t) + v_{c4}(t) \\
z_k &= x_k + w_k,
\end{aligned}
\tag{5.5.1}
$$

where $u_1(t) = \sin(25t)$, $u_2(t) = 20\sin(10t)$, $u_3(t) = 25\sin(5t)$, and $u_4(t) = 15\sin(30t)$ for $t \in [0, 10s]$ and $u_1(t) = u_2(t) = u_3(t) = u_4(t) = 0$ for $t > 10s$. In this problem we estimate

$p_1, \ldots, p_7$ which are constants. The estimation result of normalized parameters, $\frac{\hat{p}_1}{p_1}, \ldots, \frac{\hat{p}_7}{p_7}$, using conventional CDUKF is shown in Fig. 5.4. It indicates that estimate parameters drift and then diverge while the system state orbits along the sliding surfaces ($x_1(t) - x_2(t) = 0$ or/and $x_3(t) - x_4(t) = 0$, illustrated in Fig. 5.5). Fig. 5.6 shows the estimation of normalized parameters using the algorithm in Section 5.4.2. The largest error of parameter estimation

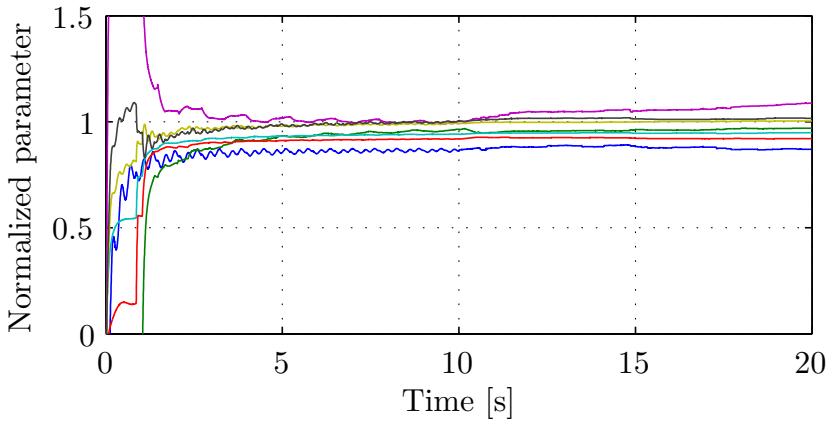

Figure 5.4: Parameter estimation using conventional CDUKF

at steady state is about 15%.

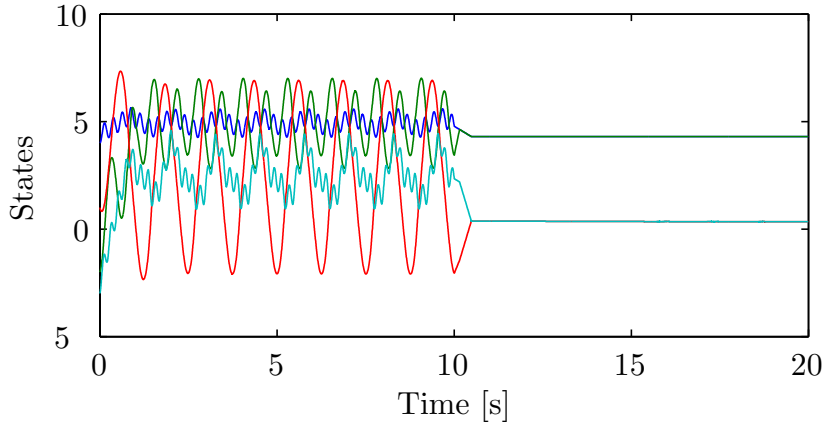

Figure 5.5: Actual state: x_1 (blue), x_2 (green), x_3 (red), and x_4

5.5.2 Application to Friction Estimation for Adaptive Control

Friction estimation is very important for adaptive friction compensation control. [43], [58] and [51] considered adaptive position control for DC motor. [43] tried to estimate the dynamic parameters of LuGre model using model-based observer, whereas [58] used sliding-mode-observer-based to estimate the dynamic parameters of LuGre model, and total moment of inertia. The disadvantage of using dynamic model of friction is that prior known static friction parameters, which are identified from individual experiments, is required. Extended

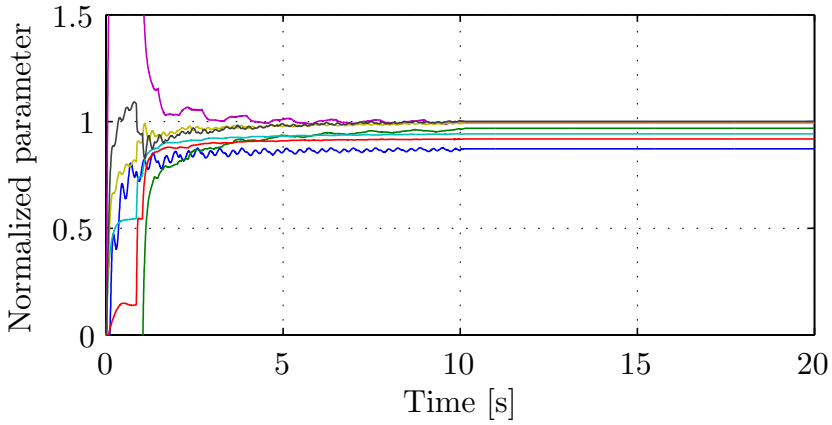

Figure 5.6: Parameter estimation using the proposed algorithm

Kalman-Bucy filter (EKBF) is used by [51] to estimate friction which is modeled as second-order random walk. The drawback is that performance over other compensation methods is not very significant. In our work, we consider an adaptive compensation of static friction which is modeled as

$$F_f = (\alpha_0 + \alpha_1 e^{-(\omega/\omega_s)^2})\text{sign}(\omega) + \alpha_2\omega, \tag{5.5.2}$$

where ω is angular velocity; ω_s is Stribeck velocity; $\alpha_0 + \alpha_1$ is static friction; α_0 is Coulomb friction; and α_2 is coefficient of viscous friction. We use the the proposed algorithm to estimate the friction from a model of DC motor as following,

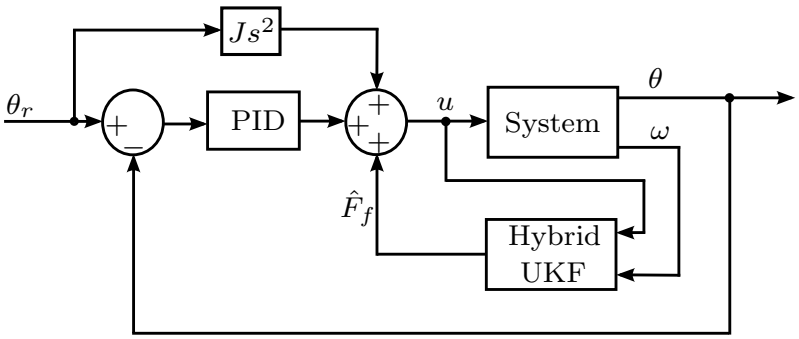

Figure 5.7: Block diagram of adaptive control

$$\dot{\omega}(t) = \frac{1}{J}[-\text{sign}(\omega) \quad -e^{-(\omega/\omega_s)^2}\text{sign}(\omega) \quad -\omega] \times \begin{bmatrix} \alpha_0 \\ \alpha_1 \\ \alpha_2 \end{bmatrix} + \frac{u}{J} \tag{5.5.3}$$

where J is the total moment of inertia of the motor and u is control torque. The shape of basis function $\Phi(\omega) = \frac{1}{J}[-\text{sign}(\omega) \quad -e^{-(\omega/\omega_s)^2}\text{sign}(\omega) \quad -\omega]^T$ around $\omega = 0$ is significantly varied by ω_s. The motivation of using the algorithm is as follows. [51] considers an adaptive control in two different cases, contact up and contact down. Friction coefficients and empirical constant, Stribeck velocity ω_s, are different for both cases (contact up: $\omega_s = 0.01$; contact down: $\omega_s = 2.4$). Intuitively, in spatial motion ω_s varies between 0.01 and 2.4 upon

the direction of contact. Therefore, we are not able to select an exact basis function for all cases.

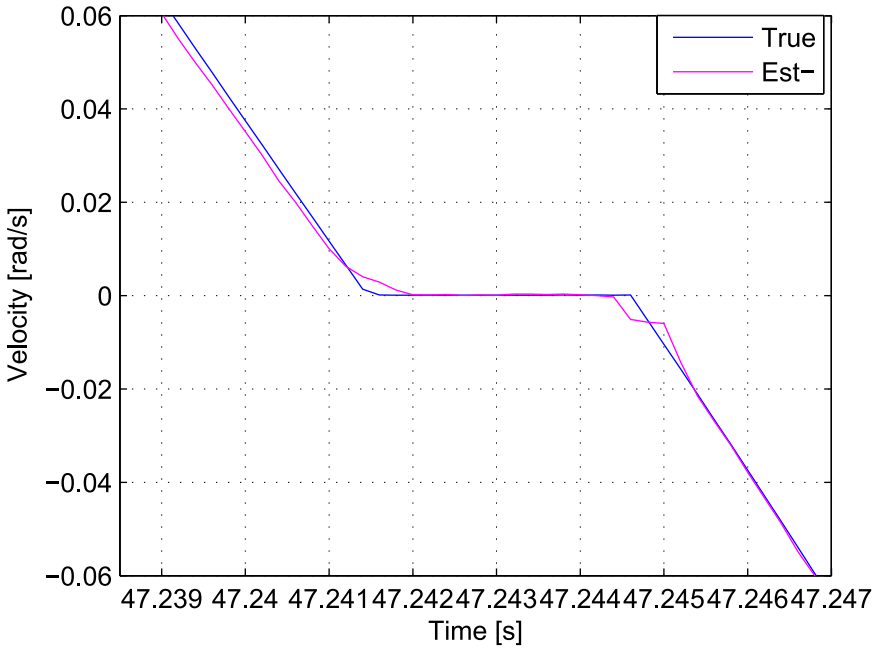

Figure 5.8: Velocity estimation

In this work, we simulate a control system (shown in Fig. 5.7 with $\theta_r(t) = 2.8\sin(0.02\pi t)$ $\sin(2\pi t)$) in the case of contact down, but $\omega_s = 0.01$ is selected for estimation algorithm, meaning that biased basis function is used and therefore, the model error is $\mathcal{E}(x, t, \theta_{\text{ideal}}) = \frac{\alpha_1}{J}(e^{-(\omega/0.01)^2} - e^{-(\omega/2.4)^2})\text{sign}(\omega)$ which is bounded for all $\omega \in \mathbb{R}$ and $t > 0$. The time-evolution parameter, $\theta(t) = [\alpha_0 \quad \alpha_1 \quad \alpha_2]^T$, are no longer constant, which are illustrated by estimation result in Fig. 5.9. The results of friction estimation and tracking error are shown in Fig. 6.7 and 6.8 respectively. In comparison with the result of [51], tracking error is reduced about 70%.

To clarify the condition (5.2.9), we also simulate the system with another choice of bias basis function, $\Phi_1(\omega) = \frac{1}{J}[-\text{sign}(\omega) \quad -\omega^2\text{sign}(\omega) \quad -\omega]^T$ which yields unbounded model error, $\mathcal{E}(x, t, \theta_{\text{ideal}}) = \frac{\alpha_1}{J}(\omega^2 - e^{-(\omega/2.4)^2})\text{sign}(\omega)$. Fig. 5.12 indicates divergence of estimation. However, it is interesting to note that at low velocity friction estimation approach the true one because the model error is small. But when velocity is large, friction estimation diverge very fast as the model error is proportional to ω^2.

5.6 Estimation Effectiveness of Joint State and Parameter Model

In this section we will show the limitation of model simplification which was proposed in the Section 5.2. We consider a control scheme which is tracking control of nonlinear stochastic

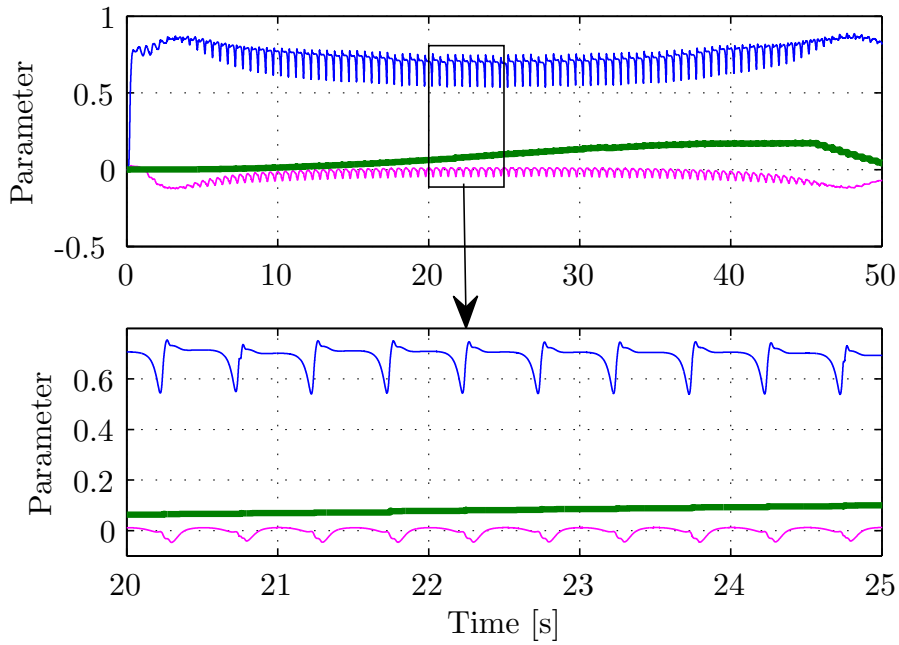

Figure 5.9: Time-evolution of parameter: $\hat{\alpha}_0$, $\hat{\alpha}_1$ and $\hat{\alpha}_2$ from the top to bottom respectively

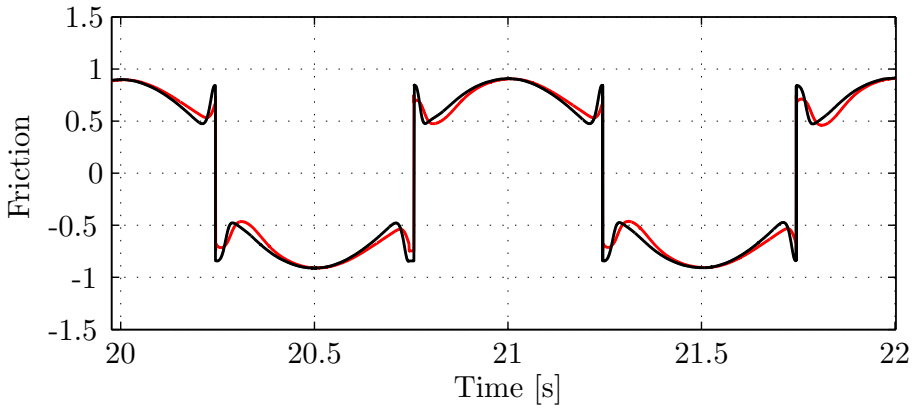

Figure 5.10: Friction estimation: black line is actual one; red line is estimation

systems with actuator nonlinearity. We use existing adaptive controller including parameter update law and control law, which can achieve exponential tracking of a class of nonlinear deterministic system. However, the controller cannot be practically applied since the presence of observation noise leads to divergence of parameter update law. Furthermore, the sensitivity of the control law signal induces bursting behavior which may, in practice, damage actuators. We modify both the parameter update law and the control law to avoid divergence and reduce the sensitivity. In addition, we consider two type of filtering techniques, i.e. classical Kalman filter to estimate joint state and parameter of a simplified linear time varying model, and continuous-discrete unscented Kalman filter to estimate state and all unknown parameters of the system. The effectiveness of our proposed control method is clarified by a numerical example of a second order dynamical system with dead-zone nonlinearity. Then,

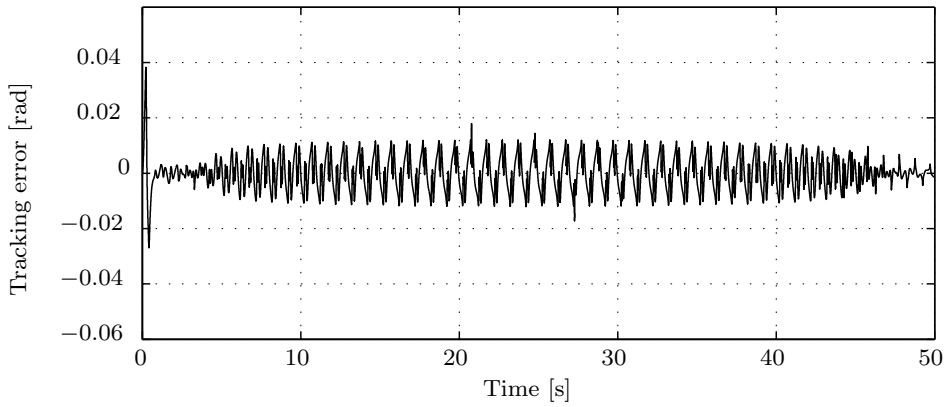

Figure 5.11: Performance

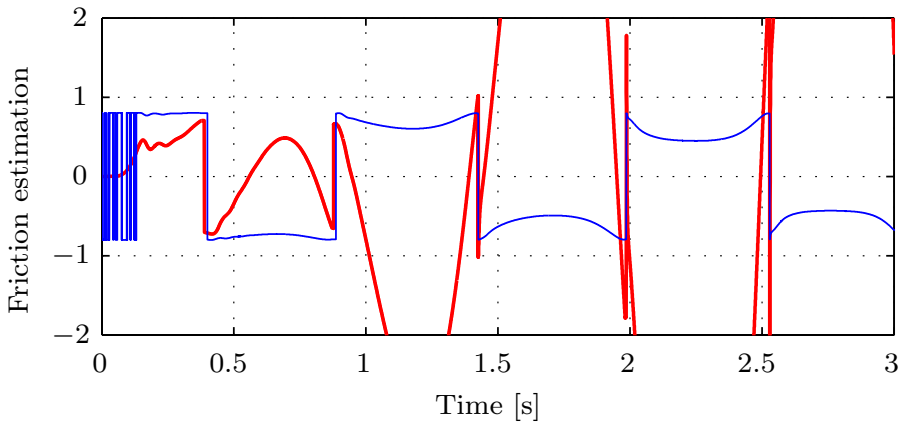

Figure 5.12: Actual friction (blue) and estimation (red)

tracking performances obtained from both filtering methods are compared.

5.6.1 Overview on Nonlinear Systems with Actuator Nonlinearity

Control problem of uncertain nonlinear system with actuator nonlinearity has been a challenging problem for decades, [59, 60, 61, 62]. Actuator nonlinearity exist in a wide range of physical systems and devices such as piezoelectric actuators, electromagnetism, electronic relay circuits, smart materials, etc [62]. The actuator nonlinearities such as dead-zone, backlash and hysteresis are commonly investigated as they are generally nonsmooth and highly nonlinear, and are usually a cause of instability and poor performance. Controller designs along with stability analyses have been done by many researchers. Recently, [62] provided controller design method based on Lypunov-function approach. The controller can achieve tracking error converging to zero exponentially, which is verified by mathematical analysis and two numerical examples. It is analytically proved that the adaptation of the controller is based on a monotonically increasing parameter whose time derivative, involving exponential of time and tracking error, converges to zero as the tracking error converges to zero at a

faster rate than the divergence rate of the exponential term. It is intuitive that the controller is not applicable for a stochastic system since tracking error for such system converges to a bounded interval around zero. In our work, we consider a remedy of this adaptation, and discuss the behavior of designed actuator input signal. In addition, since the system considered in this work is uncertain due to unknown parameter as in [62], we consider to use a robust filtering for state observer.

We use two type of filtering methods, which can deal with high process uncertainty. A classical KF is to estimate state and parameter of a simplified joint state and parameter model, which has the form of linear time varying, and CDUKF is used to estimate state and all unknown parameters of the system.

5.6.2 Problem Statement

System Model and Control

A class of system that we consider is the same as in [62], which is, for completeness, written as

$$\begin{aligned} x^{(n)}(t) + \sum_{i=1}^{r} a_i Y_i(x(t), \dot{x}(t), \ldots, x^{(n-1)}(t), t) \\ = bu(t) + d(t), \\ u(t) = N(v(t)), \end{aligned} \tag{5.6.1}$$

where plant parameters a_i are unknown constants, control gain b is unknown constant, $d(t)$ denotes bounded external disturbance and Y_i are known functions, $N(.)$ represents an actuator uncertainty, $v(t)$ is actuator input, and $u(t)$ is actuator output which is not available for measurement. In [62], two types of actuator nonlinearity are considered, backlash-like hysteresis and dead-zone, both of which can be written in one general form as

$$u(t) = cv(t) + \bar{d}(v), \tag{5.6.2}$$

where c is positive and $\bar{d}(v)$ is bounded. Substituting (5.6.2) into (1) yields

$$\begin{aligned} x^{(n)}(t) + \sum_{i=1}^{r} a_i Y_i(x(t), \dot{x}(t), \ldots, x^{(n-1)}(t), t) \\ = \rho v(t) + D(t), \end{aligned} \tag{5.6.3}$$

where $\rho = bc$, and $D(t) = b\bar{d}(v) + d(t)$. Since b is unknown, ρ is unknown, but $\rho >$ is positive as b and c are positive. $D(t)$ is bounded since $d(t)$ and $\bar{d}(v)$ are bounded. Let $y = [x, \dot{x}, \ldots, x^{(n-1)}]^T$, $y_d = [x_d, \dot{x}_d, \ldots, x_d^{(n-1)}]^T$ and the tracking error

$$e = y - y_d, \tag{5.6.4}$$

that is, $e = [e_1, e_2, \ldots, e_n]^T$, implying that

$$e_1 = x - x_d, \quad e_2 = \dot{x} - \dot{x}_d, \ \ \ldots, \ e_n = x^{(n-1)} - x_d^{(n-1)}. \tag{5.6.5}$$

From (5.6.3) to (5.6.5), the dynamic equation of the tracking error is given by

$$\dot{e} = Ae + B\left[-\sum_{i=1}^{r} a_i Y_i(y, t) + \rho v(t) + D(t) - x_d^{(n)}(t)\right], \tag{5.6.6}$$

where

$$A = \begin{bmatrix} 0 & 1 & 0 & \dots & 0 \\ 0 & 0 & 1 & \dots & 0 \\ \vdots & \ddots & \ddots & \ddots & \vdots \\ 0 & 0 & 0 & \dots & 1 \\ 0 & 0 & 0 & \dots & 0 \end{bmatrix}, \quad B = \begin{bmatrix} 0 \\ 0 \\ \vdots \\ 0 \\ 1 \end{bmatrix}, \tag{5.6.7}$$

Some constants and variables used for adaptive control scheme are defined as follows [62]:

A positive definite matrix $\mathsf{P} = \mathsf{P}^T$ is obtained from

$$[(A + \sigma_1 I) + Bk]^T \mathsf{P} + \mathsf{P}[(A + \sigma_1 I) + Bk] = -\mathsf{Q}, \tag{5.6.8}$$

where $\sigma_1 > 0$ is a design parameter, k is a constant matrix satisfying that $(A + \sigma_1 I) + Bk$ is stable, $\mathsf{Q} = \mathsf{Q}^T > 0$ is a given matrix, that is,

$$(A + Bk)^T \mathsf{P} + \mathsf{P}(A + Bk) = -\mathsf{Q} - 2\sigma_1 \mathsf{P} < -2\sigma_1 \mathsf{P}; \tag{5.6.9}$$

$$f(y,t) = \sum_{i=1}^{r} \sqrt{|Y_i(y,t)|^2 + h_i} + \sqrt{\| e \|^2 + h} + 1; \tag{5.6.10}$$

$$d_0 = \sup_{t \geq 0} \left[|D(t)| + |x_d^{(n)}| \right]; \tag{5.6.11}$$

$$\theta = \max\{|a_1|, \dots, |a_r|, \| k \|, d_0\}; \tag{5.6.12}$$

$$\theta^* = \frac{\theta}{\rho}, \tag{5.6.13}$$

where $h,\ h_i,\ i = 1, 2, \dots, r$, are positive design constants. Then the control law and parameter update law are designed as following [62]

$$v(t) = -\frac{e^T \mathsf{P} B \hat{\theta}^2(t) f^2(y,t)}{e^T \mathsf{P} B \tanh[l^{-1} e^T \mathsf{P} B \exp(2\sigma_2 t)] \hat{\theta}(t) f(y,t) + l \exp(-2\sigma_2 t)}, \tag{5.6.14}$$

$$\dot{\hat{\theta}} = \gamma \exp(2\sigma_1 t) |e^T \mathsf{P} B| f(y,t), \tag{5.6.15}$$

where $l,\ \sigma_1$ are positive design constants, $\gamma > 0$ is adaptive gain, and σ_2 satisfies $\sigma_2 > \sigma_1$, $\hat{\theta}$ is the estimate of θ^*, $\hat{\theta}(0) \geq 0$.

In practice, the system (5.6.3) is disturbed by noise, so that the parameter update given by (5.6.15) diverges at steady-state since the tracking error does not exponentially converge to zero. Instead, it converges to a bounded interval. Therefore, the controller is not realizable.

Controller Modification

In deterministic case, the right hand side of (5.6.15) converges to zero as the tracking error e converge to zero at faster rate than the divergence rate of $\exp(2\sigma_1 t)$, which implies that the parameter $\hat{\theta}$ converges to a constant. Since the tracking error converges to zero exponentially, there is no significant difference if $\hat{\theta}$ is set to a constant after the tracking error is once within tolerance. Let

$$t^* = \min_{t \geq 0}\{t \quad | \quad |e_1| < \epsilon_e\}, \tag{5.6.16}$$

where $\epsilon_e > 0$ is a desired tracking tolerance. Then the the proposed modified parameter update law is given by

$$\begin{cases} \dot{\hat{\theta}}_m = \gamma \exp(2\sigma_1 t)|e^T \mathsf{P} B| f(y,t), & \text{if } t < t^* \\ \dot{\hat{\theta}}_m = 0, & \text{otherwise.} \end{cases} \tag{5.6.17}$$

On the other hand, let

$$v^*(t) = -\frac{e^T \mathsf{P} B \hat{\theta}^2 f^2(y,t)}{|e^T \mathsf{P} B| \hat{\theta} f(y,t) + l \exp(-2\sigma_2 t)}. \tag{5.6.18}$$

By using the inequality

$$0 \leq x \tanh(\frac{x}{a}) \leq |x|, \quad \text{for } \ \forall a > 0, \tag{5.6.19}$$

we have

$$|v(t)| \geq |v^*(t)|. \tag{5.6.20}$$

For $t \to \infty$ we get $v^*(t) \to -\hat{\theta} f(y,t)$ sign$(e^T \mathsf{P} B)$. At steady-state for a stochastic system, $e^T \mathsf{P} B$ changes its sign frequently as the tracking error e converge to a bounded interval around zero. Therefore, $v^*(t)$ induces bursting signal, and so does $v(t)$, according to (5.6.20). This may damage actuators. To remedy the problem we propose to use filtering technique to obtain state observer and a modification to the control law which is governed by

$$v_m(t) = -\frac{\hat{e}^T \mathsf{P} B \hat{\theta}_m^2 f^2(\hat{y},t)}{|\hat{e}^T \mathsf{P} B| \hat{\theta}_m f(\hat{y},t) + l \exp(-2\sigma_2 t) + \epsilon_v} \tag{5.6.21}$$

where the introduced parameter $\epsilon_v > 0$ is to reduce the sensitivity of the control law, $\hat{y}$ is estimated state, and the estimate tracking error $\hat{e}$ is defined by

$$\hat{e} = \hat{y} - y_d. \tag{5.6.22}$$

5.6.3 Simplified Models for Estimation

Simplified Linear Time Varying Model

The model (5.6.3) is simplified as following

$$x^{(n)}(t) = \beta(t) v_m(t) + \nu_x(t), \tag{5.6.23}$$

where $\beta(t)$ is assumed to be a time varying parameter governed by

$$\dot{\beta}(t) = \nu_\beta(t), \tag{5.6.24}$$

and $\nu_x(t)$ and $\nu_\beta(t)$ are assumed to be white Gaussian noises. Suppose all the states $x, \dot{x}, \ldots, x^{(n-1)}$ can be measured. Then the state-space representation of (5.6.23) and (5.6.24) can be written as

$$\dot{\mathcal{X}} = \mathcal{A}(t)\mathcal{X} + \nu(t) \tag{5.6.25}$$

$$z_k = \mathcal{H}\mathcal{X}_k + w_k, \tag{5.6.26}$$

where $\mathcal{X} = [x, \dot{x}, \ldots, x^{(n-1)}, \beta]^T$ and z_k are $n+1$-dimensional state and n-dimensional measurement respectively, $\nu = [0_{1\times(n-1)}, \nu_x, \nu_\beta]^T$ has spectral density $\mathcal{Q}_c$, w_k is white Gaussian noise with covariance R, $\mathcal{A}$ and $\mathcal{H}$ are defined by

$$\mathcal{A}(t) = \begin{bmatrix} 0 & 1 & 0 & \ldots & 0 & 0 \\ 0 & 0 & 1 & \ldots & 0 & 0 \\ \vdots & \ddots & \ddots & \ddots & \ddots & \vdots \\ 0 & 0 & 0 & \ldots & 1 & 0 \\ 0 & 0 & 0 & \ldots & 0 & v_m(t) \\ 0 & 0 & 0 & \ldots & 0 & 0 \end{bmatrix}$$

$$\mathcal{H} = [I_n \quad 0]$$

(I_n is n-dimensional identity matrix). (5.6.26) implies that all the states $\mathcal{X}_k$ can be measured. It is noted that the pair $(\mathcal{A}, \mathcal{H})$ is observable for non-zero $v_m(t)$.

In order to implement classical KF, the process equation (5.6.25) is discretized over sampling time T as following,

$$\mathcal{X}_{k+1} - \mathcal{X}_k = \mathcal{A}(kT)\mathcal{X}_k T + \mu_k, \tag{5.6.27}$$

where $\mathcal{X}_k = \mathcal{X}(kT)$, $\frac{d\mu(t)}{dt} = \nu(t)$, and μ_k has covariance matrix $\mathcal{Q} = \mathcal{Q}_c T$. Let $A_k = A(kT)T + I_{n+1}$, then (5.6.27) can be rewritten as

$$\mathcal{X}_{k+1} = \mathcal{A}_k \mathcal{X}_k + \mu_k. \tag{5.6.28}$$

Thus, the classical KF can be easily implemented to the system of (5.6.28) and (5.6.26).

Nonlinear Joint State and Parameter Model

By taking the advantage of known nonlinear functions Y_i of the system introduced in (5.6.1), in the following, we consider an estimation of state and all the unknown parameters of the system. Let a parameter vector $p = [a_1, \ldots, a_r, \rho, D]^T$, then the joint state and parameter of the stochastic model of (5.6.3) is given by

$$\begin{aligned} \begin{bmatrix} \dot{y}(t) \\ \dot{p}(t) \end{bmatrix} &= \begin{bmatrix} Ay + B\Phi^T(y,t)p(t) \\ 0 \end{bmatrix} + v_c(t) \\ z_k &= h_d(y_k, t_k) + w_k, \end{aligned} \tag{5.6.29}$$

where, z_k is measurement, $\Phi^T(y,t) = [-Y_1(y,t), \ldots, -Y_r(y,t), v_m(t), 1]$, $v_c(t)$ is assumed to be white Gaussian noise with spectral density Q_c, h_d is nonlinear discrete-time measurement model, and w_k is zero-Gaussian noise with covariance matrix R. State observer is obtained from estimation of the joint state and parameter filtering model (5.6.29).

CDUKF algorithm is implemented for the proposed problem formulation (5.6.29). Let q be the dimension of the process equation, then

$$q = n + r + 2.$$

The algorithm following is provided in the form of less computational complexity and without resetting covariance matrix as used in the previous.

Algorithm: CDUKF for joint state and parameter model

1. UKF associated weights, $W_i^{(m)}$, and $W_i^{(c)}$; $i = 0, \ldots, 2q$

2. Initilization $\quad \hat{y}_{0|0}$, $\hat{p}_{0|0}$, $P_{0|0}$

3. Time update
   During $t \in [KT \quad (k+1)T]$, do the following tasks.
   - Sampling

$$\begin{aligned}\mathcal{Y}(t) = &\left[\begin{bmatrix} \hat{y}(t) \\ \hat{p}(t) \end{bmatrix}, \quad \cdots \quad , \begin{bmatrix} \hat{y}(t) \\ \hat{p}(t) \end{bmatrix} \right] \\ &+ \sqrt{q+\lambda} \begin{bmatrix} 0 & \sqrt{P}(t) & -\sqrt{P}(t) \end{bmatrix} \\ Y(t) = &[I_n \mid 0]\mathcal{Y}(t), \quad \Theta(t) = [0 \mid I_{r+2}]\mathcal{Y}(t)\end{aligned}$$

   Denote that $[\cdot]_i$ is the $(i+1)^{\text{th}}$ column of $[\cdot]$.
   - Compute

$$\begin{aligned}f_i(\mathcal{Y}(t), t) &= A[Y(t)]_i + B\Phi^T([Y(t)]_i, t)[\Theta(t)]_i \qquad (i = 0, \ldots, 2q) \\ \hat{f}(\mathcal{Y}(t), t) &= \sum_{i=0}^{2q} W_i^{(m)} f_i(\mathcal{Y}(t), t)\end{aligned}$$

   - Integrate

$$\begin{aligned}\dot{\hat{y}}(t) =& \hat{f}(\mathcal{Y}(t), t) \\ \dot{P}(t) =& \sum_{i=0}^{2q} W_i^{(c)} \left(\begin{bmatrix} ([Y(t)]_i - \hat{y})(f_i(\mathcal{Y}(t), t) - \hat{f}(\mathcal{Y}(t), t))^T & 0 \\ ([\Theta(t)]_i - \hat{p})(f_i(\mathcal{Y}(t), t) - \hat{f}(\mathcal{Y}(t), t))^T & 0 \end{bmatrix} \right. \\ &\left. + \begin{bmatrix} ([Y(t)]_i - \hat{y})(f_i(\mathcal{Y}(t), t) - \hat{f}(\mathcal{Y}(t), t))^T & 0 \\ ([\Theta(t)]_i - \hat{p})(f_i(\mathcal{Y}(t), t) - \hat{f}(\mathcal{Y}(t), t))^T & 0 \end{bmatrix}^T \right) \\ &+ Q_c\end{aligned}$$

   At the end of the time update, the latest mean and covariance are assigned as $\hat{y}_{k+1|k}$ and $P_{k+1|k}$. Since during the time update, the parameter vector is not updated, at the end of this interval the predicted parameter is assigned as $\hat{p}_{k+1|k} = \hat{p}_{k|k}$.

4. Measurement update
   At time $(k+1)T$,
   - Resampling

$$\begin{aligned}\mathcal{Y}_{k+1|k}^{(r)} = &\left[\begin{bmatrix} \hat{y}_{k+1|k} \\ \hat{p}_{k+1|k} \end{bmatrix}, \quad \cdots \quad , \begin{bmatrix} \hat{y}_{k+1|k} \\ \hat{p}_{k+1|k} \end{bmatrix} \right] \\ &+ \sqrt{q+\lambda} \begin{bmatrix} 0 & \sqrt{P_{k+1|k}} & -\sqrt{P_{k+1|k}} \end{bmatrix} \\ Y_{k+1|k}^{(r)} = &[I_n \mid 0]\mathcal{Y}_{k+1|k}^{(r)}\end{aligned}$$

- Compute

$$
\begin{aligned}
[Z_{k+1|k}]_i &= h_d([Y^{(r)}_{k+1|k}]_i, t_k) \\
\hat{z}_{k+1|k} &= \sum_{i=0}^{2q} W_i^{(m)} [Z_{k+1|k}]_i \\
P_{zz,k+1|k} &= \sum_{i=0}^{2q} W_i^{(c)} ([Z_{k+1|k}]_i - \hat{z}_{k+1|k})([Z_{k+1|k}]_i - \hat{z}_{k+1|k})^T + R \\
P_{yz,k+1|k} &= \sum_{i=0}^{2q} W_i^{(c)} \left([\mathcal{Y}^{(r)}_{k+1|k}]_i - \begin{bmatrix} \hat{y}_{k+1|k} \\ \hat{p}_{k+1|k} \end{bmatrix} \right) ([Z_{k+1|k}]_i - \hat{z}_{k+1|k})^T \\
K_{k+1} &= P_{yz,k+1|k} P^{-1}_{zz,k+1|k} \\
\begin{bmatrix} \hat{y}_{k+1|k+1} \\ \hat{p}_{k+1|k+1} \end{bmatrix} &= \begin{bmatrix} \hat{y}_{k+1|k} \\ \hat{p}_{k+1|k} \end{bmatrix} + K_k (z_k - \hat{z}_{k+1|k}) \\
P_{k+1|k+1} &= P_{k+1|k} - K_{k+1} P_{zz,k+1|k} K^T_{k+1} \\
k &\leftarrow k+1, \text{ then go to step 3.}
\end{aligned}
$$

5.6.4 Numerical Example

As in [62], to illustrate the robustness of our proposed control method we simulate a second-order dynamical system given by

$$
\begin{aligned}
\ddot{x} = a_1 \frac{1 - \exp(-x)}{1 + \exp -x} &- a_2(\dot{x}^2 + 2x)\sin(\dot{x}) \\
&- 0.5 a_3 x \sin(3t) + bu.
\end{aligned} \tag{5.6.30}
$$

Actuator nonlinearity considered for this example is dead-zone which is illustrated by Fig. 5.13. Its model is governed by

$$
u(t) = cv(t) + \bar{d}(v), \tag{5.6.31}
$$

where

$$
\bar{d}(v) = \begin{cases} -cb_r, & v \geq b_r, \\ -cv, & b_l < v < b_r \\ -cb_l, & v \leq b_l \end{cases} \tag{5.6.32}
$$

is bounded. The parameters of the plant and the nonlinearity are selected as $a_1 = a_2 = a_3 = b = 1$, $c = 1$, $b_r = 0.5$, $b_l = -0.6$, which are assumed to be unknown. The initial condition of the controlled plant (5.6.30) is given by $x(0) = -2.5$, $\dot{x}(0) = 3.5$. The reference signal is $x_d = 2.5\sin(t)$.

From (5.6.22), the estimate tracking error is, then, defined by

$$
e = [e_1, e_2]^T, \quad e_1 = \hat{x}_1 - x_d, \quad e_2 = \hat{x}_2 - \dot{x}_d.
$$

The matrices A and B are defined as

$$
A = \begin{bmatrix} 0 & 1 \\ 0 & 0 \end{bmatrix}, \quad B = \begin{bmatrix} 0 \\ 1 \end{bmatrix},
$$

and the positive function $f(y,t)$ or $f(x_1,x_2,t)$ is given by

$$f(x_1,x_2,t) = \sqrt{\left[\frac{1-\exp(-x_1)}{1+\exp(-x_1)}\right]^2 + h_1} + \sqrt{[(x_2^2+2x_1)\sin(x_2)]^2 + h_2} + \sqrt{[0.5x_1\sin(3t)]^2 + h_3} + \sqrt{\| e \|^2 + h} + 1, \tag{5.6.33}$$

where $x_1 = x,\ x_2 = \dot{x},\ h_1,\ h_2,\ h_3$, and h are chosen as $h_1 = h_2 = h_3 = h = 0.01$. Then the

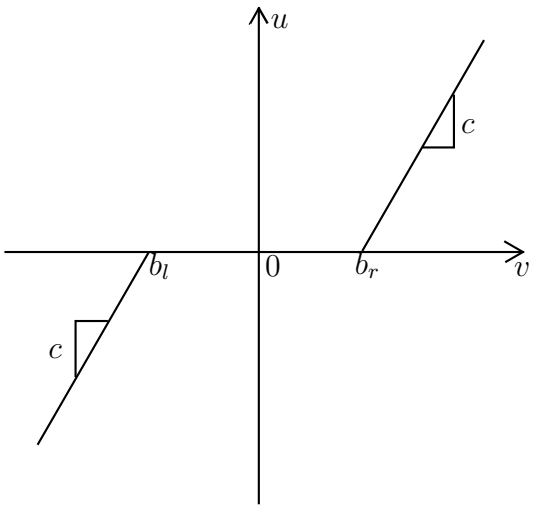

Figure 5.13: Dead-zone model

modified controller defined by (5.6.17) and (5.6.21) is applied to this example. The design parameters are selected as $\sigma_1 = 0.01$, $k = [-1,-1.1]$, $\mathsf{Q} = [6 \quad 3; 3 \quad 6]$, $\gamma = 0.1$, $\sigma_2 = 0.1$, $\hat{\theta}_m(0) = 0$, $\epsilon_e = 0.06$ and $\epsilon_v = 0.15$. For KF, larger ϵ_e and ϵ_v must be used, i.e. $\epsilon_e = 0.1$ and $\epsilon_v = 1.5$ to avoid bursting behavior of actuator designed input signal. This is because the estimate states are less accurate if KF is used for the simplified model. Solving (5.6.8) gives

$$\mathsf{P} = \begin{bmatrix} 5.8617 & 3.0586 \\ 3.0586 & 5.5584 \end{bmatrix} \tag{5.6.34}$$

For both filtering approaches, we assume that all states, $y = [x, \dot{x}]^T$, can be measured. Thus, the measurement model is given by (5.6.26). The temporal and stochastic parameters for our simulation using CDUKF are given in Table 5.1 and Table 5.2 respectively. For KF, the discretized sampling time Δt is the same as measurement interval, the covariance matrix of state equation is $\mathcal{Q} = 2.2 \times 10^{-6}[1 \quad 0 \quad 0; 0 \quad 1 \quad 0; 0 \quad 0 \quad 0.1]$, and the measurement covariance is the same as that shown in Table 5.2. Note that I_2 and I_5 appearing in Table 5.2 are 2-dimensional and 5-dimensional identity matrices respectively, and $[t_0, t_f]$ is simulation time interval.

Before we report our simulation result, we point out that only the modified parameter update law (5.6.17) can be applied to avoid divergence, whereas either the original control law (5.6.14) or the modified control law (5.6.21) can be applied. Our result is mainly discussed on the comparison of effectiveness of both control law and the comparison of tracking performance obtained from both filtering methods.

Using either control law, we obtain no significant different result of parameter from the parameter update law, which is indicated in Fig. 5.14. Also, almost the same tracking error is obtained if CDUKF is used, which is better than that obtained from classical KF as illustrated in Fig. 5.15 and Fig. 5.16. The designed actuator input signal induced by the original control law, seen in Fig. 5.17, is largely bursting which practically may damage actuator. Fig. 5.18 indicates the contribution of both modified control law and filtering effectiveness to achieve smooth designed actuator input signal.

Table 5.1: Temporal parameters (in second)

Parameters	Plant	CDUKF
$[t_0, t_f]$	[0,50]	[0,50]
Sampling time	10^{-4}	2×10^{-4}
Measurement interval	4×10^{-4}	4×10^{-4}

Table 5.2: Stochastic parameters

Parameters	Plant	CDUKF
Q_c	$10^{-4}\begin{bmatrix} 0 & 0 \\ 0 & 1 \end{bmatrix}$	$5.5 \times 10^{-3}\begin{bmatrix} I_2 & 0 \\ 0 & 0.1I_5 \end{bmatrix}$
R	$10^{-7}I_2$	$1.3 \times 10^{-6}I_2$
$[\hat{y}_{0\|0}^T \quad \hat{p}_{0\|0}^T]^T$	–	$0.01[-2.5 \quad 3.5 \quad \text{ones}(1,5)]^T$
$P_{0\|0}$	–	$10^{-2}\begin{bmatrix} I_2 & 0 \\ 0 & 0.1I_5 \end{bmatrix}$

5.7 Summery

- Straightforward implementation of estimation to joint state and parameter model of a dynamical system with discontinuity is unrealizable since the sliding vector field yields unobservable model under the sense of Filippov's convex method. We provide an algorithm which is switched to the problem of computation of deterministic system when system state is sliding. Through simulation results we also show robustness of CDUKF dealing with high uncertainty of modeling by selecting a bias basis function within limitation that guarantee stability of estimation.

- Implementation of the existing controller is not practically applicable for stochastic systems, although it can achieve exponential tracking for a class of deterministic systems. We provide modification to the controller to avoid divergence and to remedy the bursting signal of actuator input. Also, we show the contribution of filtering effectiveness together with the modified control law by showing simulation result of a numerical example of a nonlinear uncertain system with a dead-zone nonlinearity. Moreover, we point out that by taking the advantage of known nonlinear function of the system for a nonlinear filtering approach, we obtain a better result over a simplified model to use linear filtering method.

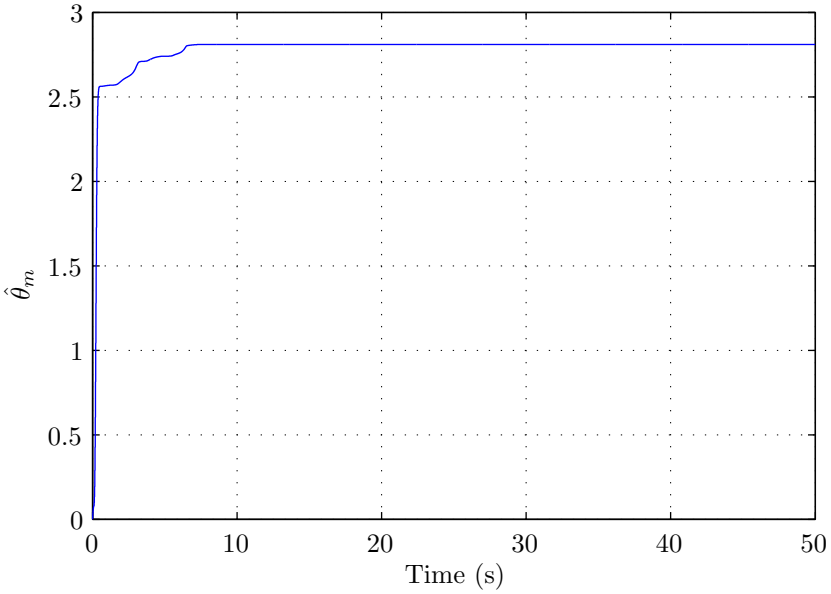

Figure 5.14: Control parameter, $\hat{\theta}_m$ (CDUKF)

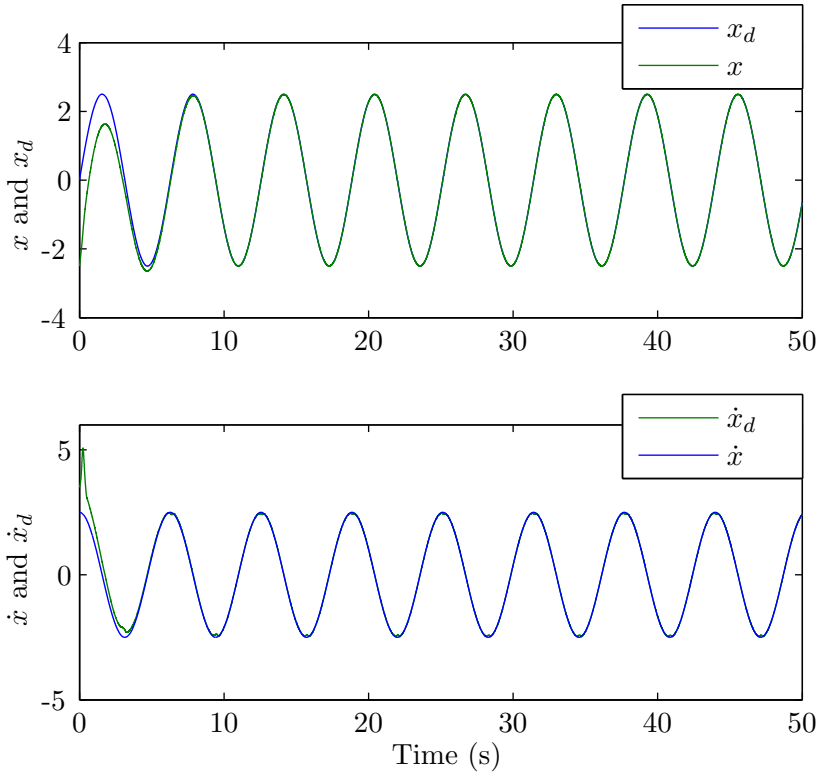

Figure 5.15: Plant states and reference (CDUKF)

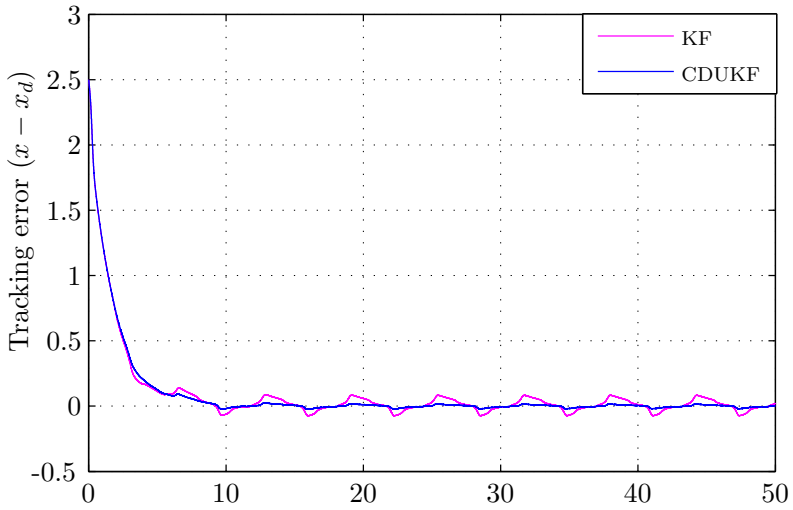

Figure 5.16: Tracking errors

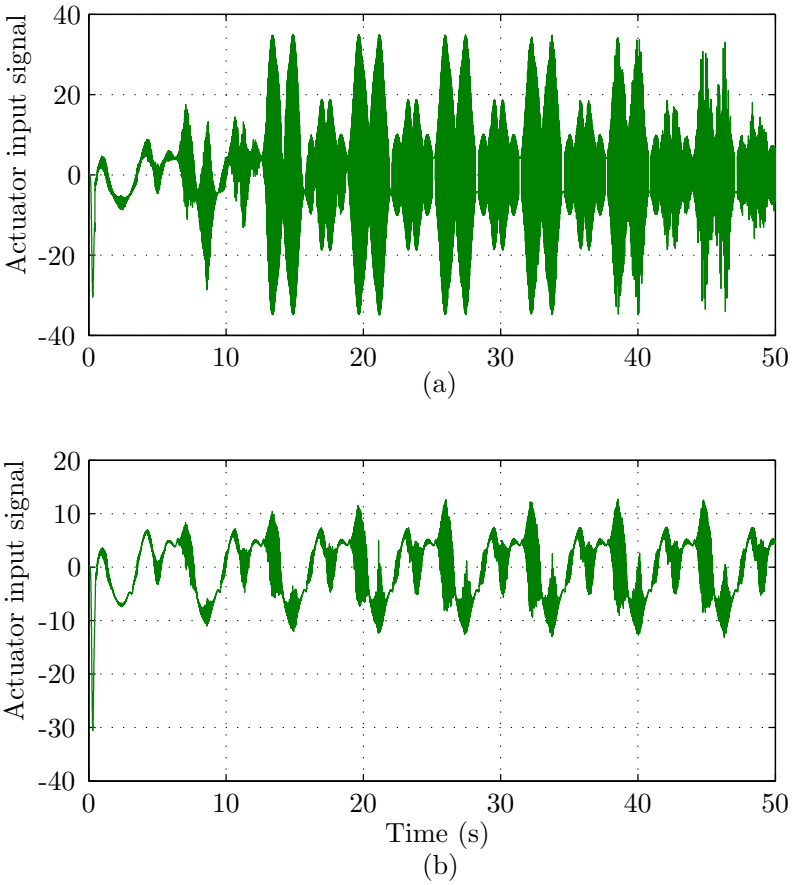

Figure 5.17: Designed actuator input signal without filtering: (a) using the original control law; (b) using the modified control law

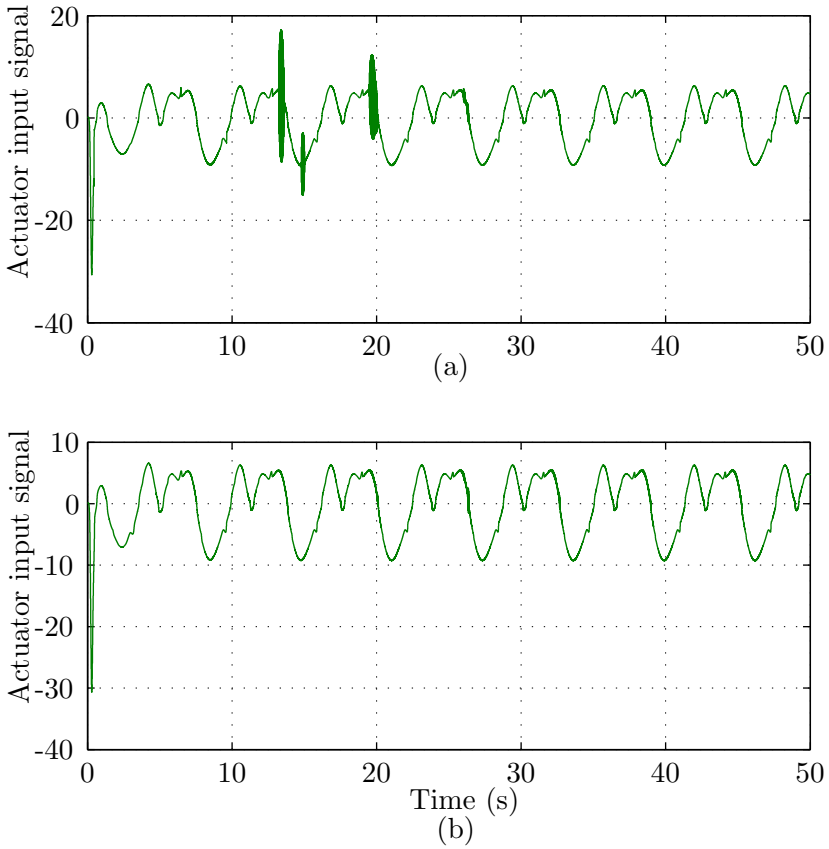

Figure 5.18: Designed actuator input signal with filtering (CDUKF): (a) using the original control law; (b) using the modified control law

Chapter 6

Receding-horizon Unscented Kalman Filter

In this Chapter, we consider another effective Kalman-type estimation algorithm for systems with discontinuous vector field. We propose an incorporation between the existing receding-horizon nonlinear Kalman filter (RNKF) and the unscented transformation, which is named receding-horizon unscented Kalman filter (RUKF). The use of unscented transformation is beneficial to discontinuous systems since it does not require partial derivatives as does the linearization technique which may incur severeness at discontinuity. An application of this algorithm to a system with discontinuous friction is considered to illustrate its performance.

6.1 Discrete Time Model

In most practical applications, state equation of a dynamical system is stochastically modeled as

$$\dot{x}(t) = f(x,t) + v_c(t) \tag{6.1.1}$$

where $x(t) \in \mathbb{R}^n$ is state; $f(x,t)$ is called drift function; and $v_c(t)$ is white Gaussian noise. This equation can be discretized as

$$\begin{aligned} x_{k+1} &= x_k + \int_{kT}^{(k+1)T} f(x,t)dt + v_k \\ &= f_d(x_k, t_k) + v_k \end{aligned} \tag{6.1.2}$$

where v_k is Gaussian noise with known covariance matrix Q. The general measurement equation is modeled in discrete time as

$$z_{k+1} = h_d(x_{k+1}) + w_{k+1} \tag{6.1.3}$$

where $z_k \in \mathbb{R}^p$ is measurement at time kT, h_d is measurement model function and w_k is measurement noise assumed to be Gaussian with known covariance matrix R.

Recently, [37] introduced the RNKF in which the Kalman filtering framework is extended to include a receding horizon in an optimization framework. The algorithm was pointed out that it can handle state constraints and is robust for estimation of parameter that evolves deterministically. Furthermore, it was proved that for linear unconstrainted systems the current estimate state is the optimal estimation of Kalman filtering, while the other

estimate states over the horizon are optimal smoothing estimation. The time update of this algorithm, however, engages linearization which is not compatible with discontinuous systems. We propose a receding-horizon unscented Kalman filter which incorporates the receding horizon framework with unscented transformation. The proposed algorithm can be summerized as follows.

Receding-horizon unscented Kalman filter

Initialization

The same as the RNKF, the RUKF starts after a window of h measurements are obtained. At any time instant k, denote $\hat{x}_{k-h|k-h}$ and $P_{k-h|k-h}$ as mean and corresponding covariance matrix respectively, both of which are assumed available. The first estimation problem is solved at time $k = h$, and it, thus, requires initialized mean and covariance at time $k = 0$, which are denoted as $\hat{x}_{0|0}$ and $P_{0|0}$ respectively. For the time corresponding to $k = 1, \ldots, h$, the estimates can be obtained with variable window sizes accordingly.

Let n_h be the number of augmented state over a window size h. Then $n_h = nh$, and the associated weights for sigma points corresponding to the augmented state are defined as following

$$\begin{aligned} W_0^{(m_h)} &= \frac{\lambda_h}{n_h + \lambda_h} \\ W_0^{(c_h)} &= \frac{\lambda_h}{n_h + \lambda_n} + (1 - \alpha^2 + \beta) \\ W_i^{(m_h)} &= \frac{1}{2(n_h + \lambda_h)}, \quad i = 1, \ldots, 2n_h \\ W_i^{(c_h)} &= \frac{1}{2(n_h + \lambda_h)}, \quad i = 1, \ldots, 2n_h \end{aligned} \tag{6.1.4}$$

where $\lambda_h = \alpha^2(n_h + \kappa) - n_h$. The positive constants α, β and κ are the method parameters. For ease of reading, we will present our whole algorithm in matrix form to calculate mean, covariance and cross-covariance matrices, which are associated with the following weight matrices,

$$\begin{aligned} w_{m_h} &= \left[W_0^{(m_h)} \cdots W_0^{(m_h)} \right] \\ W_h &= (I - [w_{m_h} \cdots w_{m_h}]) \begin{bmatrix} W_0^{(c_h)} & & \\ & \ddots & \\ & & W_{2n_h}^{(c_h)} \end{bmatrix} \\ &\quad \times (I - [w_{m_h} \cdots w_{m_h}])^T, \end{aligned} \tag{6.1.5}$$

Time update

Let us consider the time update of the state estimation over window size h, starting from filtered estimates at time k. Denote $\hat{x}_{k|k}$ and $P_{k|k}$ be *a posteriori* of mean and its error covariance matrix at time k respectively, both of which are available. The predicted estimates for all the states in the time interval $[k+1, k+h]$ are obtained by the 'open loop' propagation

of sigma points via the state equation (6.1.2). The propagated sigma points are augmented as

$$X^a_{k+h|k} = \left[X^T_{k+h|k}(k+1)\cdots X^T_{k+h|k}(k+h)\right]^T, \tag{6.1.6}$$

and the augmented mean corresponding the augmented sigma point is denoted as

$$\hat{x}^a_{k+h|k} = \left[\hat{x}^T_{k+h|k}(k+1)\cdots \hat{x}^T_{k+h|k}(k+h)\right]^T. \tag{6.1.7}$$

Then the predicted covariance matrix of the augmented states $P^a_{k+h|k}$ at the time $(k+h)^{th}$ is defined by

$$P^a_{k+h|k} = \begin{bmatrix} P^{n\times n}_{k+h|k}(k+1,k+1) & \cdots & P^{n\times n}_{k+h|k}(k+1,k+h) \\ P^{n\times n}_{k+h|k}(k+2,k+1) & \cdots & P^{n\times n}_{k+h|k}(k+2,k+h) \\ \vdots & \ddots & \vdots \\ P^{n\times n}_{k+h|k}(k+h,k+1) & \cdots & P^{n\times n}_{k+h|k}(k+h,k+h) \end{bmatrix}. \tag{6.1.8}$$

The block diagonal matrices of (6.1.8) represent the error covariance matrices in the open loop state estimates, whereas the off-diagonal matrices are the cross-covariance between the open loop state estimation errors at different time instants.

All the block elements of $X^a_{k+h|k}$, $\hat{x}^a_{k+h|k}$ and $P^a_{k+h|k} \in \mathbb{R}^{nh\times nh}$ defined in (6.1.6) to (6.1.8) are computed using unscented transformation. The i^{th} element of $X^a_{k+h|k}$ and $\hat{x}^a_{k+h|k}$ are respectively calculated by the followings,

$$\begin{aligned} X_{k+h|k}(i-1) &= \left[\hat{x}_{k+h|k}(i-1)\cdots\hat{x}_{k+h|k}(i-1)\right] \\ &\quad + \sqrt{c_1}\left[0 \quad \sqrt{P_{k+h|k}(i-1)} \quad -\sqrt{P_{k+h|k}(i-1)}\right], \\ X_{k+h|k}(i) &= f_d\left(X_{k+h|k}(i-1), u(i-1)\right), \quad \text{and} \\ \hat{x}_{k+h|k}(i) &= X_{k+h|k}(i)w_{m_1}. \end{aligned} \tag{6.1.9}$$

Then, the ii^{th} diagonal block element of $P^a_{k+h|k}$ is calculated along with the i^{th} element of $X^a_{k+h|k}$ as

$$P^a_{k+h|k}(i,i) = X_{k+h|k}(i)W_1X^T_{k+h|k}(i) + Q. \tag{6.1.10}$$

The upper triangle element of $P^a_{k+h|k}$, i.e. $P^a_{k+h|k}(i,j)$ where $i<j$, is defined by

$$P^a_{k+h|k}(i,j) = X_{k+h|k}(i)W_1X^T_{k+h|k}(j) \tag{6.1.11}$$

The complete upper triangular blocks of $P^a_{k+h|k}$ can now be calculated with these recursive relationships when the first block $P^a_{k+h|k}(1,1)$ is initialized with

$$P^a_{k+h|k}(1,1) = X_{k|k}W_1X^T_{k|k} + Q. \tag{6.1.12}$$

where $X_{k|k}$ is defined in terms of $\hat{x}_{k|k}$ and $P_{k|k}$ by the formulation of the first equation in (6.1.9). Since $P^a_{k+h|k}$ is symmetric, the lower triangle blocks are the transpose of the upper ones.

Measurement update

The predicted estimates of the augmented states are updated using all the measurements in the time window $[k+1, k+h]$ based on, again, unscented transformation. We define the augmented measurements as

$$z^a_{k+h} = \left[z^T(k+1) \cdots z^T(k+h)\right]^T. \tag{6.1.13}$$

Then the complete measurement update is as the follows

$$\begin{aligned}
\mathcal{X}^a &= \left[\hat{x}^a_{k+h|k} \cdots \hat{x}^a_{k+h|k}\right] \\
&\quad + \sqrt{c_h}\left[0 \quad \sqrt{P^a_{k+h|k}} \quad -\sqrt{P^a_{k+h|k}}\right] \\
&= \left[\mathcal{X}_1^T \cdots \mathcal{X}_h^T\right]^T \\
\mathcal{Z}^a_{k+h|k} &= \left[h_d(\mathcal{X}_1)^T \cdots h_d(\mathcal{X}_h)^T\right]^T \\
z^a_{k+h|k} &= \mathcal{Z}^a_{k+h|k} w_{m_h} \\
P^a_{zz,k+h|k} &= \mathcal{Z}^a_{k+h|k} W_h \mathcal{Z}^{aT}_{k+h|k} + R^a \\
P^a_{xz,k+h|k} &= \mathcal{X}^a_{k+h|k} W_h \mathcal{Z}^{aT}_{k+h|k} \\
K^a_{k+h} &= P^a_{xz,k+h|k} {P^a_{zz,k+h|k}}^{-1} \\
\hat{x}^a_{k+h|k+h} &= \hat{x}^a_{k+h|k} + K^a_{k+h}(z^a_{k+h} - z^a_{k+h|k})
\end{aligned} \tag{6.1.14}$$

where R^a is given by $\mathrm{diag}(R^{p\times p} \ldots R^{p\times p})$.

6.2 Application to Friction Estimation

We consider the same control system as in the previous chapter, i.e. an adaptive compensation of static friction which is modeled as

$$F_f = (\alpha_0 + \alpha_1 e^{-(\omega/\omega_s)^2})\mathrm{sign}(\omega) + \alpha_2\omega, \tag{6.2.1}$$

where ω is angular velocity; ω_s is Stribeck velocity; $\alpha_0 + \alpha_1$ is static friction; α_0 is Coulomb friction; and α_2 is coefficient of viscous friction. We use the algorithm in the previous section to estimate the friction from a model of DC motor as following,

$$\dot{\omega}(t) = \frac{1}{J}[-\mathrm{sign}(\omega), -e^{-(\omega/\omega_s)^2}\mathrm{sign}(\omega), -\omega]\alpha + \frac{u}{J} \tag{6.2.2}$$

where $\alpha = [\alpha_0, \alpha_1, \alpha_2]^T$, J is the total moment of inertia of the motor, u is control torque, and $\Phi(\omega) = 1/J[-\mathrm{sign}(\omega), -e^{-(\omega/\omega_s)^2}\mathrm{sign}(\omega), -\omega]$ is called basis function.

We simulate a control system which is illustrated by the block diagram in Fig. 6.1. The desired position is $\theta_r(t) = 2.8\sin(0.02\pi t)\sin(2\pi t)$ whose shape is indicated in Fig. 6.2, and our simulation is run up to 400 seconds. We consider the case of contact down where $\omega_s = 2.4$, and we simulate our system in two difference cases.

First, we use unbiased basis function which means that we choose the same $\omega_s = 2.4$ for estimator. The performance of tracking control obtained from using both UKF and RUKF is shown in Fig. 6.3. It indicates that tracking error using UKF is larger, especially at low velocity, (around 0, 50 and 100 seconds, the trajectory in Fig. 6.2 has small amplitude, and

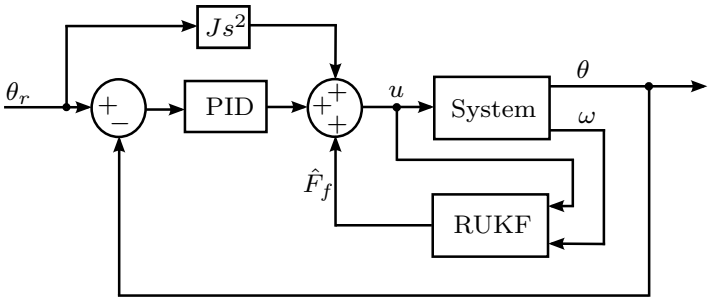

Figure 6.1: Block diagram of adaptive control using RUKF for friction estimation

so does the velocity). This is because the parameters of frication are not well estimated, as shown in Fig. 6.4. On sliding surface (at zero velocity), the system was shown unobservable in the previous chapter, and, therefore, both estimations diverge. However, convergence can be recovered when velocity is away from zero. Fig. 6.4 indicates that parameter estimation using RUKF is less sensitive than using UKF because, like RNKF, RUKF has the optimal smoothing property.

Second, we select $\omega_s = 0.01$ for estimation algorithm, meaning that biased basis function is used, as considered in the previous chapter. The temporal evolutions of estimated parameters, $\hat{\alpha}(t) = [\hat{\alpha}_0 \quad \hat{\alpha}_1 \quad \hat{\alpha}_2]^T$, are not constant, which are illustrated by estimation result in Fig. 6.5 and 6.6. The parameters, $\hat{\alpha}_0$ and $\hat{\alpha}_2$ have have fairly periodic form over 50 seconds which is the haft period of $\sin(0.02\pi t)$, so that we only show them over the last period. Whereas, the parameter $\hat{\alpha}_1$ seems to reach the steady state after about 70 seconds. The results of friction estimation and tracking error are shown in Fig. 6.7 and 6.8 respectively. In comparison with our previous result using CDUKF, tracking error obtained from using RUKF with $h = 4$ is slightly better. Furthermore, one drawback of using CDUKF is that it does not guarantee positive definite covariance matrix during the time update step [63], so resetting covariance matrix is required, and it costs much computational time if, for example, we check the sign of its all eigenvalues, 3208.7 seconds compared to 310.92 seconds for RUKF. However, Fig. 6.8 indicates that if we select too large number of horizon, tracking performance becomes worse. The reason is that, the open loop estimation of state during too long time update yields a drift away from the actual state due to uncertainty.

6.3 Summery

To handle estimation problem of discontinuous systems, we propose an estimation algorithm, receding-horizon unscented Kalman filter which extends the framework of the existing receding-horizon nonlinear Kalman filter incorporated with unscented transformation. The details of algorithm consisting of initialization, time update and measurement are explained. The algorithm is pointed out to be compatible with discontinuous systems and does not require switching method as does the continuous-discrete unscented Kalman filter used in our previous research. To clarify the proposed methods, an application to friction estimation for adaptive control is considered. In comparison with CDUKF, simulation using RUKF shows applaudable results since RUKF requires less computational time (if the horizon is not so large), and has a slightly better performance of tracking error.

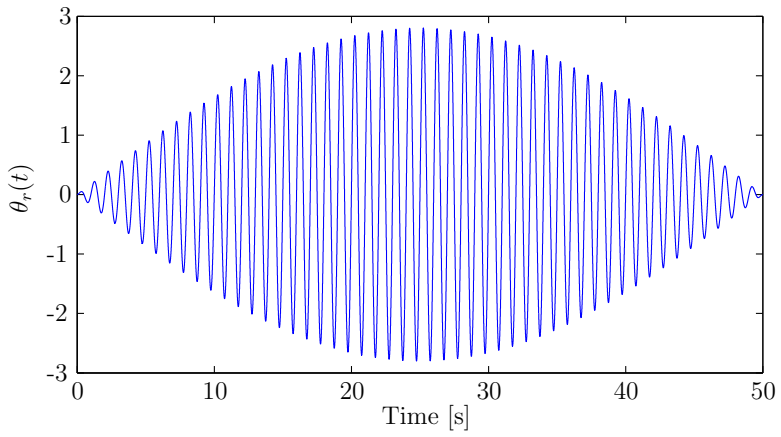

Figure 6.2: Tracking reference

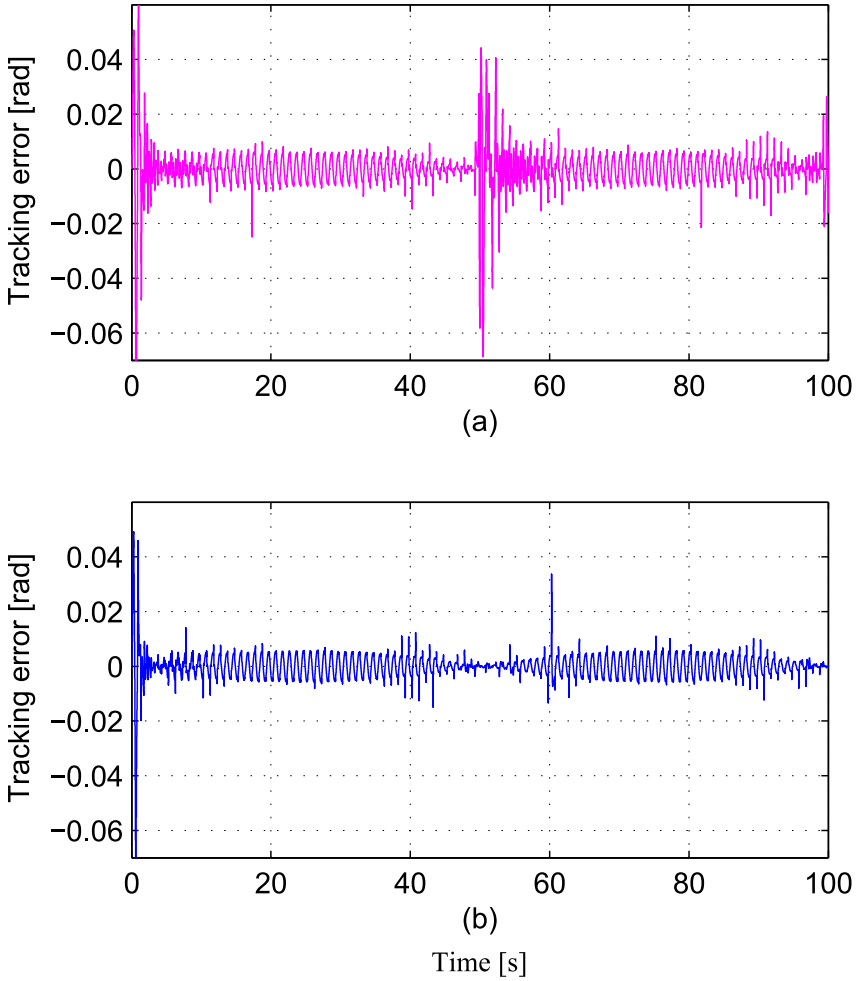

Figure 6.3: Tracking performance for unbiased model: (a) using UKF and (b) using RUKF with $h = 4$

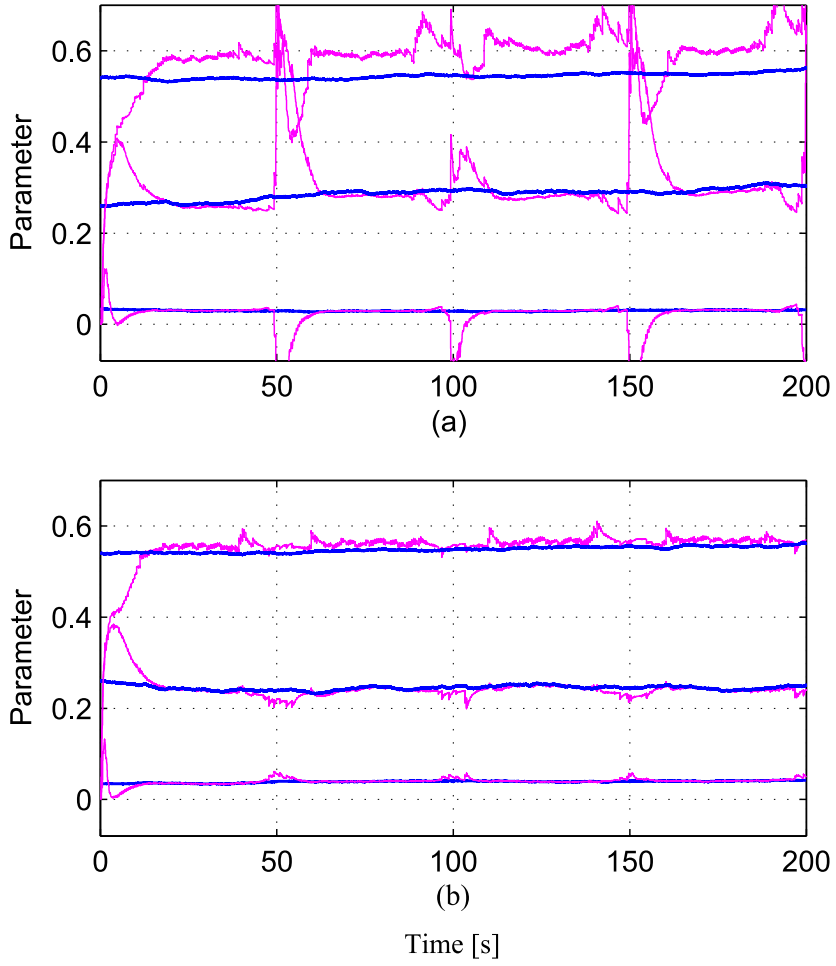

Figure 6.4: Parameter estimation for unbiased model: actual (blue) and estimate (pink); (a) using UKF and (b) using RUKF

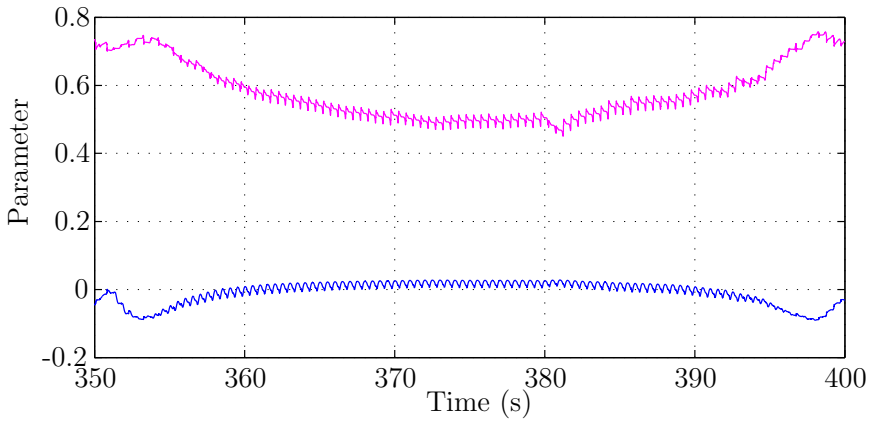

Figure 6.5: Time-evolution of parameter ($h = 4$): $\hat{\alpha}_0$ (pink) and $\hat{\alpha}_2$ (blue)

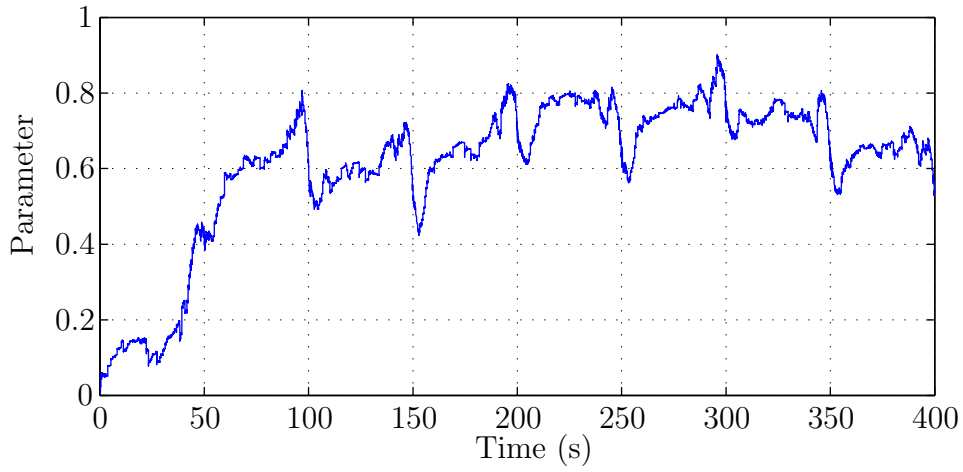

Figure 6.6: Time-evolution of parameter ($h = 4$): $\hat{\alpha}_1$

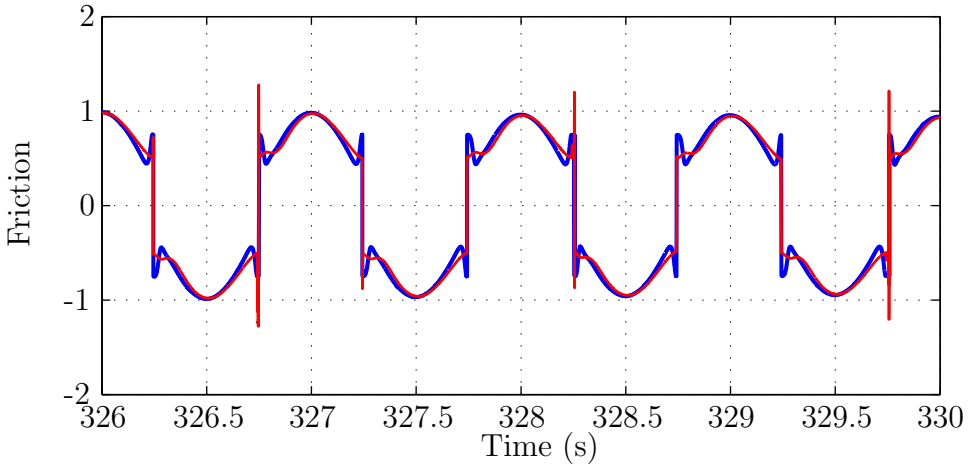

Figure 6.7: Friction: black line is actual one; red line is estimation

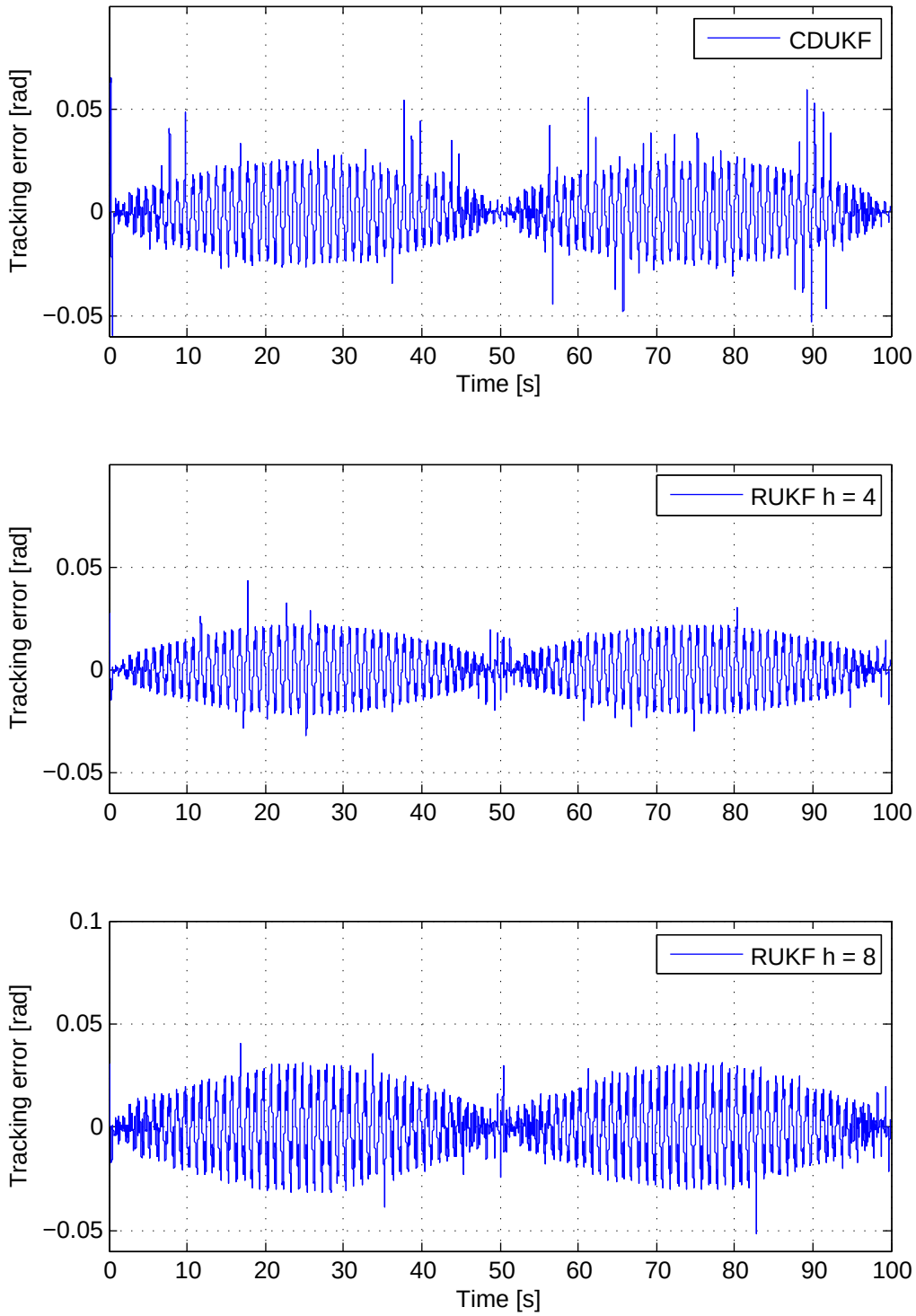

Figure 6.8: Performance

Chapter 7

Conclusions

The main contribution of this dissertation is the investigation of estimation for discontinuous dynamical systems. Firstly, we showed that common computation for such systems is not accurate when state orbit nearly reaches one or more sliding surfaces. The computational burden is chattering which is incurred due to discretization. Thus, straightforward implementation of proper standard estimation algorithms, specifically the Kalman-type filterings, cannot cope with this issue since the prediction accuracy of the algorithms relies on the effectiveness of computational method. To improve numerical accuracy, we used the extension of Filippov's convex method. Secondly, we proposed a simplification of discontinuous vector field of the dynamical systems. The simplified vector field has the form of multiplication of an arbitrary basis discontinuous-function matrix and a time-evolving parameter vector. The filtering problem of the original filtering model becomes estimation problem of joint state and parameter model. By using the Filippov's convex method to define the average vector field on discontinuity surface, we revealed that estimation of this class of dynamical model diverges when the orbit theoretically reaches sliding surface because observability condition of the joint state and parameter model does not hold. Therefore, a particular feature for estimation was proposed, that is a switch to computation of deterministic system to avoid divergence.

We also showed that the choice of the basis function has limitation that it must be selected in such a way that stability of estimation is guaranteed, i.e. the model error is at least a bounded function. As an example, we showed a result of estimation divergence if the model error is an unbounded function. Simplification technique, furthermore, has limitation beyond the stability demand. Ultimate simplification that becomes a linear joint state and parameter model results worse performance than a slightly simplified model. This implies that knowledge of nonlinear function of a dynamical model has advantage for joint state and parameter estimation for which nonlinear filtering approach is used, and it was clarified by a numerical example of tracking control of nonlinear system with actuator nonlinearity. In the control problem of this example, we also have a contribution on controller design modification since the existing controller cannot be implemented for stochastic systems.

For tracking control, CDUKF requires the switch to computation of deterministic system because the formulation of time update is sensitive to have non-positive definite covariance matrix though the orbit of state lies on sliding surface for only a short instant. The algorithms UKF and RUKF, on the other hand, do not require the switch since the time update of the algorithm always preserve positive definite covariance matrix although estimation model is not observable. However, all the estimation algorithms require the switch to avoid divergence

if the state of a system is operated on sliding surface for long time, for example regulation control.

We have some comments for future works as the follows:

In terms of practical applications, it will be more easily to implement the adaptive control scheme if we can also estimate the moment of inertia (load for general) of a the DC motor model. Furthermore, we only considered a system with symmetric model of friction, so an interesting extension of our work is to cope with asymmetric friction model. Furthermore, the presence of hysteresis in friction model which commonly exists in hydraulic systems is also a challenging issue for future consideration.

For estimation algorithms, to broaden our research scope investigation on systems with uncertain sliding surface should be done. An other crucial prospect is to develop algorithms that can handle different sets of state and parameter of hybrid model. As an example of such models, a system with asymmetric friction model consists of three individual vector fields determined by the sign of velocity, i.e. two different vector fields defined for negative and positive velocity accordingly, and the average vector field defined at zero velocity by using the Filippov's convex method. Such algorithms have potential of being used with biological systems which, in many cases, appear as discontinuous and/or hybrid systems.

Bibliography

[1] D. Karnopp, "Computer simulation of stic-slip friction in mechanical systems," *J. Of Dynamic Systems Measurement and Control*, vol. 107, No. 1, pp. 100-103, 1985.

[2] B. Armstrong-Helouvry, P. Dupont, and C. C. de Wit, "A survey of models analysis tools and compensation methods for the control of machines with friction," *Automatica*, vol. 30, no. 7, pp. 1083-1138, 1994.

[3] H. Olsson, K. Astrom, C. Canudas de Wit, M. Gafvert, and P. Lischinsky, "Friction models and friction compensation," *European Journal of Control*, vol. 4, pp. 176-195, 1998.

[4] J. Cortés, "Discontinuous dynamical systems," *IEEE Control Systems Magazine*, pp. 36-73.

[5] Q. Hui, W. M. Haddad, and S. P. Bhat, "Semistability theory for differential Inclusions with applications to consensus problems in dynamical networks with switching topology", *IEEE American Control Conference*, Seattle, WA, June 2008.

[6] J-L. Gouzé and T. Sari, "A class of piecewise linear differential equations arising in biological models," Taylor & Francis: *Dynamical Systems*, vol. 17. no. 4, pp. 299-316, 2002.

[7] R. Casey, H. de Jong, and J-L. Gouzé, "Piecewise-linear models of genetic regulatory networks: Equilibria and their stability," Springer-Verlag: *J. Mathematical Biology*, no. 52, pp. 27-56, 2005.

[8] M. Forti and P. Nistri, "Global convergence of neural networks with discontinuous neuron activations," *IEEE Trans. Circuits and Systems*, vol. 50, no. 11, pp. 1421-1435.

[9] W. M. Haddad, Q. Hui, and J. M. Bailey, "Multistability, bifurcations, and biological neural networks: A synaptic drive firing model for cerebral cortex transition in the induction of general anesthesia," in *IEEE Int. Conf. Decision and Control and European Control Conference*, Orlando, FL, December 2011.

[10] B. Brogliato, "Nonsmooth mechanics: models, dynamics, and control, 2nd ed.," New York: Springer-Verlag, 1999.

[11] F. Pfeiffer and C. Glocker, "Multibody dynamics with unilateral contacts," New York: Wiley, 1996.

[12] A. A. Agrachev and Y. Sachkov, "Control theory from the geometric viewpoint," New York: Springer-Verlag, 2004.

[13] S. Bennett, "A history of control engineering 1930-1935,". London, UK: Inst. Elect. Eng., 1993.

[14] G. A. S. Pereira, M. F. M. Campos, and V. Kumar, "Decentralized algorithms for multi-robot manipulation via caging," *Int. J. Robotics Res.*, vol. 23, no. 7-8, pp. 783-795, 2004.

[15] V. I. Utkin, "Sliding modes in control and optimization," New York: Springer-Verlag, 1992.

[16] C. Edwards and S. K. Spurgeon, "Sliding mode control: theory and applications," New York: Taylor & Francis, 1998

[17] R. C. Arkin, "Behavior-based robotics," Cambridge, MA: MIT Press, 1998.

[18] M. M. Polycarpou and P.A. Ioannou, "On the existence and uniqueness of solutions in adaptive control systems," *IEEE Trans. Automatic Control*, vol. 38, no. 3, pp. 474479, 1993.

[19] R. G. Brown and P. Y. Hwang, "Introduction to random signals and applied Kalman filtering," New York: Wiley, 1992.

[20] A. Gelb, Ed., "Applied optimal estimation," Cambridge, MA: MIT Press, 1984.

[21] J. M. Mendel, "Lessons in digital estimation theory," Englewood Cliffs, NJ: Prentic-Hall, 1986.

[22] G. C. Goodwin and K. S. Sin, "Adaptive filtering, prediction and control," Englewood Cliffs, NJ: Prentice-Hall, 1993.

[23] Y. Kleyman and I. Mochalov, "Identification of nonstationary systems," *Automatic Romote Control*, vol. 55, pp149-163, 1994.

[24] L. Ljung, "System identification: Theory for the user," Englewood Cliffs, NJ: Prentice-Hall, 1987.

[25] E. A. Misawa and J. K. Hedrick, "Nonlinear observers–A state-of-the-art survey," *ASME J. Dynamic Systems Measurement and Control*, vol. 111, pp. 344-352, 1989.

[26] G. V. Puskorius and L. A. Feldkamp, "Neurocontrol of nonlinear dynamical systems with Kalman filter trained recurrent networks," *IEEE Trans. Neural Networks*, vol. 5, pp. 279-297, 1994.

[27] K. Reif, S. Günther, E. Yaz, and R. Unbehauen, "Stochastic stability of the discrete-time extended Kalman filter," *IEEE Trans. Automatic Control*, vol. 44, no. 4, pp. 714-728.

[28] S. J. Julier, J. K. Uhlmann, and H. F. Durrant-Whyte, "A new method for the nonlinear transformation of means and covariances in filters and estimators," *IEEE Trans. Automatic Control*, vol. 45, pp. 477-482, March 2000.

[29] S. J. Julier and J. K. Uhlmann, "Unscented filtering and nonlinear estimation," *Proc. IEEE*, vol. 92, pp. 401-422, March 2004.

[30] R. M. van der, "Sigma-point Kalman filters for probabilistic inference in dynamic state-space models," Ph.D., OGI School of Sci. Eng., Oregon Health and Sci. Univ., Portland, OR, 2004.

[31] S. Särkkä, "On unscented Kalman filtering for state estimation of continuous-time nonlinear system," *IEEE Trans. Automatic Control*, vol. 52, no. 9, pp. 1631-1641, September 2007.

[32] J. Xu, Stochastic stability of the continuous-time unscented Kalman filter, *IEEE Int. Conf. Decision and Control*, Cancun, Mexico, 2008.

[33] I. Arasaratnam and S. Haykin, "Cubature Kalman filters," *IEEE Trans. Automatic Control*, vol. 54. no. 6, pp.1254-1269, June 2009.

[34] I. Arasaratnam, S. Haykin, and T. R. Hurd, "Cubature Kalman filtering for continuous-discrete systems: Theory and simulations," *IEEE Trans. Signal Processing*, vol. 58, no. 10, pp. 49774993, October 2010.

[35] P. Morreau, D. Chapelle and P. Le Tallec, Joint state and parameter estimation for distributed mechanical systems, *Comput. Meth. Appl. Mech. Eng*, vol. 197, pp. 659-677, 2008.

[36] P. Morreau and D. Chapelle, Reduced-order unscented Kalman filtering with application to parameter identification in large-dimensional systems, *ESAIM: Control, Optimisation and Calculus of Variations*, vol. 17, no. 2, pp. 380-405, 2011.

[37] R. Rengaswamy, S. Narasimhan, and V. Kuppuraj, "Receding-horizon nonlinear Kalman (RNK) filter for state estimation," *IEEE Trans. Automatic Control*, vol. 58, no. 8, pp. 2054-2059, August 2013.

[38] B. J. Sipos, "Application of the manifold-constrained unscented Kalman filter," *IEEE/ION Position, Location and Navigation Symposium*, pp.30-43, 2008.

[39] A. H. Jazwinski, "Stochastic processes and filtering theory,". New York: Academic, Ch. 6 and 9, 1970.

[40] B. Armstrong-Helouvry, "Control of machines with friction," Boston: Kluwer Academic Publisher, 1991.

[41] C. Canudas de Wit, H. Olsson, K. Astrom, and P. Lischinsky, "A new model for control system with friction," *IEEE Trans. Automatic Control*, vol. 40, no. 3, pp. 419-425, 1995.

[42] B. Friedland and Y.-J. Park, "On adaptive friction compensation," *IEEE Trans. Automatic Control*, vol. 37, no. 10, pp. 1609-1612, 1992.

[43] C. Canudas de Wit and P. Lischinsky, "Adaptive friction compensation with partially known dynamic friction model," *Int. J. Adaptive Control and Signal Processing*, vol. 11, pp. 65-80, 1997.

[44] M. Feemster, P. Vedagarbha, D. Dawson, and D. Haste, "Adaptive control techniques for friction compensation," *Mechatronics*, vol. 9, pp. 125-145, 1999.

[45] J.-H. Ryu, J. Song, and D,-S. Kwon, "A nonlinear friction compensation method using adaptive control and its practical application to an in-parallel actuated 6-dof manipulator," *Control Engineering Practice*, vol. 9, pp. 159-167, 2001.

[46] E. Papadopoulos and G. Chasparis, "Analysis and model-based control of servomechanisms with friction," *IEEE/RSJ Int. Conf. Intelligent Robots and System*, vol. 3, pp. 2109-2114, 2002.

[47] D. Putra, L. Moreau, and H. Nijmeijer, "Observer-based compensation of discontinuous friction," *IEEE Conf. in Decision and Control*, pp. 4940-4945, 2004.

[48] B. Bona, and M. Indri, "Friction compensation in robotics: an overview," *IEEE Int. Conf. on Decision and Control, and the European Control Conference*, 2005.

[49] J. C. Martinez-Rosas, and L. Alvarez-Icaza, "Adaptive compensation of dynamic friction in an industrial robot," *IEEE Int. Conf. on Control Applications, Part of 2008 IEEE Multi-Conf. Systems and Control*, San Antonio, Texas, USA, Sept 2008.

[50] L. Marton, "Adaptive friction compensation in the presence of backlash," *Control Engineering and Applied Informatics*, vol. 11, no. 1, pp. 3-9, 2009.

[51] R. R. Laura, R. Ashok, and T. Jennifer,"Adaptive friction compensation using extended Kalman-Bucy filter frcition estimation," *Control Engineering Practice*, vol. 9, no. 2, pp. 169-179, Feb 2001.

[52] P. T. Piiroinen, Y. A. Kuznetsov, "An event-driven method to simulate Filippov systems with accurate computing of sliding motions," *ACM Tranc. Mathematical Software*, Vol. 34, no. 3, 2008.

[53] A. F. Filippov, "Differential equations with discontinuous right-hand-side," Kluwer Academic Publisher, 1988.

[54] Q. Hui, W. M. Haddad, and S. P. Bhat, "Finite-time semistability and consensus for nonlinear dynamical networks," *IEEE Trans. Automatic Control*, vol. 53, no. 8, pp. 1887-1900, 2008.

[55] J. Cortés, "Distributed kriged Kalman filter for spatial estimation", *IEEE Trans. Automatic Control*, vol. 54, no. 12, pp. 2816-2827, 2009.

[56] K. Xiong, H. Y. Zhang and C. W. Chan, "Performance evaluation of UKF-based nonlinear filtering," *Automatica*, vol. 42, no. 2, pp. 261-270, 2006.

[57] H. K. Khalil, "Nonlinear systems," Prentice Hall, pp. 552-553, 2000.

[58] W. F. Xie,"Sliding-mode-observer-based adaptive control for servo actuator with friction," *IEEE Trans. Industrial Electronics*, vol. 54. no. 3, pp. 1517-1527, June 2007.

[59] G. Tao and P. V. Kokotovic, Adaptive control of systems with atuator and sensor nonlinearitites. New York: John Willey & Sons, 1996;

[60] G. Tao and F. L. Levis, Adaptive control of nonsmooth dynamic system. London: Springer-Verlag, 2001.

[61] J. Zhou and C. Wen, Adaptive backstepping control of uncertain systems. Berlin: Springer-Verlag, 2008.

[62] Z. Zhang, Exponential tracking control of nonlinear systems with actuator nonlinearity, *Preprint submitted to 19th IFAC World Congress*, 2013.

[63] S. Särkkä, A. Solin, "On continuous-discrete cubatur Kalman filtering," *16th IFAC Symp. System Identification*, vol. 16, no. 1, pp. 1221-1226, Brussels, Belgium, 2012.

Publications

Journal Papers

1. Sarot Srang and Masaki Yamakita, "Adaptive friction compensation for a position control system with Stribeck friction using hybrid unscented Kalman filter," *Int. J. Information and Communication Technology*, vol. 5, no. 3/4, pp. 283-295, 2013. (Chapter 3)

2. Sarot Srang and Masaki Yamakita, "Estimation of discontinuous dynamical systems using receding-horizon unscented Kalman filter," *IEEJ Trans. Electronics, Information and Systems*. (Chapter 6, submitted)

Conference Papers

1. Sarot Srang and Masaki Yamakita, "Application of continuous-discrete unscented Kalman filter for control of nonlinear systems with actuator nonlinearity," *IEEE The 33rd Chinese Control Conference*, 2014. (Chapter 5, Section 5.6)

2. Sarot Srang and Masaki Yamakita, "Tracking Control of Nonlinear Stochastic Systems with Actuator Nonlinearity, " *IEEE/ASME International Conference on Advanced Intelligent Mechatronics*, pp. 697-702, 2014. (Chapter 5, Section 5.6)

3. Sarot Srang and Masaki Yamakita, "On the estimation of systems with discontinuities using continuous-discrete unscented Kalman filter," *IEEE American Control Conference*, pp. 457-463, 2014. (Chapter 5, Section 5.1-5.5)

4. Sarot Srang and Masaki Yamakita, "Estimation of systems with multiple sliding surfaces," *IEEE/SICE International Symposium on System Integration*, pp. 1-6, 2013. (Chapter 5.1-5.5)

5. Sarot Srang and Masaki Yamakita, "Estimation of discontinuous friction using continuous-discrete unscented Kalman filter for adaptive compensation," *IEEE/ASME International Conference on Advanced Intelligent Mechatronics*, pp. 429-435, 2013. (Chapter 4)